ATMOSPHERIC ORGANIC AEROSOL – WATER INTERACTIONS

Dissertation

Submitted to the

Department of Chemical Engineering

University of Patras

by

MAGDALINI PSICHOUDAKI

In Partial Fulfillment of the

Requirements for the Degree of

Doctor of Philosophy

In the Department of Chemical Engineering

Patras, April 2014

ΑΛΛΗΛΕΠΙΔΡΑΣΕΙΣ ΤΩΝ ΑΤΜΟΣΦΑΙΡΙΚΩΝ

ΟΡΓΑΝΙΚΩΝ ΣΩΜΑΤΙΔΙΩΝ ΜΕ ΤΟ ΝΕΡΟ

Υπό την

Μαγδαλινή Ψυχουδάκη

Εργαστήριο Μελέτης Ατμοσφαιρικής Ρύπανσης
Τομέας Μηχανικής Διεργασιών και Περιβάλλοντος
Τμήμα Χημικών Μηχανικών, Πανεπιστήμιο Πατρών

ΕΠΤΑΜΕΛΗΣ ΕΞΕΤΑΣΤΙΚΗ ΕΠΙΤΡΟΠΗ

Σ. ΠΑΝΔΗΣ, Καθηγητής
Τμ. Χημικών Μηχανικών, Παν/μιο Πατρών
Πρόεδρος της εξεταστικής επιτροπής

Π. ΚΟΥΤΣΟΥΚΟΣ, Καθηγητής
Τμ. Χημικών Μηχανικών, Παν/μιο Πατρών

Γ. ΛΥΜΠΕΡΑΤΟΣ, Καθηγητής
Τμ Χημικών Μηχανικών, ΕΜΠ

Α. ΝΕΝΕΣ, Καθηγητής
Τμ. Επιστημών της Γης και της Ατμόσφαιρας,
Τμ. Χημικής & Βιομοριακής Μηχανικής
Ινστιτούτο Τεχνολογίας της Georgia, US

Ν. ΜΙΧΑΛΟΠΟΥΛΟΣ, Καθηγητής
Τμ. Χημείας, Παν/μιο Κρήτης

Ε. ΠΑΠΑΕΥΘΥΜΙΟΥ, Αναπ. Καθηγήτρια
Τμ. Χημείας, Παν/μιο Πατρών

Χ. ΠΑΡΑΣΚΕΥΑ, Επικ. Καθηγητής
Τμ. Χημικών Μηχανικών, Παν/μιο Πατρών

Those who desire to understand, who are looking to find that which is eternal, without beginning and end, will walk together with greater intensity, will be a danger to everything which is unessential, to unrealities, to shadows. They will concentrate. They will become the flame, because they understand.

~ Jiddu Krishnamurti ~

Acknowledgements

I would like to thank my advisor, Dr. Spyros Pandis for providing me excellent guidance and invaluable scientific advice and also for giving me the opportunity to meet and collaborate with distinguished scientists of the field. I would also like to acknowledge Dr. Thanos Nenes with whom I have spent precious time in Georgia Tech. He was always communicative, helpful and supportive and provided me knowledge, valuable material and hands-on experience. I would also like to thank a number of people with whom I collaborated and earned valuable experience: Dr. Evangelia Kostenidou, Michael Pikridas and all the members of Professor Spyros Pandis group for creative collaboration and problem sharing, also Dr. Giorgos Kouvarakis and Dr. Katerina Bougiatioti for their hospitality and collaboration during field campaigns and also during my visit in Georgia Tech. Last but not least, I thank my beloved friends and family, I deeply appreciate their continuous support and encouragement.

This research has been co-financed by the European Union (European Social Fund – ESF) and Greek national funds through the Operational Program "Education and Lifelong Learning of the National Strategic Reference Framework (NSRF) - Research Funding Program: THALES. Investing in knowledge society through the European Social Fund: "Sources and physicochemical properties of fine and ultrafine aerosol particles that affect the regional climate of Greece".

Abstract

Atmospheric aerosols are responsible for adverse health effects and uncertain climate forcing. Depending on their composition, they can directly affect climate by scattering or absorbing solar radiation and they can also indirectly affect by serving as cloud condensation nuclei (CCN). While the chemistry and physical properties of the inorganic components of the aerosols are more or less known, the same does not stand for the organic components. Hygroscopic water soluble organic material can enhance the water absorption of the particles, affecting their climate forcing. This dissertation explores the hygroscopic properties of atmospheric organic aerosol, the first part of the thesis is dedicated to the development and analysis of methods for the measurement of water soluble organic aerosol, while the second part investigates the hygroscopic properties and CCN activity of organic particulate matter emitted by different sources or produced in the atmosphere through oxidation of volatile organic compounds.

Atmospheric particles can be directly emitted in the atmosphere (POA) or formed via oxidation of volatile organic compounds in the atmosphere (SOA). The former (primary) are in general less water soluble compared to the latter (secondary). The term water soluble organic carbon (WSOC) has been operationally defined and has been often used to estimate the concentration of SOA in the absence of biomass burning. Biomass burning is an exception because the corresponding primary particles do contain significant amounts of water soluble compounds. The traditional WSOC measurement method is based on filter sampling followed by total organic carbon (TOC) analysis, with varying volumes of water used for the WSOC extraction.

In order to estimate the mass fraction of a compound that will dissolve in water during WSOC extraction, two models were developed. The ideal organic solution model is

based on the assumption that organic species form a single ideal organic solution within the particle and each organic compound is dissolved in this organic phase. This model predicts that the fraction of a compound that will dissolve in the available volume of water depends on the aqueous solubility of the compound, the atmospheric concentration of the rest water insoluble compounds and the *P* parameter. The *P* parameter is introduced here to include all sampling parameters and is proportional to the water volume available and inversely proportional to the sample volumetric flow rate, the fraction of the filter's surface used for the analysis and the sampling time. In general, high *P* parameter values lead to the extraction of less water soluble material.

In the other extreme, the independent compounds model was developed based on the assumption that the dissolution of a single compound is not affected by the presence of others. In this case, the corresponding fraction of a compound in the WSOC will depend on the solubility of the compound, its atmospheric concentration, and the *P* parameter. Based on ambient measurements of the chemical composition of WSOC as well as thermodynamic data based on both experimental and model findings we have concluded that the predictions of the ideal organic solution are closer to the truth for the atmospheric aerosol. A *P* parameter value of 0.1 cm^3 m^{-3} is proposed to be used for WSOC filter analysis, under typical atmospheric concentrations of organic aerosol in order to achieve the extraction of water soluble species (e.g., sugars, mono- and poly-acids, HULIS) and avoid the extraction of low solubility compounds (e.g., PAHs, alkanes). Higher values should be applied when measuring in high organic aerosol concentrations.

A system for the continuous measurement of WSOC has been developed and tested. The Steam Samper-TOC is based on the Steam-Jet Aerosol Collector and may also be

extended of the total organic aerosol measurement. The Steam Sampler-TOC uses steam produced in a heated tube to condense on the particles of the sampled air forming droplets. The liquid sample is driven by piston pumps to a TOC analyzer for the estimation of the WSOC concentration. The system in its current configuration collects PM_3 particles with a *P* parameter of 44 cm^3 m^{-3}. The Steam Sampler-TOC was evaluated by producing sucrose particles which were dried and driven to the Steam Sampler and an SMPS. The measurements showed a very good agreement, over a wide range of concentrations (R^2= 0.98). The instrument was also tested in a field site near Patras. An average 2.5 μg m^{-3} of water soluble organic aerosol concentration was estimated for the period of sampling. The water soluble organic mass measurements had poor correlation with the oxygenated organic aerosol and was in quite good agreement with the total organic aerosol concentration measured in PM_1. These findings were attributed to the different cut-off point of the different instruments and the high *P* parameter of the system. However, decreasing the *P* parameter is challenging because of the relatively large volume necessary for the TOC sample analysis.

The CCN activity of SOA particles from both anthropogenic and biogenic sources is investigated in the second part of the thesis. Biomass burning emissions are a major source of fine atmospheric particles on a global scale. Wood burning has been extensively used for domestic heating in many Greek cities over the last years. In Chapter 4 the findings of a one month campaign at the center of Athens during January of 2013 are presented. PM_1 particles were dominated by organics (58%) during the study. The biomass burning aerosol levels peaked during the night shortly before midnight. A smaller morning peak of hydrophobic OA observed in the morning was attributed to traffic.

The average critical supersaturation diurnal profile of particles with diameter of 80-100 nm was rather flat with an increase during the morning due to the hydrophobic traffic emissions. Smaller particles had larger variations of their critical supersaturation due to differences in their sources and chemical composition. An average hygroscopicity parameter κ was estimated for these particles. The average diurnal profile of κ had a minimum in the morning when traffic emissions dominated and was rather constant during the night when biomass burning emissions prevailed. The highest degree of chemical heterogeneity and the lowest activated fraction were observed during the morning rush hour. Hygroscopicity showed a weak correlation with the O:C ratio of the organics. The hygroscopicity parameter of organic particles was found to range from 0.06 to 0.21. During the night when biomass burning particles were dominant the average hygroscopicity parameter value was around 0.09.

The oxidation of volatile biogenic emissions is responsible for the formation of most of the atmospheric SOA on a global scale. Monoterpenes are some of the most important VOCs with α-pinene being the most dominant among them. This precursor can react with ozone and consequently with other oxidative agents in the atmosphere forming biogenic SOA. Ozonolysis and photochemical oxidation experiments by OH radicals of α-pinene were conducted in an environmental chamber and the results are presented in Chapter 5. Two types of experiments were conducted seeded and non-seeded. In the former ammonium sulfate particles were used as seeds. A volume of α-pinene was introduced into the chamber and then O_3 was added. After a couple of hours OH radicals were produced in the chamber by HONO photolysis. The CCN active fraction and the activation diameter of the particles remained constant during the ozonolysis and aging reactions. The hygroscopicity of pure SOA particles was estimated and was found not to change significantly during each experiment. An average hygroscopicity of 0.12±0.02

was estimated for either fresh or aged α-pinene SOA. The relationship of the hygroscopicity of the organic aerosol with the number of oxygen over the number of carbon atoms ratio was also investigated. The hygroscopicity of pure biogenic organic particles and the O:C ratio correlated well (R^2=0.53) and κ can be expressed as $\kappa=(0.29\pm0.005)\cdot(O:C)$. The water soluble fraction of the α-pinene SOA was measured using the Steam Sampler-TOC. The soluble fraction of the SOA after one hour of ozonolysis exceeded 0.9 and reached 1 within 2 hours after the initiation of ozonolysis. The photo-oxidation of the SOA with OH radicals did not affect the water soluble fraction of the SOA however the fraction was already close to unity at the time of HONO injections.

Table of Contents

List of Figures

List of Tables

Abbreviations

AMS: Aerosol Mass Spectrometer

BC: Black Carbon

BSOA: Biogenic Secondary Organic Aerosol

CCN: Cloud Condensation Nuclei

CCNC: Cloud Condensation Nuclei Counter

EC: Elemental Carbon

FULIS: Fulvic-like Substance

HOA: Hydrocarbon-like Organic Aerosol

HR-AMS: High Resolution Aerosol Mass Spectrometer

HULIS: Humic-like Substance

LVOA: Low Volatility Organic Aerosol

NO_x: NO + NO_2

OA: Organic Aerosol

OOA: Oxygenated Organic Aerosol

OC: Organic Carbon

PAH: Polycyclic Aromatic Hydrocarbon

PM: Particulate Matter

PMF: Positive Matrix Factorization

POA: Primary Organic Aerosol

RH: Relative Humidity

SMCA: Scanning Mobility CCN Analysis

SMPS: Scanning Mobility Particle Sizer

SOA: Secondary Organic Aerosol

VOC: Volatile Organic Compound

WIOC: Water Insoluble Organic Carbon

WIOA: Water-Insoluble Organic Aerosol

WSOC: Water Soluble Organic Carbon

WSOA: Water Soluble Organic Aerosol

WSOM: Water Soluble Organic Mass

Chapter 1

Introduction

1.1 Atmospheric aerosols

Atmospheric aerosols or particulate matter (PM) are suspended liquid or solid particles in the Earth's atmosphere. They are characterized by their size (diameter), mass, chemical composition, physical and chemical properties and play an important role in the physical and chemical processes occurring throughout the atmosphere.

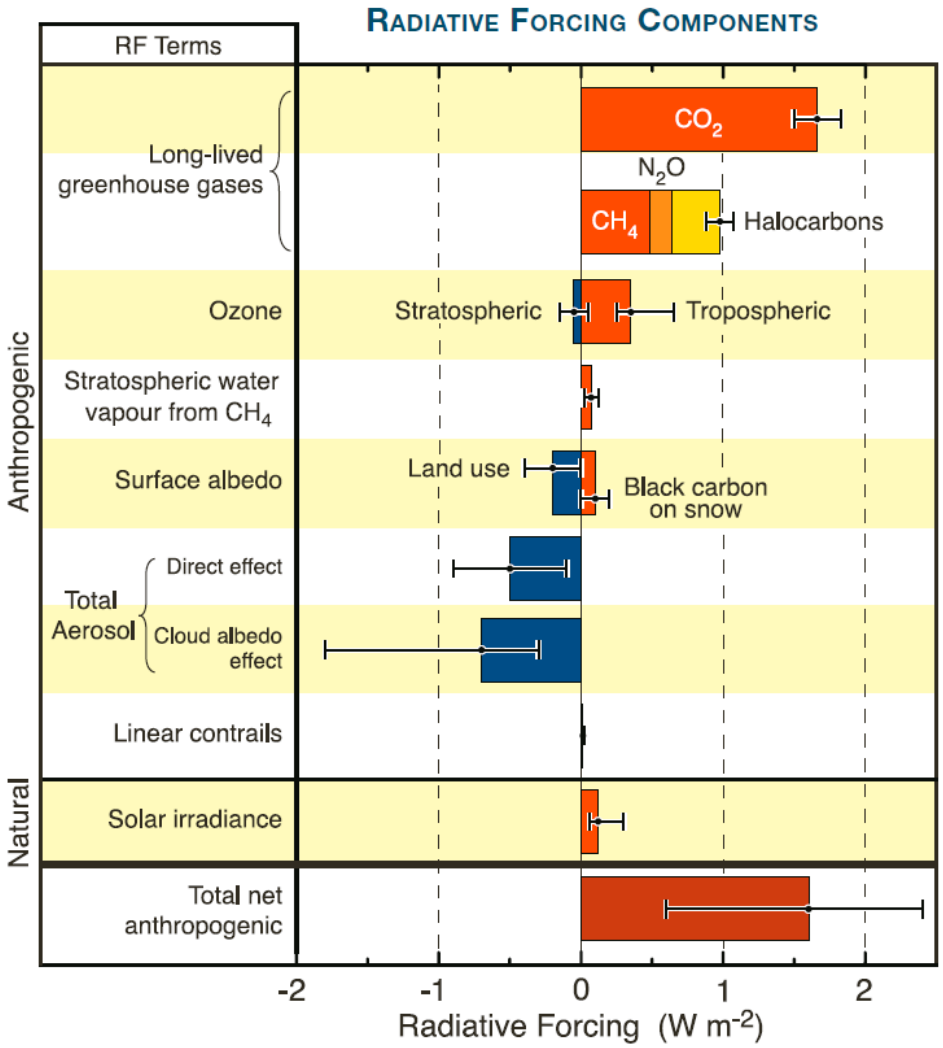

Figure 1.1: Principal components of the radiative forcing of our planet during the last 250 years. The error bars illustrate the range of uncertainty for each factor (IPCC, 2007). The radiative forcing of aerosols is the most uncertain.

For example, black carbon (BC), one of the components of atmospheric PM, has the ability to absorb light and consequently has a warming effect on climate (Hansen et al.,

2000). Particles composed of sulfates, organics, etc can scatter solar radiation, having a direct cooling effect on climate (Charlson et al., 1992).

In addition to their direct effect, the indirect effect of aerosols on climate is also important. Particles can serve as cloud condensation nuclei (CCN) on which water can condense and form cloud droplets. The size and the composition of the particles determine their ability to act as CCN. Thus, particles that consist of compounds with high water affinity are better CCN compared to particles with hydrophobic components. The impact of aerosols on climate forcing is still highly uncertain. Figure 1.1 illustrates the principal factors contributing to the total radiative forcing of the Earth's climate, including the greenhouse gases and the aerosol's direct and indirect effect (IPCC, 2007). The indirect effect presents the highest uncertainty among all components.

Atmospheric particles have adverse health effects. An extreme example is the severe smog event in London in 1952, which caused thousands of deaths in a few days (Brimblecombe, 1987). Fine particle levels have been found to correlate with increased mortality (Dockery et al, 1993). The adverse health effects are caused by both short and long term exposure to high PM concentrations, according to the World Health Organization (WHO) and are caused by the penetration of the particles to the thoracic region of the respiratory system. Globally, 3% of cardiopulmonary and 5% of lung cancer deaths are attributed to the atmospheric particles (WHO, 2013). An increase by 10 μg m^{-3} of $PM_{2.5}$ (atmospheric particulate matter of diameter less than 2.5 μm) of concentration leads to the increase of the long-term risk of cardiopulmonary mortality by 6-13%. These health effects, so far, appear to correlate mostly with fine particulate mass and not with individual components. However, many components of PM are known to

be toxic. For example, polycyclic aromatic hydrocarbons (PAHs) are known carcinogens, while diesel exhaust engine has been classified as carcinogenic by the International Agency for Research on Cancer. There is also evidence that combustion-related particle emissions are more dangerous, compared to other sources (WHO, 2013).

The diameter of atmospheric particles ranges from a few nanometers to tens of micrometers. A typical size distribution of atmospheric aerosols in an urban area is shown in Figure 1.2.

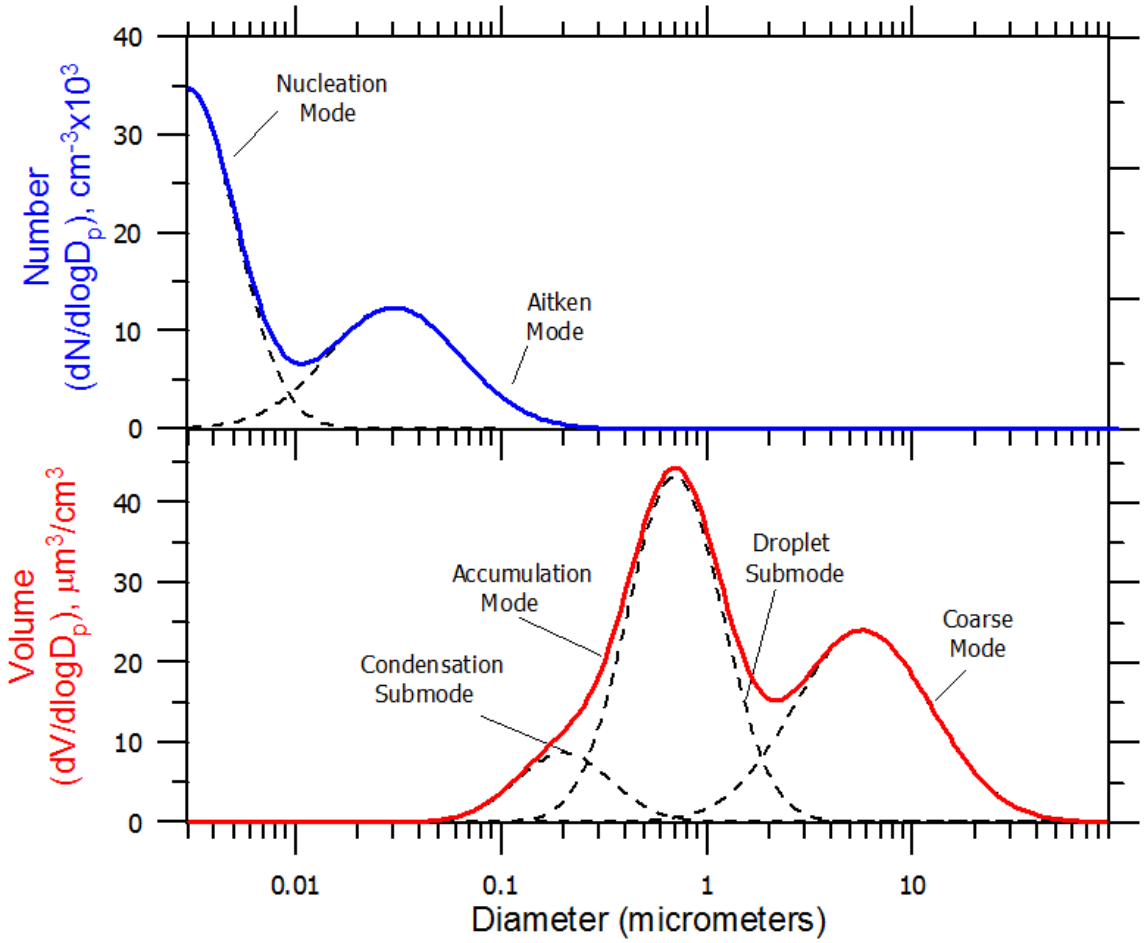

Figure 1.2: Typical number (upper) and volume (lower) distribution of atmospheric aerosols in an urban area (Seinfeld and Pandis, 1996).

Most of the particles (in number) are smaller than 100 nm. Two different modes are present in the number distribution, the nuclei mode, with particles less than 10 nm in

diameter and the Aitken mode, with diameters ranging from 10 to 100 nm. The ultrafine particles (diameter less than 100 nm) have though very small contribution to the total aerosol mass, due to their small sizes. Most of the aerosol mass is contributed by particles larger than 100 nm. The accumulation mode (Figure 1.2) spans diameters from 100 nm to 2.5 μm and accounts for a significant fraction of the aerosols mass concentration (Seinfeld and Pandis, 2006).

In general, atmospheric particles are classified in two major classes: "*fine*" and "*coarse*", where fine particles have diameters less than 2.5 μm in diameter and particles larger than 2.5 μm are considered as coarse. The two modes have different origin, chemical composition and optical properties, differ in their deposition patterns in the respiratory tract and are removed from the atmosphere by different mechanisms. The composition and size of atmospheric particles continuously changes due to reactions in the gas phase and subsequent condensation of low volatility products, evaporation, coagulation, etc. The chemical composition of atmospheric particles depends on the geographic area and on the corresponding sources. In general, aerosol particles emitted naturally by evaporation of water from sea spray, volcano eruptions, corrosion of materials (e.g., rocks, sand) belong to the coarse mode. Anthropogenic emissions are almost exclusively in the fine mode with fossil fuel combustion, wood burning, industrial emissions and transportation to be the most important sources.

Tropospheric aerosols contain sulfate, ammonium, nitrate, sodium, chloride ions, trace metals, carbonaceous material, crustal elements and water. The carbonaceous fraction consists of both organic and black (or elemental) carbon. Water is an abundant component of PM and dominates the chemical composition of aerosols at relative

humidity higher than 80% (Hanel, 1976). The absorption of water by aerosols affects their physical and chemical properties and strongly alters their interactions with solar radiation, affecting their climate forcing and visibility. Activation of particles in a supersaturated environment and transformation to cloud or fog droplets provides the reacting medium for heterogeneous reactions in the atmosphere and increases the size of particles (Seinfeld and Pandis, 1996; Khlystov et al., 2005).

1.2 Organic aerosols

Organic compounds are one of the most significant components of atmospheric PM, representing 20-90% of the total aerosol mass concentration. There are tens of thousands of different chemical species in atmospheric PM and only a small fraction of them have been identified and quantified (Kanakidou et al., 2005). Organic aerosols are either emitted directly in the atmosphere in the particulate phase and in this case are called primary organic aerosols (POA) or are formed in the atmosphere through gas-to-particle conversion processes (secondary OA or SOA). Atmospheric oxidants, such as O_3, OH and NO_3 react with organic vapors forming more oxygenated and less volatile species, which can then partition between the gas and the particle phases. Both biogenic and anthropogenic precursors can lead to the formation of secondary organic aerosols (SOA) with the biogenic volatile organic compounds (VOCs) being responsible for most of the SOA globally (Tsigaridis and Kanakidou, 2003).

In general, POA components are hydrophobic, with the exception of biomass burning emissions. SOA is in general more hygroscopic and water soluble, because oxidation reactions lead to the formation of oxygenated species. The extent of oxidation, the

hygroscopic properties and the aqueous solubility of the organic compounds reveal information about their sources, atmospheric processing, and age.

1.2.1 CCN properties of organic aerosols

Twenty years before or so the water uptake of the aerosols was attributed only to their inorganic components. Saxena et al. (1995) stressed the potential role of water-soluble organic species on the hygroscopic behavior of the particles. The Köhler theory which was developed in 1930s aimed at predicting the growth of a particle in an aqueous supersaturated environment (Seinfeld and Pandis, 1996; Raymond and Pandis, 2002). Köhler assumed that a particle is composed of a completely soluble salt, such as NaCl and $(NH_4)_2SO_4$ and combined the solute or Raoult effect (decrease of water vapor pressure because of the presence of the solute) with the curvature or Kelvin effect (increase of the vapor pressure due to the curvature of the droplet) to predict the CCN activation of the salts (Figure 1.3) by the balance between the two phenomena (Cruz and Pandis, 1997). The Köhler equation gives the equilibrium saturation S_{eq} as a function of the radius of the droplet formed. The Köhler equation is expressed as follows:

$$S_{eq} = \ln(RH) = \frac{2\sigma_W M_W}{RT\rho_W a} - \frac{3\nu m_s M_W}{4\pi M_s \rho_W a^3} \tag{1.1}$$

where S_{eq} is the equilibrium saturation, σ_w the solution surface tension, M_w and M_s the molecular weights of water and solute respectively, R the ideal gas constant, T is the temperature, ν the number of ions in which the solute dissociates, m_s the solute mass, ρ_w the water density and a is the radius of the droplet. Equation 1.1 expresses the equilibrium curve from which the critical saturation and the critical radius can be derived:

$$S_c = \sqrt{\frac{4A^3}{27B}} \tag{1.2}$$

$$a_c = \sqrt{\frac{3B}{A}} \tag{1.3}$$

The critical saturation, S_c, expresses the saturation above which a particle will activate, meaning that it will start absorbing water and grow to become a cloud droplet. The terms A and B are expressed as follows:

$$A = \frac{4M_W\sigma_W}{RT\rho_W} \tag{1.4}$$

$$B = \frac{6n_sM_W}{\pi\rho_W} \tag{1.5}$$

The radius a_c expresses the corresponding size limit, above which the particles can activate at saturation S_c. Particles that can activate at a given saturation are defined as CCN, for this saturation.

The water absorption by organics is highly uncertain. Laboratory and field measurements have suggested that organic species in mixed aerosols can both increase or decrease the water uptake of particles (Dick et al., 2000; Khlystov et al., 2005). Organic compounds can alter the particle hygroscopicity by lowering the surface tension or by gradual dissolution in the growing droplets, affecting the critical size. Other studies found that only a fraction of the measured CCN could be attributed to the inorganic species and that organic species can increase the water uptake of the particles as well (Saxena et al., 1995; Shulman et al., 1996; Raymond and Pandis, 2002).

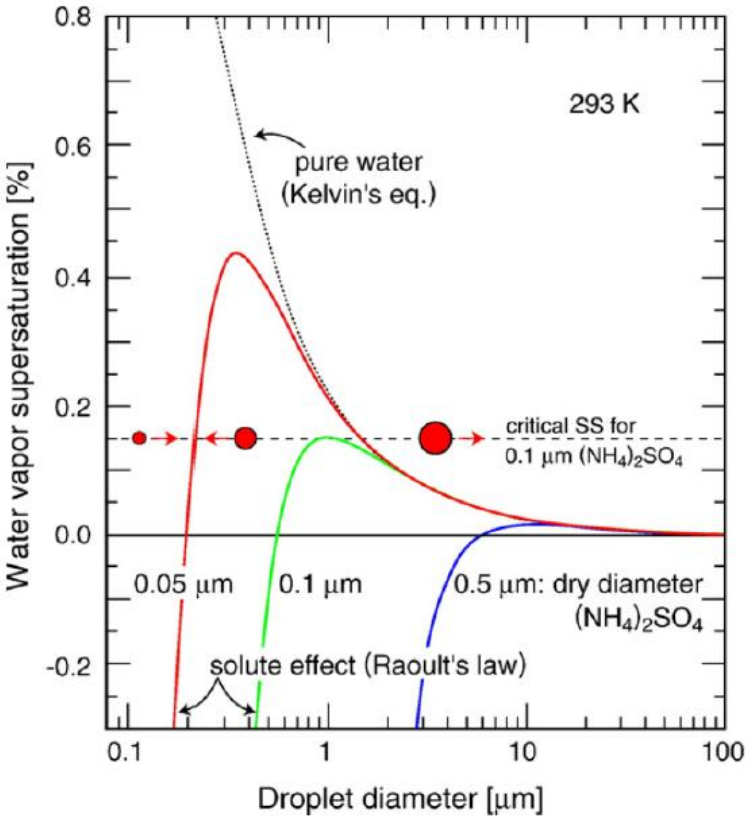

Figure 1.3: Köhler curves (droplet diameter versus the water vapor supersaturation) of pure water and different sized $(NH_4)_2SO_4$ particles (Andreae and Rosenfeld, 2008).

Organic compounds with high water affinity can have a hygroscopic behavior comparable with the inorganic compounds, contribute to the water uptake of atmospheric PM and consequently can act as CCN (Saxena et al., 1995; Ansari and Pandis, 2000; Cruz and Pandis, 2000; Dick et al., 2000).

The diameter of a particle strongly depends on its water content which is a function of the relative humidity and the chemical composition of the particle. The relationship between the size and composition of the particles and the relative humidity are required for climate predictions. In general, the increase of the mass fraction of the organic species keeping the particle size constant leads to a decrease of the hygroscopicity and the water uptake by the aerosols (Mochida et al., 2008). Since organics usually comprise

the dominant fraction of atmospheric PM, their water affinity is crucial for the overall hygroscopic and CCN behavior of the aerosol.

1.2.2 Water Soluble Organic Carbon (WSOC)

The water soluble organic species present in atmospheric aerosols are usually referred to as water soluble organic carbon (WSOC). The WSOC is an operationally defined quantity, since the dissolution of a compound in water depends not only on the solubility of the compound but on the amount of water or the concentration of the solution and other extraction parameters as well (Sullivan and Weber, 2006). While there is no direct method to estimate the levels of SOA, under certain conditions the oxygenated fraction is expected to be comprised almost entirely of secondary organic species although some fraction of the SOA may not be soluble (Zhang et al., 2005). WSOC measurements by the existing methods have often shown a strong correlation of WSOC and oxygenated organic aerosol (OOA) concentrations, revealing that the origin of WSOC is mostly secondary (Miyazaki et al., 2006; Kondo et al., 2007). In general, WSOC is expected to approximate the SOA, presenting similar seasonal and diurnal variations (Kang et al., 2004; Zhang et al., 2007). In the absence of biomass burning WSOC has been used as an indicator of SOA (Docherty et al., 2008).

Many identified components of WSOC, such as dicarboxylic acids or polyacids have been found to enhance the CCN activity of particles. Other compounds that have been found among the water soluble organic fraction are mono acids, sugars, humic-like substances (HULIS, high molecular weight heterogeneous organic species found in terrestrial and aquatic environments), alcohols, amines, phenols and polyconjugated species (Graber and Rudich, 2006; Mayol-Bracero et al., 2002; Facchini et al., 1999).

The methods for the measurement of WSOC can be divided in two major classes, off-line and on-line. The off-line measurement includes sample collection on the surface of a quartz-fiber filter which is afterwards immersed in a volume of water in order to extract the water soluble species. A sonicator bath or mechanical shaking (shaker baths or hand-shaking) are often applied in order to promote the extraction. However, uncertainties concerning the effect of such procedures combined with the fact that there is no protocol or standard volume of water used in such extractions, can lead to differences in the measured water soluble fraction. Furthermore, evaporation of semivolatile species and contamination of the sample during the filter preparation or during the analysis and absorption of organic species by the quartz filter media may induce errors in the measured WSOC.

The on-line methods of the WSOC measurement present many advantages compared to the off-line, filter based sampling of WSOC. They offer much higher resolution, which from 24 hours (typical) decreases to a few minutes, allowing for the better understanding of diurnal variations and of the sensitivity to sources. The positive and negative sampling artifacts involved in the off line sampling are also avoided.

In this work, we have developed a novel instrumentation for the continuous measurement of WSOC. The Steam Sampler is based on the Steam-Jet-Aerosol Collector which has been used for the continuous monitoring of the concentration of the main soluble inorganic species present in the aerosols. A full description of this instrument is given in Chapter 2.

1.3 Motivation and objectives of this thesis

Water is the single most important component of atmospheric aerosols and as a result its interactions with the major pollutants are extremely important for both climate change and air quality. The water affinity and hygroscopic properties of organic aerosols are highly uncertain. While the hygroscopic properties of inorganic PM are well characterized, organics behavior can range from hydrophobic to quite hydrophilic. The range of solubilities of organics covers several orders of magnitude (Psichoudaki and Pandis, 2013). The main goal of this work is to improve our understanding of the hygroscopic properties of atmospheric particles of different types and sources.

While the term WSOC has been used for almost 20 years, it has only been operationally defined. One of the objectives of this work is to define the WSOC by taking into account its chemical composition and the solubility of contributing species. This work examines the measurement methods of the WSOC and based on the thermodynamic behavior of the particles and WSOC measurements a new definition of the WSOC is proposed. The definition is in terms of water solubility rather than in terms of extraction parameters. A new parameter *P* is proposed to describe the currently used techniques.

Even if the correct *P* parameter is applied for the measurement of WSOC, sampling artifacts like gas-adsorption by the filter media or evaporation of volatile species and low time-resolution sampling will still interfere. The second objective was thus to develop and evaluate a simple and cost effective system for the continuous monitoring of atmospheric WSOC.

In the last part of this work the hygroscopic properties of particles emitted by different sources were quantified. The financial crisis in Greece has created atmospheric pollution problems in many cities due to the use of fireplaces. The hygroscopic properties of urban aerosols, measured during winter in the center of the capital of Greece, Athens, during winter were characterized. The approach adopted included combination of the CCN-activation measurements with detailed chemical composition measurements by an Aerosol Mass Spectrometer. The results of this work are presented in Chapter 4.

Biogenic VOCs are the most important organic aerosol precursors on a global scale. The CCN behavior and the water soluble fraction of SOA from the ozonolysis and further oxidation with OH radicals of the most important monoterpene, α-pinene was therefore investigated.

1.4 References

Andreae, M.O., Rosenfeld, D. Aerosol-cloud-precipitation interactions. *Earth-Science Reviews, **2008***, 89(1-2):13-41.

Ansari, A.S., Pandis, S.N. Water absorption by secondary organic aerosol and its effect on inorganic aerosol behavior. *Environ. Sci. Technol.*, **2000**, 34, 71-77.

Brimblecombe, P. The big smoke – A history of air pollution in London since Medieval times. London, Methuen & Co. Ltd, **1987**.

Cerully, K.M., Raatikainen, T., Lance, S., Tkacik, D., Tiitta, P., Petaja, T., Ehn, M., Kulmala, M., Worsnop, D.R., Laakosonen, A., Smith, J.N., Nenes, A. Aerosol hygroscopicity and CCN activation kinetics in a boreal forest environment during the 2007 EUCAARI campaign. *Atmos. Chem. Phys*., **2011**, 11, 12369-12386.

Charlson, R.J., Schwartz, S.E., Hales, J.M., Cess, R.D., Coakley, J.A., Hansen, J.E., Hofmann, D.J. Climate forcing by anthropogenic aerosols. *Science*, **1992**, 255 (5043), 423-430.

Cruz, C.E., Pandis, S.N. A study of the ability of pure secondary organic aerosol to act as cloud condensation nuclei. *Atmos. Environ.*, **1997**, 31, No 15, 2205-2214.

Cruz, C.E., Pandis, S.N. Deliquescence and hygroscopic growth of mixed inorganic-organic atmospheric aerosol. *Environ. Sci. Technol.*, **2000**, 34, 4313-4319.

Dick, W.D., Saxena, P., McMurry, P.H. Estimation of water uptake by organic compounds measured during the southeastern aerosol and visibility study. J. Gepohys. Res., **2000**, 105, 1471-1479.

Docherty, K.S., Stone, E.A., Ulbrich, I.M., DeCarlo, P.F., Snyder, D.C., Schauer, J.J., Peltier, R.E., Weber, R.J., Murphy, S.M., Seinfeld, J.H., Eatough, D.J., Grover, B.D., Jimenez, J.L. Apportionment of primary and secondary organic aerosols in Southern

California during the 2005 study of organic aerosols in riverside (SOAR). *Environ. Sci. Technol.* **2008**, *42*, 7655-7662.

Dockery, D.W., Pope, C.A., Xu, X.P., Spengler, J.D., Ware, J.H., Fay, M.E., Ferris, B.G., Speizer, F.E. An association between air pollution and mortality in 6 United States cities. *New England Journal of Medicine*, **1993**, 329 (24), 1753-1759.

Facchini, M.C., Fuzzi, S., Zappoli, S., Andracchio, A., Gelencér, A., Kiss, G., Krivácsy, Z., Mészáros, E., Hanson, H.C., Alsberg, T., Zebühr, Y. Partitioning of the organic aerosol component between fog droplets and interstitial air. *J. Geophys. Res.* **1999**, *104*, No D21, 26,821-26,832.

Graber, E.R., Rudich, Y. Atmospheric HULIS: How humic-like are they? A comprehensive and critical review. *Atmos. Chem. Phys.* **2006**, 6, 729-753.

Hanel, G. The properties of atmospheric aerosol particles as functions of relative humidity and thermodynamic equilibrium with surrounding moist air. *In Advances in Geophys.*,**1976**, Vol 19. Academic Press, New York, 73-188.

Hansen, J., Sato, M., Ruedy, R., Lacis, A., Oinas, V. Global warming in the twenty-first century: An alternative scenario. *Proceedings of the National Academy of Sciences of the United States of America*, **2000**, 97, (18), 9875-9880.

IPCC, 2007: Summary for policymakers. Intergovernmental Panel on Climate Change **2007**: The physical science basis. Contribution of working group I to the fourth assessment report of the intergovernmental panel on climate change [Solomon, S., Qin, D., Manning, Z., Chen, M., Marquis, M., Averyt, K.B., Tignor, M., Miller, H.L.]. Cambridge University Press, NY, USA.

Kanakidou, M., Seinfeld, J.H., Pandis, S.N., Barnes, I., Dentenerm F.J., Facchini, M.C., Van Dingenen, R., Ervens, B, Nenes, A., Nielsen, C.J., Swietlicki, E., Putaud, J.P., Balkanski, Y., Fuzzi, S., Horth, J., Moortgat, G.K., Winterhalter, R., Myhre, C.E.L.,

Tsigaridis, K., Vignati, E., Stefanou, E.G., Wilson, J. Organic aerosol and global climate modelling: A review. *Atmos. Chem. Phys.*, **2005**, 5, 1053-1123.

Kang, E., Toohey, D.W., Brune, W.H. Dependence of SOA oxidation on organic aerosol mass concentration and OH exposure: experimental PAM chamber studies. *Atmos. Chem. Phys.* **2011**, *11*, 1837-1852.

Khlystov, A., Stanier, C.O., Takahama, S., Pandis, S.N. Water content of ambient aerosol during the Pittsburgh Air Quality Study. *J. Geophys. Res.*, **2005**, Vol 110, D07S10.

Mayol-Bracero, O.L., Guyon, P., Graham, B., Roberts, G., Andreae, M.O., Decesari, S., Facchini, M.C., Fuzzi, S., Artaxo, P. Water-soluble organic compounds in biomass burning aerosols over Amazonia 2. Apportionment of the chemical composition and importance of the polyacidic fraction. *J. Geophys. Res.* **2002**, *107*, No D20, 8091.

Miyazaki, Y., Kondo, Y., Takegawa, N., Komazaki, Y., Fukuda, M., Kawamura, K., Mochida, M., Okozawa, K., Weber, R.J. Time-resolved measurements of water-soluble organic carbon in Tokyo. *J. Geophys. Res.* **2006**, *111*, D23206, doi:10.1029/2006JD007125.

Mochida, M., Kuwata, M., Miyakawa, T., Takegawa, N., Kawamura, K., and Kondo, Y.: Relationship between hygroscopicity and cloud condensation nuclei activity for urban aerosols in Tokyo, *J. Geophys. Res.*, **2006**, 111, D23 204.

Petters, M.D., Kreidenweis, S.M. A single parameter representation of hygroscopic growth and cloud condensation nucleus activity. *Atmos. Chem. Phys.*, **2007**, 7, 1961-1971.

Psichoudaki, M., Pandis, S.N. Atmospheric aerosol water-soluble organic carbon measurement: A theoretical analysis. *Environ. Sci. Technol.*, **2013**, 47, 9791-9798.

Raymond, T.M., Pandis, S.N. Cloud condensation of single-component organic aerosol particles. *J. Geophys. Res.*, **2002**, 107, NO. D24, 4787, doi:10.1029/2002JD002159.

Saxena, P., Hildemann, L.M., McMurry, P.H., Seinfeld, J.H. Organics alter hydroscopic behavior of atmospheric particles. *J. Geophys. Res.* **1995**, *100*, 18,755-18,770.

Seinfeld, J.H., Pandis, S.N. Atmospheric chemistry and physics: From air pollution to climate change. 2nd edition. Wiley, New York, **2006**.

Shulman, M.L., Jacobson, M.C., Charlson, R.J., Synovec, R.E., Young, T.E. Dissolution behavior and surface tension effects of organic compounds in nucleating cloud droplets. *Geophys. Res. Lett.* **1996**, *23*, 277-280.

Sullivan, A.P., Weber, R.J.,. Chemical characterization of the ambient organic aerosol soluble in water: 1. Isolation of hydrophobic and hydrophilic fractions with a XAD-8 resin. *J. Geophys. Res.*, **2006**, 111, D05314.

Tsigaridis, K., Kanakidou, M. Global modeling of secondary organic aerosol in the troposphere: a sensitivity analysis. *Atmospheric Chemistry and Physics*, **2003,** *3*, 1849-1869.

World Health Organization, Regional Office for Europe. Health effects of particulate matter. Policy implications for countries in Eastern Europe, Caucasus and central Asia. WHO, **2013**.

Zhang, Q., Alfarra, M.R., Worsnop, D.R., Allan, J.D., Coe, H., Canagaratna, M.R., Jimenez, J.L. Deconvolution and quantification oh hydrocarbon-like and oxygenated organic aerosols based on the aerosol mass spectrometry. *Environ. Sci. Technol.*, **2005**, 39, (13), 4938-4952.

Zhang, Q., Jimenez, L., Canagaratna, M.R., Allan, J.D., Coe, H., Ulbrich, I., Alfarra, M.R., Takami, A., Middlebrook, A.M., Sun, Y.L., Dzepina, K., Dunlea, E., Docherty, K., DeCarlo, P.F., Salcedo, D., Onasch, T., Jayne, J.T., Miyoshi, T., Shimono, A.,

Hatakeyama, S., Takegawa, N., Kondo, Y., Schneider, J., Drewnick, F., Borrmann, S., Weimer, S., Demerjian, K., Williams, P., Bower, K., Bahreini, R., Cottrell, L., Griffin, R.J., Rautiainen, J., Sun, J.Y., Zhang, Y.M., Worsnop, D.R. Ubiquity and dominance of oxygenated species in organic aerosols on anthropogenically-influenced Northern Hemisphere midlatitudes. *Geophys. Res, Lett.* **2007**, *34*, L13801, doi:10.1029/2007GL029979.

Chapter 2

Atmospheric Aerosol Water Soluble Organic Carbon Measurement: A Theoretical Analysis

2.1 Introduction

Organic particulate matter represents one of the least understood components of atmospheric aerosols, although it typically represents more than half of the fine (less than 1 μm) particle mass (Facchini et al., 1999; Kanakidou et al., 2005; Sullivan et al., 2006). Organic aerosol emissions result from a wide range of both natural and anthropogenic sources, such as biomass burning, combustion of fossil fuels, industrial emissions, meat cooking operations, cigarette smoking and biogenic emissions (Schauer et al., 1996; Jacobson et al., 2000; Donahue et al., 2009). Organic compounds can either be emitted in the gas or the particulate phase. If the saturation concentration of a compound is low enough, most of it remains in the particulate phase in ambient conditions and is regarded as Primary Organic Aerosol (POA). On the other hand, organic compounds with high saturation concentrations remain entirely in the gas phase, where some of them can be oxidized to form species with lower volatility that can condense and form secondary organic aerosol (SOA). Semivolatile species move from phase to phase but also get oxidized forming more polar products (Donahue et al., 2009).

In general, SOA constituents are more water soluble compared to their precursors and POA components (Kondo et al., 2007; Kang et al., 2011). Thus, an indicator of whether organic aerosol is primary or secondary is its water soluble fraction. The Water Soluble Organic Carbon (WSOC) is considered to be a major fraction of the SOA, presenting similar seasonal and diurnal variations (Sullivan et al., 2006; Kondo et al., 2007; Zhang et al., 2007; Miyazaki et al., 2006). Some WSOC components are emitted as primary particles, especially during biomass combustion, and others are produced as a result of reactions in the gas and aqueous phases (Miyazaki et al., 2006; Sullivan et al., 2006;

Kondo et al., 2007). WSOC has been used as a tracer for secondary organic aerosol (SOA) in the absence of biomass burning (Docherty et al., 2008). WSOC concentrations measured by a Particle-Into-Liquid Sampler (PILS) have been strongly correlated with oxygenated organic aerosol (OOA) concentrations estimated from aerosol mass spectrometry (Kondo et al., 2007). OOA is considered to be water soluble or partially water soluble and is also regarded as a good approximation of SOA (Miyazaki et al., 2006; Kondo et al., 2007).

Until the early 90s the water uptake of atmospheric particles was attributed solely to inorganic species. Saxena et al. (1995) stressed the importance of water soluble compounds in atmospheric particles and found that organic species can significantly alter the hygroscopic behavior of particles. Saxena and Hildemann (1996) proposed a list of compounds that can contribute to the water soluble fraction of the aerosols. At that time, an effort to quantify the fraction of WSOC in atmospheric samples began, with Facchini et al. (1999) publishing some of the first WSOC measurements in fog and interstitial air. The aerosol samples were collected on pre-fired quartz filters and the carbon content measurement was carried out by a Total Organic Carbon (TOC) analyzer. Their findings revealed increased concentration of water soluble polar compounds in the fog samples, compared with the interstitial air. Since then, numerous semiempirical approaches have been used for the WSOC measurement, mainly based on quartz filter sampling by a high or low volume sampler followed by TOC analysis, varying the volume of water used for the compounds' extraction, duration and technique of extraction.

The water soluble organic fraction of aerosols is likely to be composed of compounds containing mostly oxygenated groups such as -COOH, -COH, -C=O, -COC-, -CNO_2, $CONO_2$, and -CNH_2 (Sullivan et al., 2004). Although identified species account for a small fraction of the measured WSOC, aliphatic dicarboxylic acids, sugars, aliphatic alcohols, aliphatic and aromatic carboxylic acids, polyacids, aldheydes, and ketones are expected to dominate the water soluble fraction (Facchini et al., 1999; Mayol-Bracero et al., 2002).

WSOC can account for 40 to 80% of the total organic carbon, depending on the location and season ((Sullivan et al., 2004; Anderson et al., 2008). WSOC is of major importance, due to its ability to influence the interactions of aerosols with water and thus alter the hydroscopicity of atmospheric particles and their ability to act as cloud condensation nuclei (Saxena et al., 1995). Water-soluble organic compounds in aerosols can be quite hygroscopic and organic particles therefore can act as CCN (Cruz and Pandis, 1997). Shulman et al. (1996) have proposed that slightly soluble organic compounds affect cloud droplet growth by two mechanisms: gradual dissolution in the growing droplets which affects the critical size, and lowering of surface tension which decreases critical supersaturation.

WSOC is generally operationally defined, since a variety of different off-line methods have been developed for its measurement. Given the wide range of solubilities and ambient concentrations of the organic compounds along with the variability of the volume of water available for their extraction, different results by different methods are expected. Research has revealed discrepancies between WSOC concentrations measured by different techniques, which were attributed to sampling artefacts, differences in

solution concentrations and incomplete extraction (Sullivan et al., 2004). It is not clear whether the details of the extraction methods affect the result of the analysis for the determination of WSOC, what is the solubility range of the compounds extracted by the common extraction methods and therefore what chemical species are expected to be measured by these methods. The goal of this work is to develop a theoretical framework for the interpretation of WSOC measurements. The implications of this work for the optimization of WSOC measurement methods are also discussed.

2.2 Off-line WSOC measurement

A typical off-line WSOC sampling technique includes sample collection on pre-combusted quartz fiber filters followed by extraction, filtration and analysis. An amount of water is used for the extraction of the filter and afterwards the liquid sample is filtered through a 0.2 or 0.45 μm pore size filter to remove suspended insoluble particles and filter debris (Facchini et al., 1999; Huang et al., 2006; Hagler et al., 2007; Duval et al., 2008; Viana et al., 2006; Saarikoski et al., 2007). Filter samples are collected by either low or high-volume air samplers. Sampling is usually carried out for 24 h, but the sampling time can range from a few hours to several days. The duration of the extraction can range from 5 minutes even to 36 hours and soaking, sonication and hand-shaking is usually applied to promote the extraction (Facchini et al., 1999; Viana et al., 2006; Saarikoski et al., 2007; Huang et al., 2006; Hagler et al., 2007; Duval et al., 2008). In most cases, part of the filter is used for the WSOC analysis and the rest of the filter is used for the measurement of the concentration of other compounds or repetitions.

2.2.1 Ideal Organic Solution Model

Let us assume first that the organic species in the aerosol particles form a single ideal organic solution. In this case, each organic compound is assumed to be dissolved in the organic phase of the particle. If we define as $m_A(aq)$ the mass of compound A from a sample that will be dissolved in the water in the WSOC measurement, V_w the volume of water used for the extraction of the filter, the aqueous concentration of A assuming phase equilibrium will satisfy:

$$\frac{m_A(aq)}{V_W} = x_A S_A \tag{2.1}$$

where x_A is the mole fraction of A in the organic phase and S_A its saturation concentration in the aqueous phase.

Some of the other organic compounds of the aerosol will also dissolve in water. If m_{OA} is the total mass of all the organic compounds collected on the filter and f_{WSOC} is the fraction of the water soluble compounds, the mass of the organics that will remain in the organic phase of the aerosol will be equal to $m_{OA}(1-f_{WSOC})$. If $m_A(org)$ is the mass of compound A that will remain dissolved in the organic phase, M_A its molecular weight and M_{OA} the average molecular weight of the compounds that remain in the organic phase then (1) becomes:

$$\frac{m_A(aq)}{V_W} = \frac{\frac{m_A(org)}{M_A}}{\frac{m_A(org)}{M_A} + \frac{m_{OA}(1-f_{WSOC})}{M_{OA}}} S_A \tag{2.2}$$

Assuming for simplicity that $M_A \approx M_{OA}$:

$$\frac{m_A(aq)}{V_W} = \frac{m_A(org)}{m_A(org) + m_{OA}(1-f_{WSOC})} S_A \tag{2.3}$$

To further simplify the problem, the mass of a single compound in the organic solution is assumed to be significantly lower than the mass of the organic phase ($m_A(org) << m_{OA}(1-f_{WSOC})$), resulting in:

$$\frac{m_A(aq)}{V_W} = \frac{m_A(org)}{m_{OA}(1-f_{WSOC})} S_A \quad (2.4)$$

The total mass of the compound A, $m_A(tot)$ in both aqueous and organic phases is:

$$m_A(tot) = m_A(org) + m_A(aq) \quad (2.5)$$

Combining (4) and (5):

$$m_A(tot) = m_A(aq)\left(\frac{V_W S_A + m_{OA}(1-f_{WSOC})}{V_W S_A}\right) \quad (2.6)$$

The fraction, f_A, of the compound A that will dissolve in water, is:

$$f_A = \frac{m_A(aq)}{m_A(tot)} \quad (2.7)$$

Combining equations (6) and (7):

$$f_A = \frac{V_W S_A}{V_W S_A + m_{OA}(1-f_{WSOC})} \quad (2.8)$$

If Q is the air sampling flow rate, Δt is the total sampling time, and f the fraction of the filter analyzed, f_A can be expressed in terms of atmospheric concentrations, by dividing by $Q \cdot f \cdot \Delta t$:

$$f_A = \frac{\frac{V_W S_A}{Qf\Delta t}}{\frac{V_W S_A}{Qf\Delta t} + C_{OA}(1 - f_{WSOC})} \quad (2.9)$$

Defining parameter *P* as:

$$P = \frac{V_W}{Q \cdot f \cdot \Delta t} \quad (2.10)$$

The fraction f_A of the compound A extracted in the WSOC, will be:

$$f_A = \frac{S_A P}{S_A P + C_{OA}(1 - f_{WSOC})} \quad (2.11)$$

The *P* parameter is expressed in volume of water per volume of air (cm^3 m^{-3}) and includes information about the sampling and the WSOC analysis. It practically represents the availability of water for the extraction of the soluble organic compounds of aerosols of the sampled volume of air. Table 1 summarizes the values of *P* for different WSOC measurement approaches in the literature. *P* usually ranges from 0.01 to 1 cm^3 m^{-3} and in many cases is around 0.1 cm^3 m^{-3}. Only in a few cases *P* exceeds significantly 1 cm^3 m^{-3}. Higher *P* values will lead to the extraction of more compounds and/or higher fractions of WSOC. According to Equation (11), the fraction of compound A, that will be measured as WSOC, is practically independent of its concentration in the particulate phase. It depends though on the total concentration of the other organic compounds not dissolved in the water during the extraction, the solubility of the compound and the *P* parameter.

The impact of the *P* parameter on the results of such WSOC analysis is presented in Figure 1. The fraction of a compound that will be included in the WSOC is calculated

for high, medium, and low *P* values. A high *P* parameter value of 1 cm^3 m^{-3} allows the total extraction (more than 90% of a compound's mass) of organic species with solubility exceeding 10^{-2} g L^{-1}, for typical ambient water insoluble organic aerosol (WIOA) concentrations of 1 to 10 μg m^{-3}.

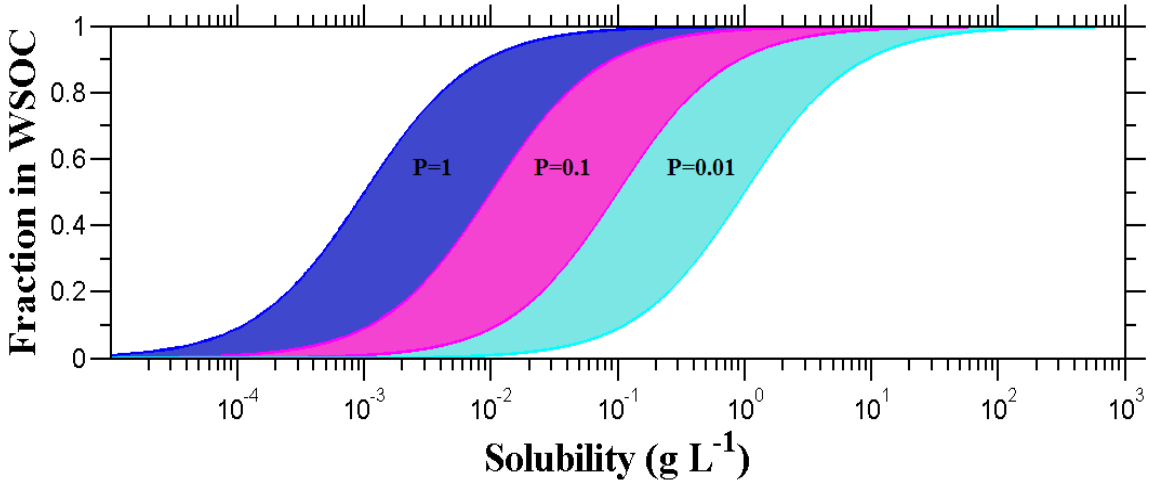

Figure 2.1: Fraction of a compound that will be extracted in the WSOC, according to the ideal organic solution model, for three different values of the *P* parameter: 1 (blue), 0.1 (magenta) and 0.01 cm^3 m^{-3} (cyan). The shown range for each P corresponds to water insoluble organic mass concentration of 1 (left side) to 10 μg m^{-3} (right side of each shaded area).

Species start contributing partially to the WSOC (more than 10% of their mass) when their solubility exceeds 10^{-4} g L^{-1}. Lower values of *P* lead to the extraction of fewer compounds and/or lower fraction of their mass. The corresponding solubility thresholds for total extraction, for the intermediate (0.1 cm^3 m^{-3}) and low (0.01 cm^3 m^{-3}) *P* values are approximately 0.1 and 1 g L^{-1} respectively. It is clear from Figure 1 that a change of *P* by a factor of 10 can alter the contributing species solubility limit by 10. Also a change by an order of magnitude on the insoluble organic aerosol concentration will

have the same impact on the contributing solubility range. On the other hand, such a change will not have the same effect on the fraction f_A of a specific compound.

Table 1: *P* parameter calculated for various sampling and extraction methods based on the fraction of the filter used, *f*, the sampler's flow rate, *Q*, the sampling time, Δ*t*, and the volume of water used for the extraction, V_w.

Study	*f*	*Q* (m^3 min^{-1})	Δ*t* (h)	V_w (cm^3)	P parameter (cm^3 m^{-3})
Duarte et al. (2007)	1	1.13	168	150	0.01
Murásky et al. (2011)	0.25	0.5	96	20	0.03
Sullivan et al. (2011)	0.095	1.13	72	20	0.04
Huang et al. (2006)	0.75	0.03	72	5	0.05
Huang et al. (2006)	0.75	0.03	48	5	0.08
Wang et al. (2005)	0.027	1.1	24	4	0.09
Kumagai et al. (2012)	0.25	0.03	336	15	0.11
Wang et al. (2005)	0.027	1.1	24	5	0.12
Decesari et al. (2001)	0.5	0.05	24	6	0.17
Li et al. (2012)	0.034	1.13	24	10	0.18
Urban et al. (2012)	0.008	1.14	48	4.5	0.18
Yang et al. (2005)	0.056	1.11	12	10	0.22
Ram and Sarin (2011)	0.25	1.1	13	50	0.23
Ram and Sarin 2011)	0.25	1.1	11	50	0.28
Feng et al. (2006)	0.011	1.13	24	5	0.28
Rengarajan et al. (2012)	0.25	1.1	10	50	0.3
Hagler et al. (2007)	0.407	0.02	80	10	0.31
Kudo et al. (2012)	0.25	0.04	23	5	0.36
Pathak et al. (2011)	1	0.02	24	10	0.42
Viana, et al. (2006)	0.008	0.5	24	5	0.82
Kudo et al. (2012)	0.25	0.02	23	5	0.87
Salma et al. (2007)	0.024	0.31	12	5	0.92
Wozniak et al. (2012)	0.082	1.7	24	200	0.99
Zhang et al. (2012)	1	0.02	24	30	1.25
Urban et al. (2012)	0.008	1.14	6.5	4.5	1.3
Ruellan and Cachier (2001)	1	0.04	3	10	1.33
Prieto-Blanco et al. (2010)	0.125	0.04	24	10	1.45
Duvall et al. (2008)	0.38	0.02	23	16	1.83
Wozniak et al. (2012)	0.082	0.8	24	200	2.1
Saarikoski et al. (2007)	0.058	0.024	72	15	2.46
Cheng et al. (2011)	1	0.007	24	40	4.15
Mandalakis et al. (2011)	0.003	0.5	24	10	4.65
Park et al. (2012)	1	0.017	6	40	6.65
Saarikoski et al. 2007)	0.058	0.024	24	15	7.38
Ruellan and Cachier (2001)	1	0.04	0.5	10	8

Regarding for example, a compound with a solubility of 10^{-2} g L^{-1}, by increasing the concentration of WIOA from 1 to 10 μg m^{-3}, its fraction will decrease from almost 60% to 10%. For WIOA=1μg m^{-3}, a change of *P* from 0.1 to 1 cm^3 m^{-3} will increase the contribution of the compound from 60% to 90%.

Figure 2.2 presents the aqueous solubility range of various chemical groups of organic species that can be found in atmospheric aerosols.

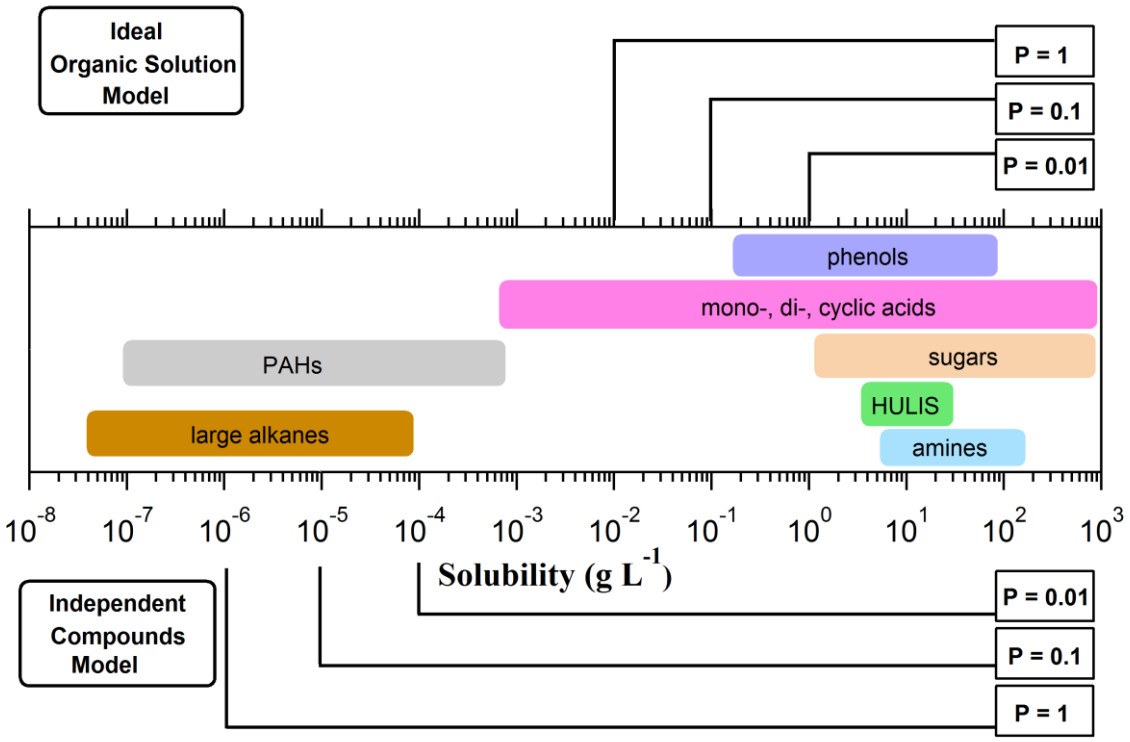

Figure 2.2: Solubility ranges of various organic compound classes found in atmospheric aerosols and predicted solubility range for full extraction of a compound by the ideal organic solution model and independent compounds model, for different *P* parameter values. The lines above and below indicate the solubility limit above which all species are fully extracted for typical organic aerosol concentrations.

When the *P* parameter of the method applied is 1 cm^3 m^{-3}, sugars, acids, alcohols, phenols, humic and fulvic-like substances (HULIS and FULIS respectively), amines,

and other highly water soluble compounds, such as poly-conjugated species, will be included in the measured WSOC. Some polycyclic aromatic compounds such as pyrene and fluoranthene will also contribute partially to the WSOC. Extraction methods with *P* values close to 0.1 cm^3 m^{-3} include in the WSOC all the above soluble species but cannot extract any PAHs. Low *P* value methods which use low volumes of water for the extraction of large areas of probably "over-loaded' filters, tend to exclude organic species from the WSOC.

In the case of *P* equal to 0.01 cm^3 m^{-3}, sugars, HULIS and amines will be included in the WSOC, while some other highly water soluble species, like specific acids (e.g. succinic or suberic acid) and phenols, will only partially contribute to the WSOC. These results are based on no assumptions on kinetics limitations or matrix effect, regarding the dilution of the less soluble compounds. Kinetics limitations have been observed in soil systems, however it is not known how similar this system can be compared with the aerosols (Cornelissen et al., 1998).

Without the assumption that the average molecular weight of the WSOC compounds is not equal to the average organic compounds' molecular weight, and an equation between these two is: $M_A=\alpha M_{OA}$, then equation 11 is transformed:

$$f_A = \frac{S_A P}{S_A P + \alpha C_{OA}(1 - f_{WSOC})} \quad (12)$$

The predictions of the model can be different in some cases, e.g. when the compound A is HULIS, which have been found to have molecular weights between 40-500 more or less (Graber and Rudich, 2006). In this case, the α factor can reach 10 and the

corresponding fraction f_A will be affected as if the *P* parameter or the solubility would decrease by one order of magnitude.

If the mass of compound A is not significantly lower than the total mass of the rest of the organic species in the remaining organic solution, the result is a quadratic algebraic equation. The mass of the compound A in the aqueous phase is thus given by:

$$m_A(aq) = \frac{1}{2}\left\{ m_A(tot) + V_W S + m_{OA}\left(1 - f_{WSOC}\right) - \left[\left(m_A(tot) + V_W S + m_{OA}(1 - f_{WSOC}) \right)^2 - 4 m_A(tot) V_W S \right]^{1/2} \right\} \quad (13)$$

The fraction of the compound that will be extracted in the WSOC can be obtained by dividing by $m_A(tot)$:

$$f_A = \frac{m_A(tot) + V_W S + m_{OA}(1 - f_{WSOC}) - \left[\left(m_A(tot) + V_W S + m_{OA}(1 - f_{WSOC}) \right)^2 - 4 m_A(tot) V_W S \right]^{1/2}}{2 m_A(tot)} \quad (14)$$

The fraction of the compound A that will be part of the WSOC in this case depends on its ambient concentration as well.

For typical aerosol concentrations, we can now classify organic species into three categories, based on the extent of their contribution (or lack of) to the WSOC.

Class I: Regardless of the sampling and extraction method and WIOA ambient concentration, compounds the solubility of which exceeds 10 g L^{-1} will be measured (more than 90% of their mass) as WSOC. Sugars, many phenols, alcohols, amines, acids and part of HULIS are members of this class.

Class II: Depending on the *P* parameter and on the concentration of the WIOA, species which fall within the solubility range between 10^{-4} and 10 g L^{-1}, will be at least partially included in the WSOC. The extent of the contribution of the members of this class depends on their solubility, the total ambient concentration of the insoluble organic species and the *P* parameter. Some phenols, acids (with more than 6-8 carbon atoms), aromatic species and part of HULIS fall within this class. If the concentrations of these intermediate solubility compounds are high, then significant differences between different WSOC measurement methods will exist.

Class III: Regardless of the sampling and extraction method and of the WIOA concentration, compounds with solubility lower than 10^{-4} g L^{-1} will not be extracted (less than 10% of their mass) in the WSOC. Most polycyclic aromatic hydrocarbons and alkanes with more than 8 carbon atoms are members of this class.

For significantly elevated WIOA concentrations (>100 μg m^{-3}), relevant for source sampling, the high total WIOA content of the samples prevents the extraction of various compounds into water, according to Equation 11. Figure 3 depicts the fraction of a single compound that can be extracted in the WSOC for an intermediate value of P=0.1 cm^3 m^{-3} as a function of the WIOA. For a total WIOA concentration of 100 μg m^{-3}, species with solubility that exceeds 10 g L^{-1} will be measured (>90% of their mass) as WSOC. Species with lower solubility, from 0.1 to 10 g L^{-1}, which is actually the solubility range of most mono- and di-acids with less than 10 carbon atoms, will contribute only partially to the WSOC in this case. Species with solubility less than 0.1 g L^{-1} will be practically excluded (contribute with <10% of their mass) from the WSOC. For even higher WIOA concentrations of 1 mg m^{-3}, these thresholds are shifted higher

by one order of magnitude. In this case, even highly water soluble small mono- and di-acids, (see Table 2) are only partially contributing to the WSOC, while species with solubility less than 1 g L^{-1} will not contribute significantly. Consequently, WSOC measurements under high organic concentration loadings often used during source sampling will tend to give low WSOC values unless higher *P* values are used.

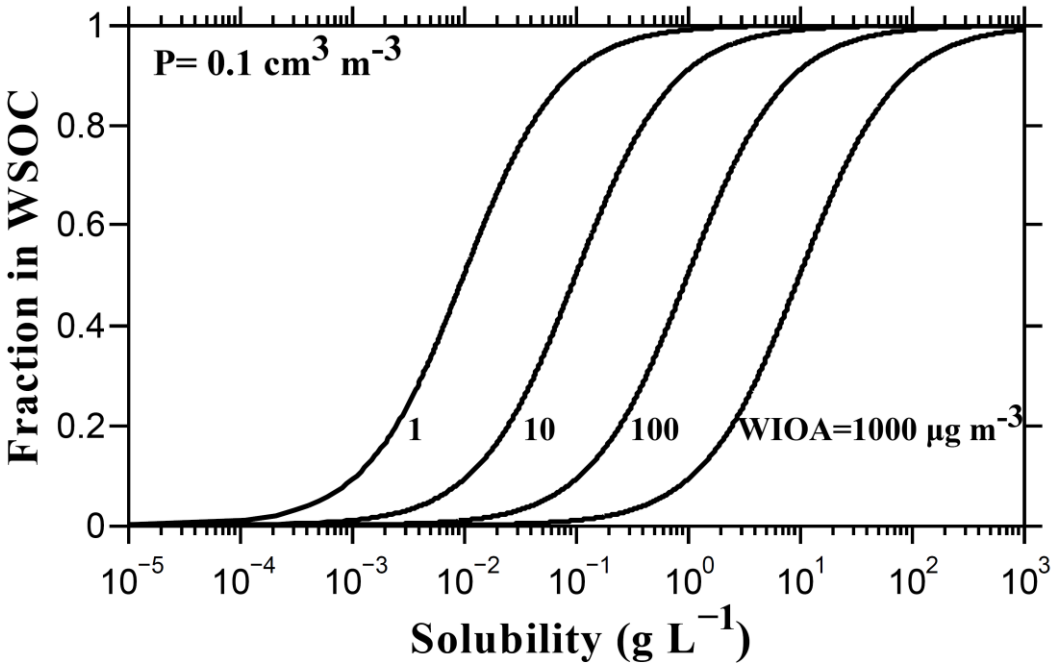

Figure 2.3: Fraction of a compound that will be extracted in the WSOC, for an intermediate *P* parameter value (0.1 cm^3 m^{-3}) for typical (1, 10 µg m^{-3}) and elevated (100, 1000 µg m^{-3}) concentrations of total water insoluble organic aerosol concentrations (WIOA).

2.2.2 Independent Compounds Model

The above analysis has been based on the hypothesis that the organic components in the aerosol form an ideal organic solution. In the other extreme it may be assumed that the dissolution of a single compound is not affected by the presence of the other components. It was also assumed that the aqueous solutions past the extraction will be

sufficiently dilute. This approach will be referred to as the independent compounds model.

The mass m_A of the organic compound A that can be dissolved during the extraction (assuming that the system reaches equilibrium), will be equal to $V_W \cdot S_A$ and $m_{A(tot)}$ in this case will be equal to $C_A \cdot f \cdot Q \cdot \Delta t$. Now the fraction of A in the aqueous phase is given by:

$$f_A = \frac{V_W \cdot S_A}{f \cdot Q \cdot \Delta t \cdot C_A} \qquad \text{(for } f_A \leq 1\text{)} \qquad (2.14)$$

or using the *P* parameter from equation (10):

$$f_A = \frac{P \cdot S_A}{C_A} \qquad \text{(for } f_A \leq 1\text{)} \qquad (2.15)$$

The independent compounds model predicts that the water soluble fraction of A is proportional to the *P* parameter and the solubility of the compound, S_A and inversely proportional to its ambient concentration, C_A. When the numerator exceeds the denominator in Equation (15) then f_A is equal to unity. This case corresponds to high availability of water for the extraction of the specific compound, complete dissolution and 100% contribution of the compound to the WSOC. Figure 4a depicts the water soluble fraction of a compound, as a function of its solubility, for different ambient concentrations, as predicted by the independent compounds model, for P=0.01 $cm^3\ m^{-3}$. Despite the low *P* parameter value, the model predicts that organics with solubility higher than 10^{-2} g L^{-1} always contribute to the WSOC more than 90% of their mass, regardless of their ambient concentration, while species with solubility less than 10^{-5} g L^{-1} do not contribute significantly. Alkanes are practically excluded from the WSOC in

this case, while some relatively water soluble PAHs, like pyrene, phenanthrene and fluoranthene (Table 1) can contribute a significant fraction of their mass or even all of it to the WSOC, depending on their ambient concentration. Organic acids, sugars, phenols, amines, HULIS and other polyconjugated organic species can dominate the WSOC composition in this case.

As *P* increases the corresponding curves for the intermediate (Figure 4b) and higher *P* parameter values (Figure 4c) shift to the left. The *P* value of 0.1 cm^3 m^{-3} permits species with solubility that exceeds 10^{-6} g L^{-1} to contribute partially and species with solubility that exceeds 10^{-3} g L^{-1} to contribute totally to the WSOC, regardless of their ambient concentration. Species that have 10 ng m^{-3} concentrations in the atmosphere and a solubility that exceeds the value of 10^{-5} g L^{-1} have at least 10% participation in the WSOC, which can reach 100% if their solubility exceeds 10^{-4} g L^{-1}. Such compounds include acids, sugars, phenols, HULIS and amines, but also anthracene, retene, benzo[a]anthracene, pyrene, triphenylene, etc., depending on the solubility and concentration combination of the species.

The high *P* parameter value of 1 cm^3 m^{-3} leads to the extraction of organics with even lower water solubility. Species with solubility more than 10^{-7} g L^{-1} contribute to the WSOC more than 10%, if their atmospheric concentration is 1 ng m^{-3}. Species that have an atmospheric concentration of 10 ng m^{-3} can contribute practically all their mass when their solubility is higher than 10^{-5} g L^{-1}. Thus, the elevated *P* value allows almost all polycyclic aromatic compounds, present in the OA and regarded as water-insoluble, to be included partially or fully, depending on their solubilities and ambient concentrations.

Small or even long-chained alkanes, from decane to even hexacosane, will also be measured as WSOC.

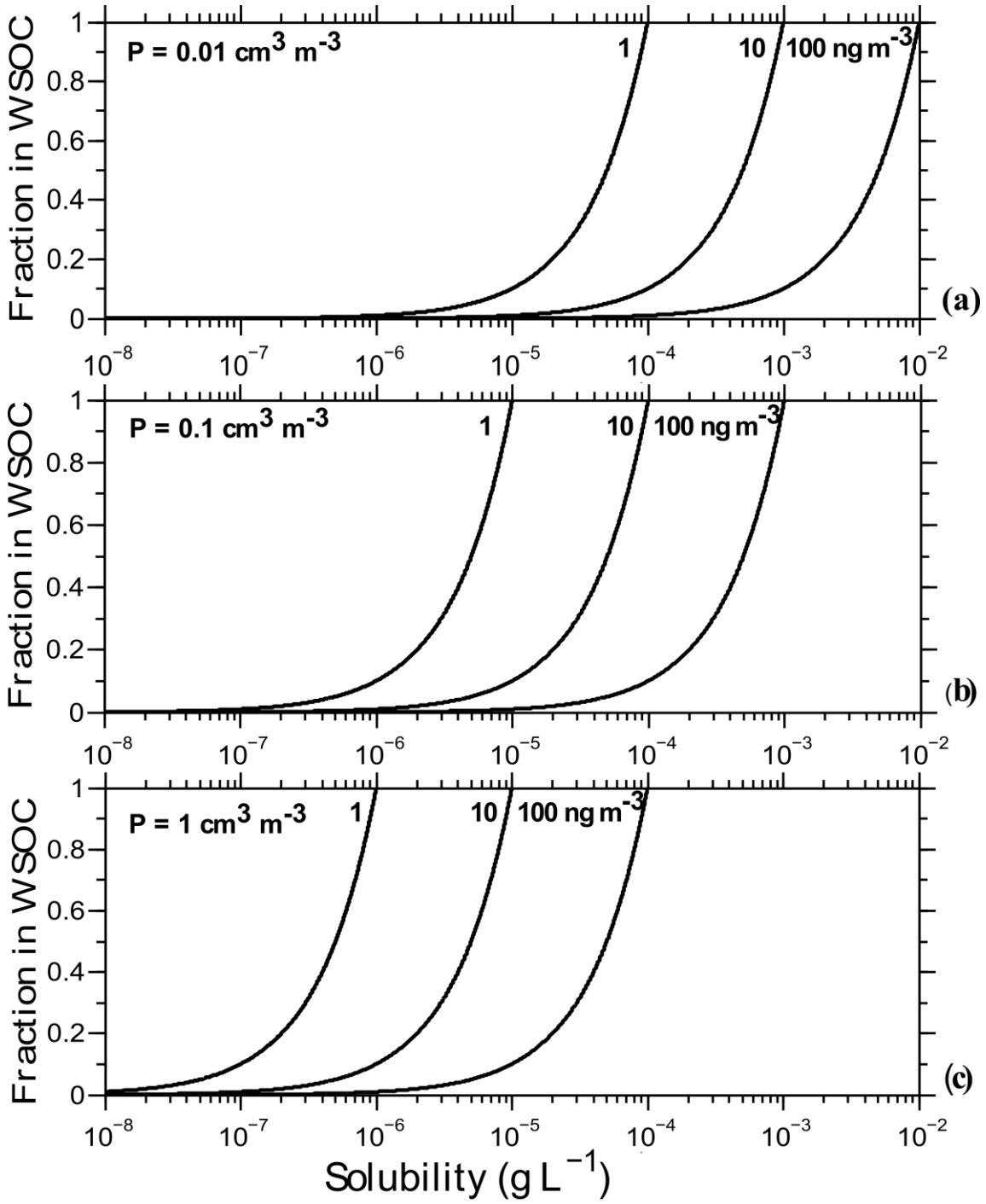

Figure 2.4: Water soluble fraction of a compound as a function of its solubility and ambient concentration, as predicted by the ideal compounds model: (a) for low, (b) intermediate and (c) high value of *P*.

Table 2. Solubilities of various organic compounds present in aerosols, at 25°C.

Compound – Abbreviation	Chemical Formula	Solubility ($g\ L^{-1}$)	Solubility Reference
Sugars			
mannose	$C_6H_{12}O_6$	2500	a
sucrose	$C_{12}H_{11}O_{22}$	2000	a
levoglucosan	$C_6H_{10}O_5$	1000	estimated
glucose	$C_6H_{12}O_6$	909	a
fructose	$C_6H_{12}O_6$	407	a
lactose	$C_{12}H_{11}O_{22}$	200	a
maltose	$C_{12}H_{11}O_{22}$	93	a
Acids			
glutaric	$C_5H_8O_4$	1160	b
malonic	$C_3H_4O_4$	1161	b
citric	$C_6H_8O_7$	750	b
oxalic	$C_2H_2O_4$	120	b
succinic	$C_4H_6O_4$	88	b
adipic	$C_6H_{10}O_4$	25	b
L-aspartic	$C_4H_7NO_4$	5	c
benzoic acid	$C_7H_6O_2$	2.1	d
suberic	$C_8H_{14}O_4$	2.4	c
azelaic	$C_9H1_6O_4$	1.8	d
decanoic	$C_{10}H_{20}O_2$	0.15	d
palmitic	$C_{16}H_{32}O_2$	$7.2\ 10^{-3}$	d
Phenols			
catechol	$C_6H_6O_2$	450	d
phenol	C_6H_6O	82	d
o-cresol	C_7H_8O	32	d
2,4,6 trinitrophenol	$C_6H_3N_3O_7$	13	d
pentachlorophenol	C_5HCl_5O	0.021	d
Polycyclic Aromatic Hydrocarbons, PAHs			
naphthalene	$C_{10}H_8$	0.031	e
acenaphthene	$C_{12}H_{10}$	$1.5\ 10^{-3}$	d
phenanthrene	$C_{14}H_{10}$	$1.3\ \ 10^{-3}$	f
fluoranthene	$C_{16}H_{10}$	$2.6\ 10^{-4}$	d
pyrene	$C_{16}H_{10}$	$1.3\ 10^{-4}$	d
anthracene	$C_{14}H_{10}$	$4.5\ 10^{-5}$	d
anthracene	$C_{14}H_{10}$	$4.5\ 10^{-5}$	d
chrysene	$C_{18}H_{12}$	$2.0\ 10^{-6}$	e
perylene	$C_{20}H_{12}$	$4.0\ 10^{-7}$	d
benzo [ghi] perylene	$C_{22}H_{12}$	$3.0\ 10^{-7}$	f
coronene	$C_{24}H_{12}$	$1.0\ 10^{-7}$	e

Alkanes			
cyclohexane	C_6H_{12}	0.058	d
hexane	C_6H_{14}	$9.8\ 10^{-3}$	d
n-heptane	C_7H_{16}	$2.4\ 10^{-3}$	d
octane	C_8H_{18}	$7.3\ 10^{-4}$	d
decane	$C_{10}H_{22}$	$1.5\ 10^{-5}$	d
octadecane	$C_{18}H_{38}$	$6\ 10^{-6}$	d
docosane	$C_{22}H_{46}$	$6\ 10^{-6}$	d
tetracosane	$C_{24}H_{50}$	$4\ 10^{-6}$	d
HULIS		5-20	g

[a] Rosenorn et al. (2006)

[b] Saxena and Hildemann (1996)

[c] Huff Hartz et al. (1996)

[d] CRC Handbook of Chemistry and Physics 90th edition (2010)

[e] Seinfeld and Pandis (1996)

[f] Pio et al. (2000)

[g] Salma et al. (2008)

Even for the case of long-chained alkanes, which are traditionally regarded as insoluble in water, the high *P* parameter applied could allow them to contribute to the WSOC. Octadecane and docosane, which have similar solubilities of approximately $6x10^{-6}$ g L^{-1}, can contribute more than half of their mass to the WSOC, for atmospheric concentrations of 10 ng m^{-3}. Their fraction in the WSOC will be lower for higher ambient concentrations, according to the independent compounds model. Using a low *P* of 0.01 cm^3 m^{-3} a wide range of polycyclic aromatic species with solubilities that exceed 10^{-5} g L^{-1} are also included in the WSOC. High *P* parameter value of 1 cm^3 m^{-3} can lead to the extraction of an even wider range of PAHs (those with solubility higher than 10^{-7} g L^{-1}) as well as various long-chained alkanes containing up to 30 or even 40 carbon atoms. Based on the above, we can now classify organic compounds into three main categories, regarding their contribution to the WSOC fraction:

Class I ($S_A > 10^{-2}$ g L^{-1}): 100% of the compound mass will be included in the WSOC, regardless of the *P* parameter and their ambient concentration, since the typical concentration of a single compound in ambient organic aerosol rarely exceeds 100 ng m^{-3}. Levoglucosan could be an exception, as it has been identified as the most abundant water-soluble compound measured in aerosols emitted by biomass burning (Nolte et al., 2001; Mochida and Kawamura, 2004). Its high expected solubility, however, allows levoglucosan to fall within this class, even if its concentration exceeds 1 μg m^{-3}.

Class II (10^{-7} g $L^{-1} < S_A < 10^{-2}$ g L^{-1}): The water soluble fraction of a compound in this case depends on the total ambient concentration of the compound, the *P* parameter and its solubility as well. Increasing the solubility or the *P* parameter leads to the increase of the contribution of the compound in the WSOC, while increase of its ambient concentration leads to the decrease of its corresponding fraction in the WSOC.

Class III ($S < 10^{-7}$ g L^{-1}): Species in this category are never present in the WSOC.

According to the hypothesis of non-interacting compounds in the aerosol, the fraction of the organic species extracted in the WSOC depends on their atmospheric concentration. According to Figure 4, an organic species can have a significant contribution (more than 90% of its mass) to the WSOC (thus referring to compounds with atmospheric concentrations higher than 1 ng m^{-3}) if its solubility is above a threshold. This threshold solubility in the case of the low *P* parameter value is near 10^{-4} g L^{-1}, for the intermediate *P* of 0.1 is 10^{-5} g L^{-1} and is 10^{-6} g L^{-1} for the value of 1 cm^3 m^{-3}.

2.3 Synthesis of the Results

The independent compounds and the ideal organic solution models are two rather extreme cases, with the truth lying probably between them. Regardless of the *P* value and the atmospheric concentrations of the other organic species, compounds with solubilities higher than 10^{-2} g L^{-1} will always be included in the WSOC with more than 90% of their mass, according to the independent compounds model. The corresponding threshold solubility according to the ideal organic solution model is 10 g L^{-1}. Thus, the value of 10 g L^{-1} is a robust threshold for participation in the measured WSOC (Figure 2) and such species can be treated as water soluble. In the other end, the lower corresponding solubility threshold is 10^{-7} g L^{-1} for the independent compounds model and 10^{-4} g L^{-1} for the ideal organic solution model. Such species can be treated as water insoluble. This unfortunately leaves a wide range of 10^{-7} to 10 g L^{-1} of compound solubilities where their behavior in the WSOC measurements will depend on their interactions with the other organic species, their atmospheric concentrations, and the measurement protocol.

The existence of highly soluble organic species in the WSOC, such as small mono, di and polyacids, such as citric, oxalic, adipic, glutaric, maleic or succinic acid is predicted by both the independent compounds and the ideal solution models under normal atmospheric concentrations. Sugars are expected as well to be included in the WSOC due to their high solubility. Amines, along with various phenols, such as cresols and catechol are also predicted to be part of the WSOC by both models. Furthermore, species like keto-carboxylic acids and other multifunctional compounds will probably be included in the WSOC. Humic and fulvic acids, which are considered to be natural acidic organic polymers, are in the solubility range where they will be mostly part of the

WSOC. The quantitative extraction of HULIS and FULIS can be assured by the use of intermediate or high *P* parameter value. Although the water solubility of highly oxidized compounds, such as hydroxyacids or deoxysugars, is in most cases unknown, such species are expected to possess a high enough solubility in water (> 10 g L^{-1}), due to the high extent of their oxidation and to their polarity and they participate in the WSOC fraction. Both models predict the participation of the above species in the WSOC.

On the other hand, species like the large PAHs, coronene, perylene and benzoperylene that have solubilities of the order of 10^{-7} g L^{-1} can be considered as water insoluble from the WSOC measurement point of view. The concentrations of long-chained alkanes (more than 10 carbon atoms) tend to decrease with increasing carbon number (Yang et al., 2005; Xingru et al., 2009). As a result their solubility does not allow their participation in the WSOC under all conditions.

A number of species with significantly high ambient concentrations (like fluoranthene, benzoanthracene, and benzoperylene) have solubilities in the intermediate range from 10^{-5} to 10^{-3} g L^{-1}. In this range, the independent compounds model predicts even 100% extraction of various PAHs (e.g., fluoranthene or pyrene) for intermediate and high *P* values), while the ideal organic solution model less than 10%.

The ideal organic solution model also predicts that a wide range of long chained acids, with more than 10 carbon atoms will contribute significantly to the WSOC, if $P \geq 0.1$ cm^3 m^{-3}. Along with long chained acids, some polycyclic aromatic compounds, such as phenanthrene or acenaphthene can also be found in the water soluble fraction, since these compounds' solubilities allow them to be extracted according to the ideal organic

solution model. The independent compounds model predicts that these compounds are fully contributing to the WSOC.

2.4 Application to Ambient Measurements

The experimental efforts to chemically characterize the water soluble fraction of aerosols have all concluded that acidic compounds are a major fraction of WSOC. Mayol-Bracero et al. (2002) using HPLC-UV and GC/MS found that half of the WSOC measured in Amazonia was composed of monoacids, diacids, hydroxyacids, oxoacids and polyacidic compounds. Around 20% of the WSOC that was not retained in the HPLC column was characterized as neutral and was composed of anhydrosugars, sugars, sugar alcohols and neutral aromatics, while the rest was unaccounted. Decesari et al. (2001) analyzed the WSOC in the polluted Po Valley in Italy, by means of HPLC and H-NMR and again found that 87% of the WSOC consisted of acidic and neutral compounds. In another paper, Decesari et al. (2000) using IR and FTIR spectroscopy, UV spectroscopy, fluorescence, H-NMR found that 77% of the water soluble compounds in aerosol and fog samples were mono and di-acidic compounds, neutral/basic and polyacidic. NMR spectra also revealed interesting information about the structure of the compounds. A very low content of aromatic protons was found in the neutral/basic class, suggesting that these compounds can be mainly hydroxylated or alkoxylated aliphatic species, like alcohols and ethers. In addition, the relative abundance of H-C-O protons compared to the unsubstituted H-C protons is indicative of the presence of polyols, like deoxy-sugars, rather than aliphatic monoalcohols. Mono and dicarboxylic acids were found to be the most abundant compounds in the WSOC and aliphatic carboxylic acids, along with hydroxycarboxylic acids were dominant among acids. Furthermore, a HULIS standard was tested and appeared to have a

chromatographic behavior similar to the polyacidic fraction, suggesting the presence of macromolecular humic-like organic compounds. Krivácsy et al. (2001) reported that 50% of the WSOC in Jungfraujoch, Switzerland, separated by a two-step solid phase extraction (SPE), consisted of highly conjugated weak polyacids (humic-like substances), slightly polyconjugated, very hydrophilic and neutral compounds. Kiss et al. (2002) also employed SPE to separate WSOC collected at a rural site in Hungary into moderately hydrophilic and strongly hydrophilic and found that the more hydrophilic fraction is composed of small carboxylic acids, hydroxy-acids and polyhydroxy-acids and lacked polyconjugated structures. Sullivan et al.[3] reported the existence of a hydrophobic fraction in the WSOC along with the hydrophilic. The former consisted mainly of monocarboxylic and dicarboxylic acids with more than 4 or 5 carbons, aromatic-containing compounds, phenols, cyclic acids and humic-like substances, while the latter included saccharides, amines, carbonyls and small acids with less than 3-4 carbon atoms. The measurement in this case was performed by PILS, which normally uses high *P* parameter values.

In summary, the experimental findings agree that the WSOC fraction can be composed of acids (mono-, di- and poly-acids), HULIS, polyols, like sugars, phenols and polyconjugated species. Since there is no ability to distinguish single aromatic rings from polycyclic aromatics, the NMR aromatic protons' spectra imply the presence of polycyclic compounds in the WSOC extracts. In general, the solubility of these species exceed 10^{-3} g L^{-1}. The extraction of such species is predicted by the ideal organic solution model for the intermediate *P* parameter value, which predicts the extraction in the WSOC of the previously mentioned species, possibly along with a few PAHs of relatively high solubility (anthracene, phenanthrene, acenaphthene). Thus, the previously

described experimental findings combined with Figure 2, lead us to conclude that the ideal organic solution model predictions are closer to reality.

For typical organic aerosol concentrations, the intermediate *P* value of 0.1 cm^3 m^{-3} appears to be more suitable for the full extraction of the soluble species expected in the WSOC. The species fully extracted by this value have solubility more than 0.1 g L^{-1} and include species found in primary biomass burning emissions (e.g., sugars) and in oxidized secondary aerosol (e.g., acids). HOA-like compounds, such as aromatic species and alkanes are excluded. Higher *P* values would lead to the extraction of more HOA while lower values would exclude various acids.

A number of studies have provided support of the existence of one or two organic phases in ambient particles. Donahue et al. (2011) based on a two-dimensioned volatility-basis set (VBS) proposed that, when the background aerosol is mostly hydrocarbon-like (HOA) or particles from biomass burning (BBOA) and thus not very oxidized, then primary organic emissions can mix well with the organic aerosol and form one organic phase. On the other hand, when the background aerosol is highly oxygenated, non-polar reduced primary emissions will have a hard time mixing with this background aerosol and instead will tend to phase separate and form two organic phases, a polar and a non-polar one. Zuend et al. (2010) confirmed the above findings, asserting that the total Gibbs free energy of the system is minimized in the case of the formation of two phases instead of one. If the organic phase would consist of hydrophobic, hydrocarbon-like organics and highly oxidized, hydrophilic organics, a further phase separation of the organic phase into a low-O:C phase and a high-O:C phase could become stable according to Zuend and Seinfeld (2012). Smog chamber experiments also

confirmed the hypothesis that "like mixes well with like". Asa-Awuku et al. (2009) and Song et al. found that primary emissions of motor oil or diesel fuel and biogenic secondary organic aerosol form two distinct organic phases when mixed. Also, studies on the aqueous solubility of hydrocarbon mixtures support the formation of two phases rather than one in hydrophobic-hydrophilic systems, suggest the limitation of a compound's solubility by the presence of other molecules and confirm the validity of the organic solution model (Banergee, 1984; De Hemptine et al., 1998). The ideal organic solution model assumes that all organic aerosol species form one organic phase. In the case of formation of two different organic phases, the $C_{OA}(1\text{-}f_{WSOC})$ in Equation (11) should be replaced by the amount of the corresponding phase that does not dissolve in the water. The changes that this will cause to the above discussion should be in most cases within a factor of two and will not change drastically the above picture.

2.5 Conclusions

The measurement of Water Soluble Organic Carbon (WSOC) in atmospheric aerosol is usually carried out by sample collection on filters, extraction in ultrapure water, filtration, and measurement of the total organic carbon. In this work, the role of different conditions of sampling and extraction as well as the range of solubilities of the organic compounds that contribute to the WSOC were investigated. The sampling and extraction of WSOC can be described by a single parameter, *P*, expressing the ratio of water used per volume of air sampled on the analyzed filter. Two cases are examined in order to bound the range of interactions of the various organic aerosol components with each other. In the first we assume that that the organic species form an ideal solution in the particle and in the second that the extraction of a single compound is independent of the presence of the other organics. The ideal organic solution model predicts that species

with water solubility as low as 10^{-4} g L^{-1} contribute to the measured WSOC. In the other end, the independent compounds model predicts that low-solubility (as low as 10^{-7} g L^{-1}) compounds are part of the WSOC. Studies of the WSOC composition are consistent with the predictions of the ideal organic solution model. A value of P=0.1 cm^3 m^{-3} is proposed for the extraction of WSOC in typical organic aerosol concentrations (1-10 μg m^{-3}) while higher P values should be applied in case of heavier organic aerosol loadings (100-1000 μg m^{-3}).

2.6 References

Anderson, C., Dibb, J.E., Griffin, R.J., Bergin, M.H. Simultaneous measurements of particulate and gas-phase water-soluble organic carbon concentrations at remote and urban-influenced locations. *Geophys. Res. Lett*. **2008**, *35*, L13706, doi:10.1020/2008GL033966.

Asa-Awuku, A., Miracolo, M.A., Kroll, J.H., Robinson, A.L., Donahue, N.M. Mixing and phase partitioning of primary and secondary organic aerosols, *Geophys. Res. Lett*. **2009**, *36*, L15827, doi:10.1029/2009GL039301.

Banerjee, S. Solubility of organic mixtures in water. *Environ. Sci. Technol*. **1984**, 18, 587-591.

Cornelissen, G., Rigterink, H., Ferdinandy, M.M.A., Van Noort, P.C.M. Rapidly desorbing fractions of PAHs in contaminated sediments as predictor if the extend of bioremediation. *Environ. Sci. Technol*. **1998**, 32, 966-970.

Cruz, C.N., Pandis, S.N. Study of the ability of pure secondary organic aerosol to act as cloud condensation nuclei. *Atmos. Environ.* **1997**, *31*, No 15, 2205-2214.

De Hemptine, J.C., Delepine, H., Jose, J.C., Jose, J. Aqueous solubility of hydrocarbon mixtures. *Rev. Inst Fr. Pet.* **1998**, 53(4), 409-419.

Decesari, S., Facchini, M.C., Fuzzi, S., Tagliavini, E. Characterization of water-soluble organic compounds in atmospheric aerosol: A new approach. *J. Geophys. Res.* **2000**, *105*, D1, 1481-1489.

Decesari, S., Facchini, M.C., Matta,E., Lettini, F., Mircea, M., Fuzzi, S., Tagliavini, E., Putaud, J.-P. Chemical features and seasonal variation of fine aerosol water soluble organic compounds in the Po Valley, Italy. *Atmos. Environ.* **2001**, *35*, 3691-3699.

Docherty, K.S., Stone, E.A., Ulbrich, I.M., DeCarlo, P.F., Snyder, D.C., Schauer, J.J., Peltier, R.E., Weber, R.J., Murphy, S.M., Seinfeld, J.H., Eatough, D.J., Grover,

B.D., Jimenez, J.L. Apportionment of primary and secondary organic aerosols in Southern California during the 2005 study of organic aerosols in riverside (SOAR). *Environ. Sci. Technol.* **2008**, *42*, 7655-7662.

Donahue, N.M., Epstein, S.A., Pandis S.N., Robinson, A.L. A two-dimensional volatility basis set: 1. organic aerosol mixing thermodynamics. *Atmos. Chem. and Phys*. **2011**, *11*, 3303-3318.

Donahue, N.M., Robinson, A.L., Pandis, S.N. Atmospheric organic particulate matter: From smoke to secondary organic aerosol. *Atmos. Environ.* **2009,** *43*, 94-106.

Duvall, R.M., Majestic, B.J., Shafer, M.M., Chuang, P.Y., Simoneit, B.R.T., Schauer, J.J. The water-soluble fraction of carbon, sulphur, and crustal elements in Asian aerosols and Asian soils. *Atmos. Environ.* **2008**, *42*, 5872-5884.

Facchini, M.C., Fuzzi, S., Zappoli, S., Andracchio, A., Gelencér, A., Kiss, G., Krivácsy, Z., Mészáros, E., Hanson, H.C., Alsberg, T., Zebühr, Y. Partitioning of the organic aerosol component between fog droplets and interstitial air. *J. Geophys. Res.* **1999**, *104*, No D21, 26,821-26,832.

Graber, E.R., Rudich, Y. Atmospheric HULIS: How humic-like are they? A comprehensive and critical review. *Atmos. Chem. Phys.* **2006**, 6, 729-753.

Hagler, G.H.W., Bergin, M.H., Smith, E.A., Dibb, J.E., Anderson, C., Steig, E.J. Particulate and water-soluble carbon measured in recent snow at Summit, Greenland. *Geophys. Res. Lett.* **2007**, *34*, L16505, doi:10.1029/2007GL030110.

Huang, X.F., Yu, J.Z., He, L.Y., Yuan, Z. Water-soluble organic carbon and oxalate in aerosols at a coastal urban site in China: Size distribution characteristics, sources, and formation mechanisms. *J. Geophys. Res.* **2006**, *111*, D22212, doi:10.1029/2006JD007408.

Jacobson, M.C., Hansson, H.C., Noone, K.J., Charlson, R.J. Organic atmospheric aerosols: review and state of the science. *Reviews of Geophys*. **2000**, *38*, 267-294.

Kanakidou, M., Seinfeld, J.H., Pandis, S.N., Barnes, I., Dentener, F.J., Facchini, M.C., Van Dingenen, R., Ervens, B., Nenes, A., Nielsen, C.J., Swietlicki, E., Putaud, J.P., Balkanski, Y., Fuzzi, S., Horth, J., Moortgat, G.K., Winterhalter, R., Myhre, C.E.L., Tsigaridis, K., Vignati, E., Stefanou, E.G., Wilson, J. Organic aerosol and global climate modelling: A review, *Atmos. Chem. Phys.* **2005**, *5*, 1053-1123.

Kang, E., Toohey, D.W., Brune, W.H. Dependence of SOA oxidation on organic aerosol mass concentration and OH exposure: experimental PAM chamber studies. *Atmos. Chem. Phys.* **2011**, *11*, 1837-1852.

Kiss, G., Varga, B., Galambos, I., Ganszky, I. Characterization of water-soluble organic matter isolated from atmospheric fine aerosol. *J. Geophys. Res.* **2002**,*107*, D21,8339, doi:10.1029/2001JD000603.

Krivácsy Z., Gelencsér, Kiss, G., Mészáros, T., Sárvári, Z., Temesi, D., Varga, B., Baltensperger, U., Nyeki, S., Weingartner, E. Study of the chemical character of water soluble organic compounds in fine atmospheric aerosol at Jungfraujoch. *J. Atmos. Chem.* **2001**, *39*, 235-259.

Kondo, Y., Miyazaki, Y., Takegawa, N., Miyakawa, T., Weber, R.J., Jimenez, J.L., Zhang, Q., Worsnop, D.R. Oxygenated and water-soluble organic aerosols in Tokyo. *J. Geophys. Res.* **2007**, *112*, D01203, doi:10.1029/2006JD007056.

Mayol-Bracero, O.L., Guyon, P., Graham, B., Roberts, G., Andreae, M.O., Decesari, S., Facchini, M.C., Fuzzi, S., Artaxo, P. Water-soluble organic compounds in biomass burning aerosols over Amazonia 2. Apportionment of the chemical composition and importance of the polyacidic fraction. *J. Geophys. Res.* **2002**, *107*, No D20, 8091.

Miyazaki, Y., Kondo, Y., Takegawa, N., Komazaki, Y., Fukuda, M., Kawamura, K., Mochida, M., Okozawa, K., Weber, R.J. Time-resolved measurements of water-soluble organic carbon in Tokyo. *J. Geophys. Res.* **2006**, *111*, D23206, doi:10.1029/2006JD007125.

Mochida, M., Kawamura, K. Hydroscopic properties of levoglucosan and related organic compounds characteristic to biomass burning aerosol particles. *J. Geophys. Res.***2004**, *109*, D21202, doi:101029/2004JD004962.

Nolte, C.G., Schauer, J.J., Cass, G.R., Simoneit, B.R.T. Highly polar organic compounds present in wood smoke and in the ambient atmosphere. *Environ. Sci. Technol*. **2001**, *35* (10), 1912–1919.

Saarikoski, S., Sillanpää, M., Sofiev, M., Timonen, H., Saarnio, K., Teinilä, K., Karppinen, A., Kukkonen, J., Hillamo, R. Chemical composition of aerosols during a major biomass burning episode over northern Europe in spring 2006: Experimental and modelling assessments. *Atmos. Environ.* **2007**, *41*, 3577-3589.

Saxena, P., Hildemann, L.M., McMurry, P.H., Seinfeld, J.H. Organics alter hydroscopic behavior of atmospheric particles. *J. Geophys. Res.* **1995**, *100*, 18,755-18,770.

Saxena, P., Hildemann, L. Water-soluble organics in atmospheric particles: a critical view of the literature and application of thermodynamics to identify candidate compounds. *J. Atmos. Chem.***1996**, *24*, 57-109.

Schauer, J.J., Rogge, W.F., Hildemann, L.M., Mazurek, G.R., Cass, G.R., Simoneit, B.R.T. Source apportionment of airborne particulate matter using organic compounds as tracers. *Atmos. Environ*. **1996**, *30*, 3837-3855.

Shulman, M.L., Jacobson, M.C., Charlson, R.J., Synovec, R.E., Young, T.E. Dissolution behavior and surface tension effects of organic compounds in nucleating cloud droplets. *Geophys. Res. Lett*. **1996**, *23*, 277-280.

Song, C., Zaveri, R.A., Alexander, M.L., Thornton, J.A., Madronich, S., Ortega, J.V., Zelenyuk, A., Yu, X.-Y., Laskin, A., Maugan, D.A. Effect of hydrophobic primary organic aerosols on secondary organic aerosol formation from ozonolysis of alpha-pinene. *Geophys. Res. Lett.* **2007,** *34*, L20803, doi: 10.1029/2007GL030720.

Sullivan, A.P., Peltier R.E., Brock, C.A., de Gouw, J.A., Holloway, J.S., Warneke, C., Wollny, A.G., Weber, R.J. Airborne measurements of carbonaceous aerosol soluble in water over northeastern United States: Method development and an investigation into water-soluble organic carbon sources. *J. Geophys. Res.* **2006**, *111*, doi: 10.1029/2006JD007072.

Sullivan, A.P., Weber, R.J., Clements, A.L., Turner, J.R., Bae, M.S., Schauer, J.J. A method for on-line measurement of water-soluble organic carbon in ambient aerosol particles: Results from an urban site. *Geophys. Res. Lett.* **2004**, *31*, L13105, doi:10.1029/2004GL019681.

Viana, M., Chi, X., Maenhaut, W., Querol, X., Alastuey, A., Mikuška, P., Večeřa, Z. Organic and elemental carbon concentrations in carbonaceous aerosols during summer and winter sampling campaigns in Barcelona, Spain. *Atmos. Environ.* **2006**, *40*, 2180-2193.

Xingru, L., Xueqing, G., Xinran, L., Chenshu, L., Shanshan, Z., Yuesi, W. Distribution and sources of solvent extractable organic compounds in $PM_{2.5}$ during 2007 Chinese spring Festival in Beijing. *J.Environ. Sci.* **2009**, *21*, 142-149.

Yang, H., Yu, J.Z., Ho, S.H.H., Xu, J., Wu, W.S., Wan, C.H., Wang, X., Wang, X., Wang, L. The chemical composition of inorganic and carbonaceous materials in $PM_{2.5}$ in Nanjing, China. *Atmos. Environ.* **2005**, *39*, 3735-3749.

Zhang, Q., Jimenez, L., Canagaratna, M.R., Allan, J.D., Coe, H., Ulbrich, I., Alfarra, M.R., Takami, A., Middlebrook, A.M., Sun, Y.L., Dzepina, K., Dunlea, E.,

Docherty, K., DeCarlo, P.F., Salcedo, D., Onasch, T., Jayne, J.T., Miyoshi, T., Shimono, A., Hatakeyama, S., Takegawa, N., Kondo, Y., Schneider, J., Drewnick, F., Borrmann, S., Weimer, S., Demerjian, K., Williams, P., Bower, K., Bahreini, R., Cottrell, L., Griffin, R.J., Rautiainen, J., Sun, J.Y., Zhang, Y.M., Worsnop, D.R. Ubiquity and dominance of oxygenated species in organic aerosols on anthropogenically-influenced Northern Hemisphere midlatitudes. *Geophys. Res, Lett.* **2007**, *34*, L13801, doi:10.1029/2007GL029979.

Zuend A., Marcolli., C., Peter, T., Seinfeld, J.H. Computation of liquid-liquid equilibria and phase stabilities: implications for RH-dependent gas/particle partitioning of organic-inorganic aerosols. *Atmos. Chem. Phys.* **2010**, 7795-7820.

Zuend, A., Seinfeld J.H. Modelling the gas-particle partitioning of secondary organic aerosol: the importance of liquid-liquid phase separation. *Atmos. Chem. Phys.* **2012**, *12*, 3857-3882.

Chapter 3

Development of a method for the continuous measurement of the Water Soluble Organic Carbon (WSOC) of atmospheric aerosols

3.1 Introduction

The organic fraction of atmospheric aerosols comprises a complex mixture of probably thousands of chemical compounds. The complex chemical nature and the very low concentrations of most individual organics do not allow their full chemical speciation. Thus the classification of organic species into groups is essential for their characterization and description of their properties.

The water soluble organic carbon (WSOC) is an operationally defined term used to describe a water soluble class of organic aerosol components. WSOC can account for the major fraction of the total organic content of the aerosols, ranging from 40 to 80% (Anderson et al., 2008). WSOC compounds are formed in the atmosphere by oxidation reactions of less soluble species, which in general lead to the formation of species with higher aqueous solubility (Sullivan et al., 2006; Kondo et al., 2007; Miyazaki et al., 2006). However, WSOC compounds are also emitted during biomass burning. Thus the sources of WSOC are both biogenic and anthropogenic.

The measurement of WSOC has been traditionally carried out by filter sampling, which includes sample collection on quartz fiber filters, extraction of the soluble fraction, filtration and analysis of the total organic carbon with a TOC analyzer (Psichoudaki and Pandis, 2013). Sampling duration is usually 24 hours, but can vary from a few hours to several days. Although the filter-based non-continuous methods are widely used for the measurement of WSOC, they exhibit several disadvantages. The preparation and analysis of the filters require significant effort, thus limiting the frequency of the measurements. Sampling artifacts can also occur, due to semi-volatile organic species which may evaporate from the filter and so will not be accounted in the measurement.

Positive artifacts can also take place because of the ability of the quartz fiber filters to absorb gas-phase species or due to absorption of organic gases by the particles collected on the filter (Sullivan et al., 2004).

A number of on-line methods have gained ground lately. In 1995 a system for continuous water soluble inorganic aerosol composition measurements was developed in the Netherlands Energy Research Foundation by Khlystov et al. (1995) for the collection of the water soluble inorganic species. The system was equipped with two cyclones in series made of high density polyethylene. The Steam Jet Aerosol Collector (SJAC) was coupled with an anion and a cation chromatograph for the measurement of the water soluble inorganic ions.

The Particle-Into-Liquid Sampler (PILS) developed in Georgia Institute of Technology, was also initially designed for the continuous measurement of the major water soluble inorganic ionic components of the aerosols (Weber et al., 2001) in combination with ion chromatography. This instrument coupled with a TOC analyzer was used for the continuous measurement of WSOC and is now commercially available (Sullivan et al., 2004). PILS uses water vapor that condenses on the sampled aerosol thus leading to the formation of droplets. The droplets are driven to an impactor and then are collected with the help of additional water flowing though the instrument. The instrument has been found to measure higher water soluble fractions of organic aerosol compared with filter measurements, probably due to the high *P* parameter applied in this instrument (Sullivan et al., 2004; Psichoudaki and Pandis, 2013).

In the present work, the initial design of the SJAC for the continuous measurement of WSOC combined with a TOC analyzer (Steam Sampler-TOC) was modified. The design of the system did not include an impactor plate as the PILS, limiting particle losses inside the system. This may allow the extension of its use for the alternative measurement of WSOC and the total organic carbon (OC) and to the achievement of continuous monitoring of the water soluble fraction of the organic aerosols. The design of PILS does not allow OC measurements because insoluble particles may stick to the impactor leading to serious OC underestimation (Peltier et al., 2007). The step by step development and the evaluation of the system's performance will be presented in the following sections.

3.2.1 Description of SJAC

The initial design of the SJAC allowed the measurement of the major water soluble inorganic ions, including sulfate, nitrate, ammonium, sodium, potassium, magnesium and chloride, in combination with a pair of anion and cation chromatographs. The main components of this original version of the instrument are shown in the schematic diagram shown in Figure 3.1. SJAC consists of a steam generator, a mixing reservoir made of glass, two glass cyclones in series, two peristaltic pumps, a condenser and an air pump. The sampled air mixes with steam in the mixing reservoir, forming droplets. The liquid sample is then driven to the cyclones from where it is directed to a test tube with a peristaltic pump. The excess steam condenses in the condenser and the water is removed from the system by a peristaltic pump. SJAC uses a three-neck flask containing ultrapure water placed on an electric heating mantle, which heats the water to boiling. A peristaltic pump continuously provides the flask with ultrapure water.

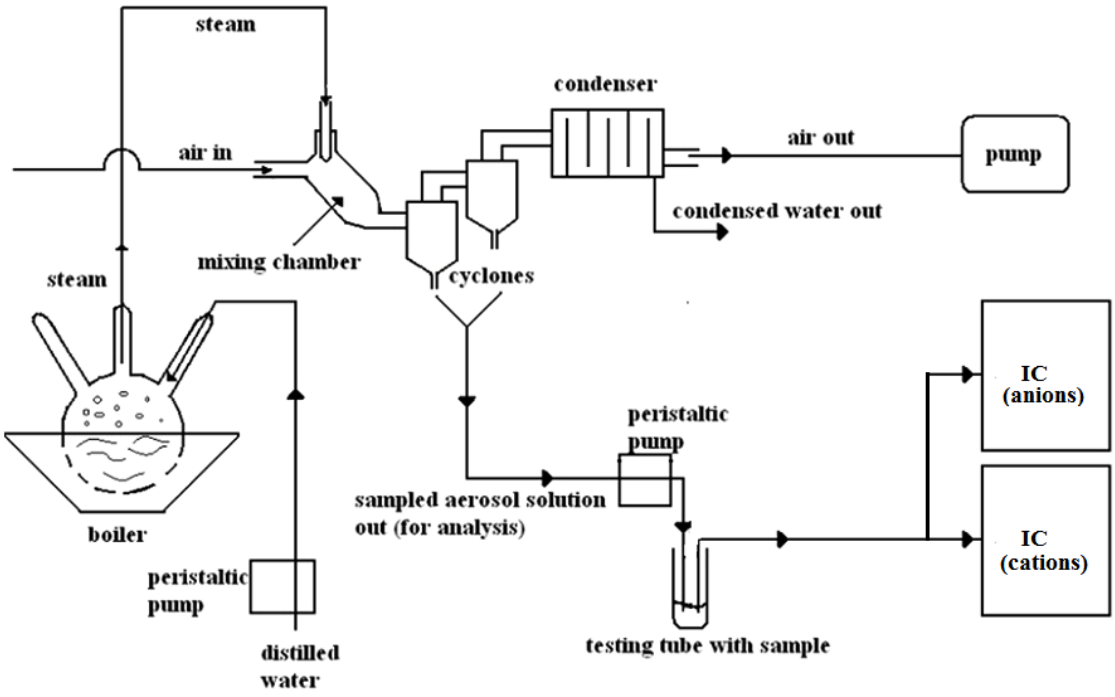

Figure 3.1: Schematic of the steam Jet Aerosol Collector used for the measurement of inorganic PM components (Kostenidou, 2010).

The air stream containing the aerosols rapidly mixes in the mixing reservoir with the steam coming from the steam generator. The resulting supersaturation causes aerosol particles to grow into droplets of at least 1 μm diameter, containing the dissolved aerosol components (Khlystov et al., 1995). The resulting solution is collected by the two cyclones, from where it is constantly pumped out by a peristaltic pump and led to a test tube and to an anion and/or cation chromatograph. The steam produced in the flask is led to the top of the mixing reservoir through a narrow tube (Figure 3.2).

The steam exits the narrow tube (operating as an orifice) as a strong jet which causes turbulence inside the reservoir. The resulting turbulence promotes the fast mixing of the air stream with the steam and as a result, air is supersaturated before most of the vapor condenses onto the reservoir walls. There is a competition between condensation on the aerosol particles' surface and condensation on the walls. Approximately 50% of the

water vapor condenses on the walls of the mixing chamber (Khlystov et al., 1995). For 3-4 g of water injected per minute mixing with an air stream with a flow rate of 22.5 L min^{-1}, the resulting supersaturation is estimated to be 200-250%. However, calculations show that even if a 10% supersaturation is achieved, the residence time inside the mixing chamber (around 0.1 s) allows particles with diameter more than 20 nm to grow and form droplets. As a result the system can collect practically all hygroscopic aerosol particles in the sampled air (Khlystov et al., 1995).

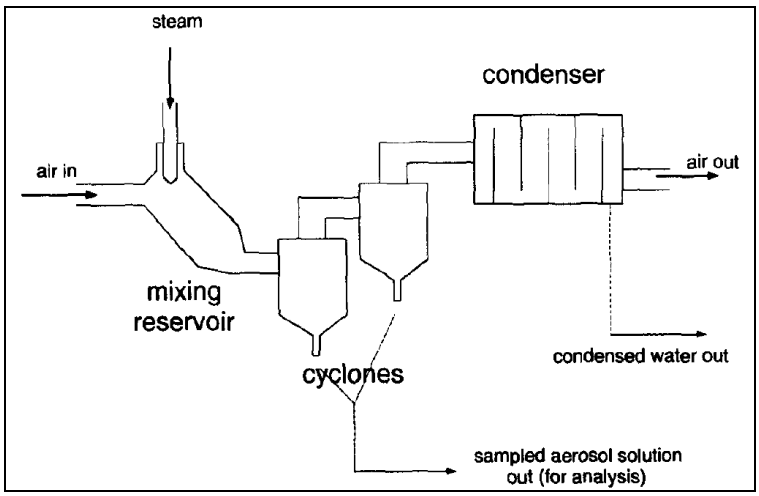

Figure 3.2: Main parts of the SJAC: A mixing reservoir where air mixes with steam, two cyclones to collect the liquid sample and a condenser to remove excess steam.

3.2.2 Modifications of the SJAC to measure WSOC

Our goal was to use the SJAC for the collection of the water soluble organic components of the aerosols and measure continuously the WSOC of atmospheric aerosols using a total organic carbon analyzer. The initial design of the SJAC was inappropriate for the collection of the WSOC due to contamination from various materials present in the system. The tubing of the peristaltic pumps, flange joints of the flask and other plastic connectors resulted in high (> 2 ppm) and unstable TOC concentrations.

In the new version of the Steam Sampler-TOC developed here the steam generation system has been replaced by a 120 cm long spiral tube of 10 mm diameter in vertical orientation, all covered by heating tape (Figure 3.3). Ultrapure water is continuously provided to this water evaporation tube, using two piston pumps providing the mixing chamber with a continuous steam flow. Each piston pump is equipped with a 5 mL glass syringe and a piston made of Teflon and continuously dispenses a programmed volume of water. The two piston pumps operate in a coordinated way so that the produced steam has a steady flow rate. An example of the stability of the sample's production flow rate is shown in Figure 3.4.

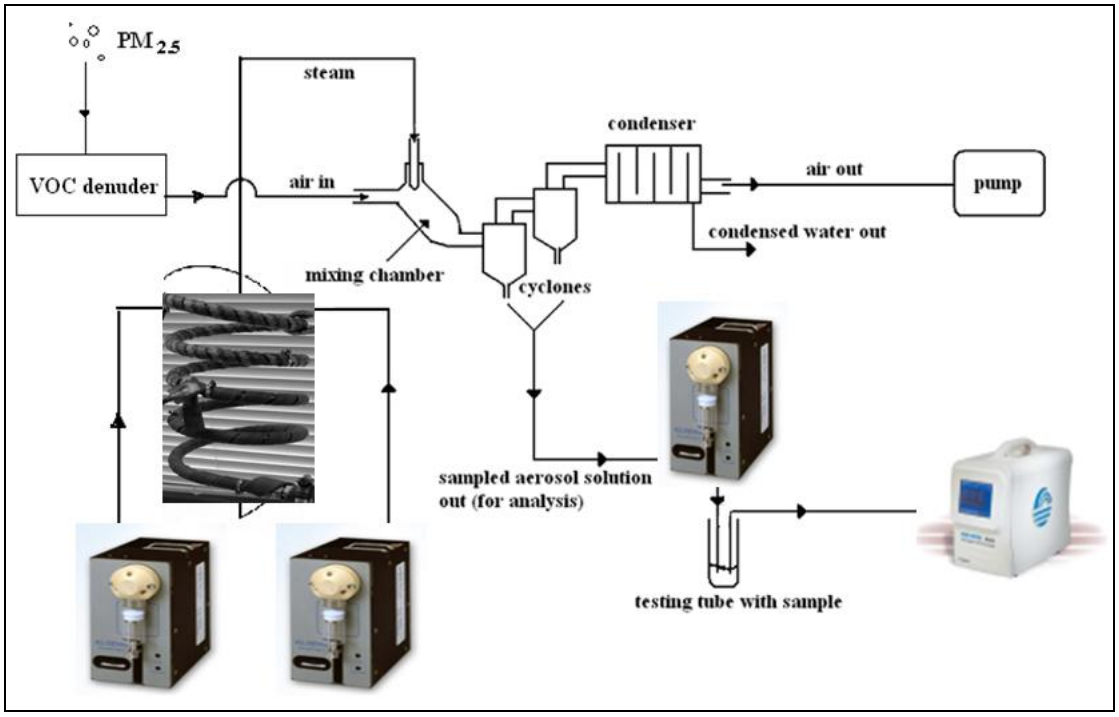

Figure 3.3: Schematic of the modified Steam Jet Aerosol Collector (Steam Sampler-TOC) developed for the WSOC measurement.

A volatile organic compound (VOC) denuder has also been added at the inlet, in order to collect the gas-phase WSOC and allow only the measurement of the particulate WSOC content.

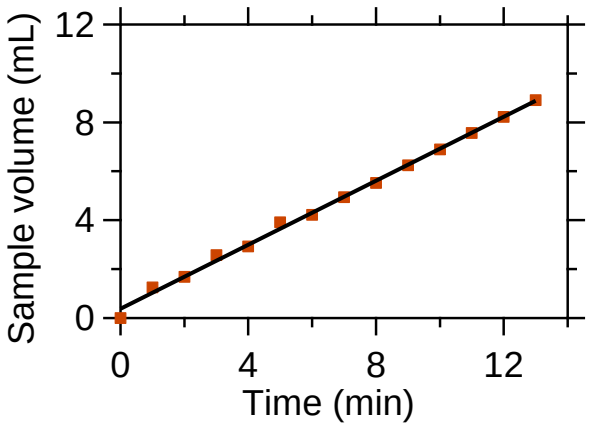

Figure 3.4: Total volume of sample flow as a function of time for the modified SJAC.

3.3 Total Organic Carbon Measurement

A commonly used instrument for the continuous measurement of the total organic carbon (TOC) is the Sievers GE TOC analyzer which offers the capability for fast on-line measurements (4 min or 4 sec in turbo mode) of the TOC content of an aqueous solution. The main parts of the instrument and the paths that the sample follows in the instrument are shown in Figure 3.5.

During the on-line operation of the instrument the sample is introduced in the analyzer via a sipper tube. After the sample introduction, a 6 M H_3PO_4 solution is injected into the sample in order to reduce the sample's pH to 2. The acidified sample is then combined with a 15% $(NH_4)_2S_2O_8$ (ammonium persulfate) solution to promote the oxidation of the organic species present in the sample and the sample travels through a mixing coil and into a stream splitter.

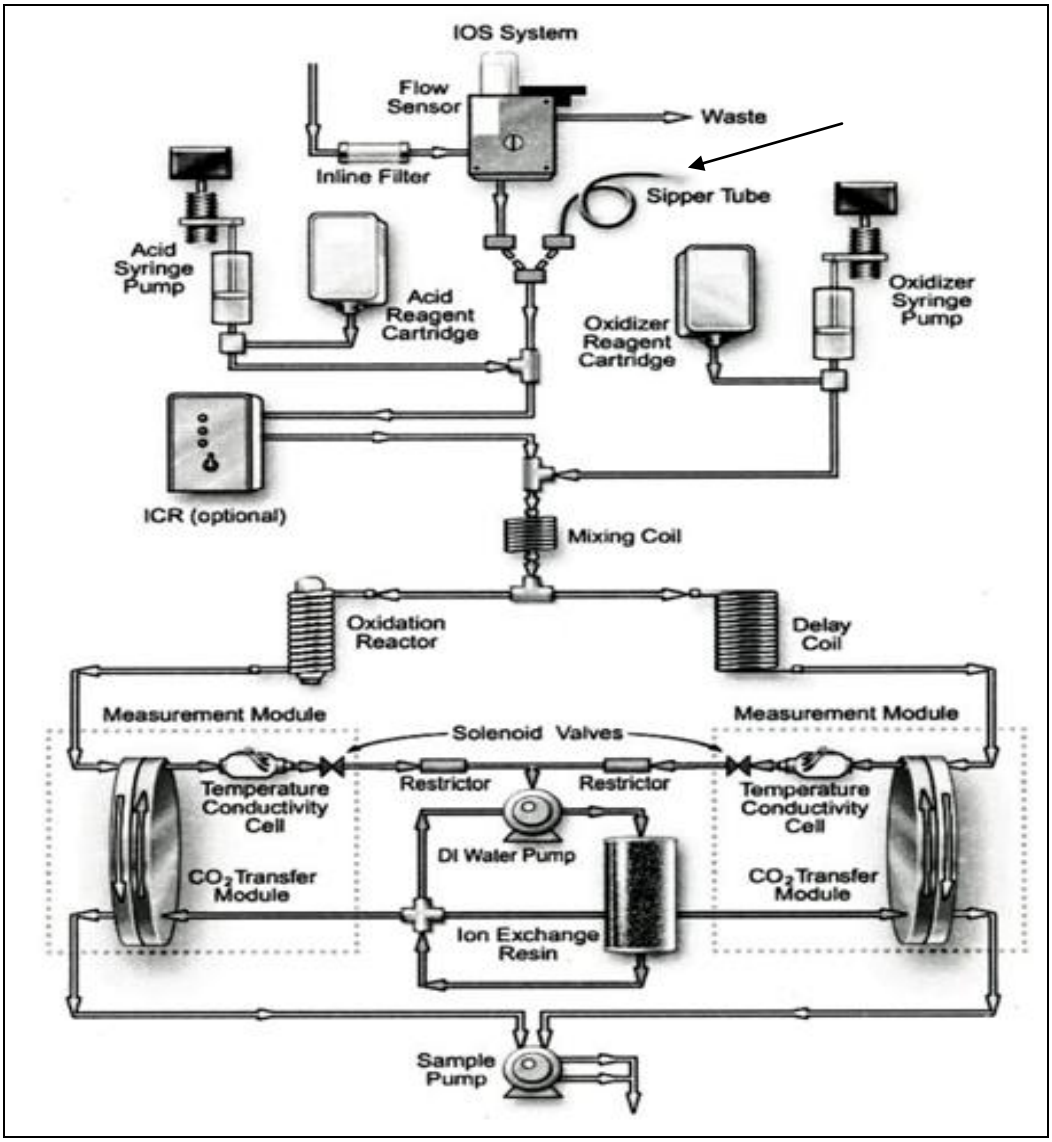

Figure 3.5: Schematic of the Sievers Total Organic Carbon Analyzer.

At the stream splitter, the sample is divided in two streams: One stream is used for the determination of the inorganic carbon content (IC) and the second for the measurement of the total carbon content (TC). The TC stream then enters the oxidation reactor, which is a spiral quartz tube wrapped around a UV lamp. The sample is thus exposed to UV light from the lamp emitting in two different wavelengths, 185 and 254 nm, resulting in complete reaction of the organic species (RH) to CO_2:

$$H_2O + hv\ (185\ nm) \rightarrow {}^{\bullet}OH + H^{\bullet} \qquad (3.1)$$

$S_2O_8^{2-} + hv\ (254\ nm) \rightarrow 2\ SO_4^{\bullet-}$ (3.2)

$SO_4^{\bullet-} + H_2O \rightarrow HSO_4^- + {}^{\bullet}OH$ (3.3)

$RH + {}^{\bullet}OH \rightarrow \ldots \rightarrow CO_2 + H_2O$ (3.4)

Both the water content of the sample and the persulfate ions promote the production of hydroxyl radicals, converting the carbon of the organic compounds to CO_2. For low TOC concentrations (< 1 ppm) the complete oxidation of the organic compounds can be achieved using only the hydroxyl radicals produced from the photolysis of H_2O.

While the TC stream is oxidized in the oxidation reactor, the IC stream passes through a delay coil, in order to have the same transit time with the TC stream through the analyzer. Afterwards, each stream is led to its respective CO_2 transfer module (Figure 3.6). The CO_2 module is a CO_2 selective gas-permeable membrane, which separates the sample side from a deionized (DI) water side and allows the transfer of CO_2 from the one side of the membrane to the other.

The DI water side is a closed loop consisting of two conductivity cells, one for the TC and one for the IC stream, a DI H_2O pump, a DI H_2O reservoir and an ion exchange resin bed. CO_2 from the sample side passes through the gas-permeable membrane into the DI water side, while the interfering compounds and oxidation by-products remain in the sample side.

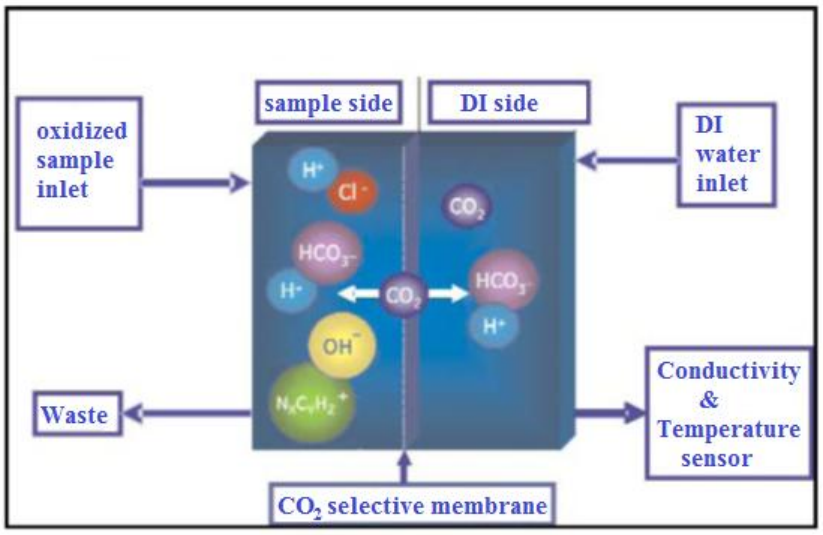

Figure 3.6: Schematic representation of the CO_2 transfer module.

The CO_2 can now form carbonic acid which rapidly dissociates to hydrogen ions and bicarbonate ions, according to:

$$CO_2 + H_2O \Leftrightarrow H_2CO_3 \Leftrightarrow H^+ + HCO_3^- \quad (3.5)$$

The reason of the initial acidification of the sample to pH values below 2 is because at this pH carbonic acid's dissociation is negligible (Figure 3.7). Bicarbonate and carbonate ion fractions are close to zero for pH below 2 and the dominant species is undissociated carbonic acid. In this way it is assured that no CO_2 produced by the oxidation of the organic species of the sample will dissociate in the acidified sample side. The produced CO_2 can then pass through the membrane to the DI side with neutral pH. There it will form carbonic acid which will dissociate to H^+ and HCO_3^-. DI water which is continuously pumped through the DI side collects the H^+ and HCO_3^- ions from the CO_2 transfer modules, delivering them to each cell for measurement of the respective conductivity. The conductivity cells contain a thermistor so that all conductivity readings are temperature corrected.

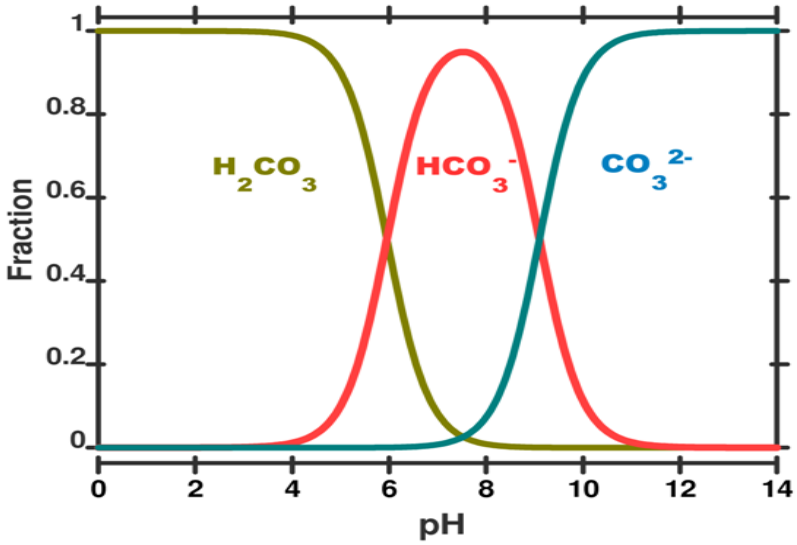

Figure 3.7: Fraction of the chemical forms of carbonic acid in water equilibrium depending on the pH. In low pH carbonic acid dominates while in pH>6 the HCO_3^- and CO_3^{-2} ions are dominant.

Finally, the conductivity readings of the TC and IC stream caused by the CO_2 present in each stream are converted to carbon concentration using calibration curves and the TOC is calculated as the difference of IC concentration from the corresponding value of TC.

3.4. Evaluation – Sampling efficiency

In order to evaluate the sampling efficiency of the redesigned Steam Sampler the setup of Figure 3.8 was used. A 0.01 g L^{-1} sucrose solution was prepared and was used into a syringe pump. The syringe pump provided the atomizer with a steady flow of the sucrose solution. In the atomizer compressed air expands through an orifice, forming a high-velocity jet in the atomizing section. There it meets with the liquid, leading to the formation of solute droplets.

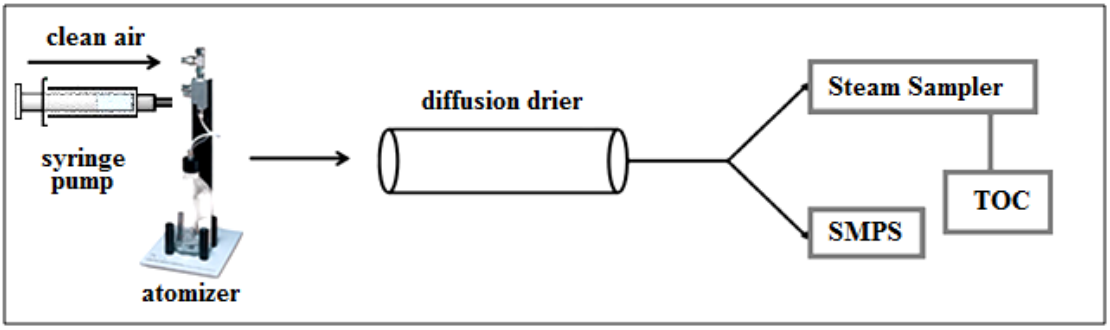

Figure 3.8: Schematic of the setup used for the evaluation of the sampling efficiency of the Steam Sampler-TOC.

The water droplets pass afterwards through a long silica gel diffusion drier where the water evaporates. The dried particles are thereafter led to the Steam Sampler for the measurement of the total water soluble organic content and to a Scanning Mobility Particle Sizer (SMPS) for the measurement of the size distribution of the particles. Since the solubility of sucrose is very high (2000 g L^{-1}) all particle mass should be measured as WSOC. The volume concentration measured by the SMPS should then correspond to the WSOC measurement.

An SMPS consists of two parts: a Differential Mobility Analyzer (DMA) and a Condensation Particle Counter (CPC). First a radioactive bipolar charger (e.g., ^{210}Po, ^{85}Kr) establishes a bipolar equilibrium charge distribution on the particles. Particles receive either positive, negative, or zero charge(s). Next, the particles enter the DMA and they are separated according to their electrical mobility. This parameter is inversely related with the particle size and is proportional to the number of charges present on the particle. The classifier separates aerosol particles by size for high resolution measurements of particle size distribution. The monodisperse aerosol exiting the classifier passes to CPC which measures the particle number concentration. By scanning quickly a wide size range (typically 20 nm to 500 nm depending on the configuration)

the result is the size distribution of the aerosol particles generated from the atomization system. Using the density of the particles the mass concentration of the aerosol sample may be estimated.

The setup shown in Figure 3.8 enables the simultaneous measurement of the water soluble sucrose particles in an air stream, by two different instruments, the Steam Sampler which gives one measurement of WSOC concentration every 4 min and one by the SMPS every 3 min.

The TOC analyzer measurements are expressed in mass of carbon per unit volume of the liquid or air sample. In order to convert the carbon mass to organic mass, the relative abundance of C in the sucrose ($C_{12}H_{22}O_{11}$) molecule is used. One mole contains 144 g of C and weighs 342.3 g. By multiplying the measured carbon mass concentration by 2.38, the TOC readings are converted to sucrose mass concentration. The SMPS number distribution is converted to volume concentration assuming spherical particles and then to mass concentration by multiplying with the sucrose's density of 1.59 g cm^{-3}.

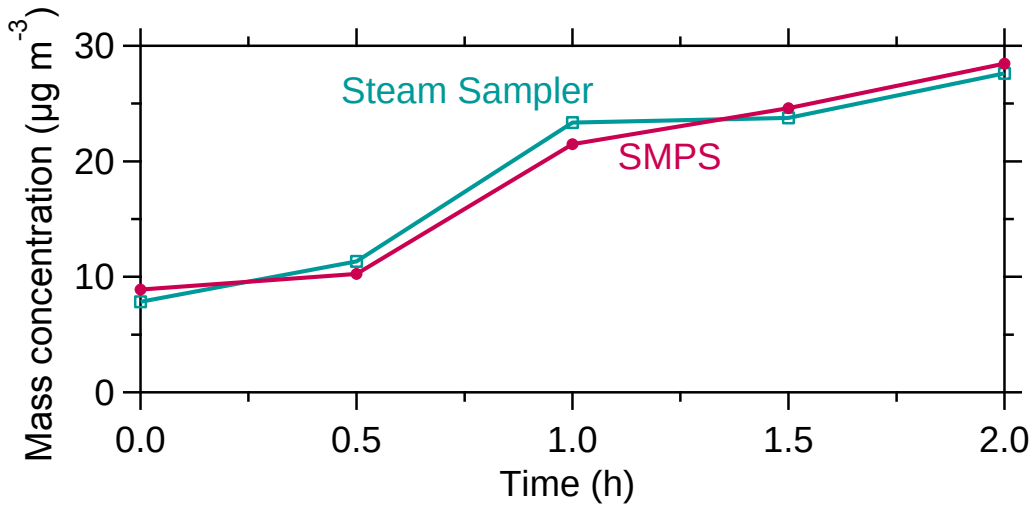

Figure 3.9: Mass concentration of sucrose particles measured by the Steam Sampler and the SMPS.

The time series of measurements of sucrose mass concentration by the Steam Sampler-TOC and the SMPS are presented in Figure 3.9. The points correspond to 30 min averages. The mass concentration of the sucrose aerosols measured by the Steam Sampler and the SMPS are consistent. The two measurements are within 10% of each other (Figure 3.10).

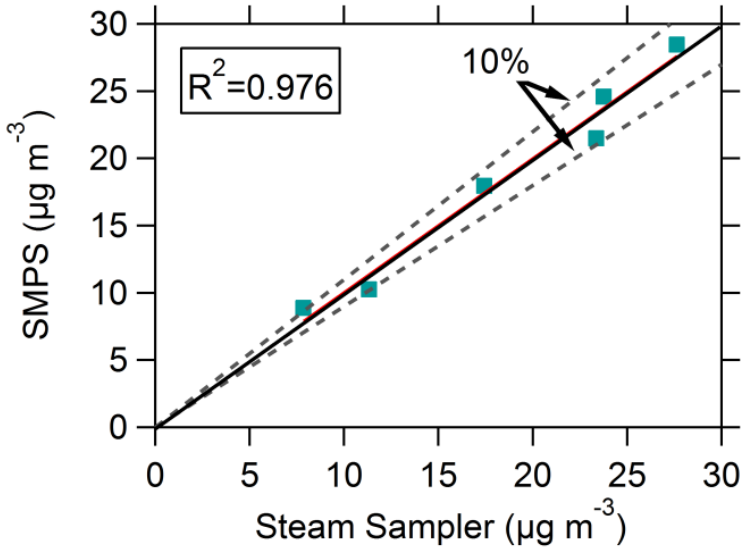

Figure 3.10: Comparison of 30-min averaged simultaneous measurements of sucrose particle mass concentrations by the SMPS and the modified Steam Sampler. Dashed lines correspond to 10% deviation from unity.

3.5 Field-testing of the Steam Sampler-TOC

We tested this system in Patras, by sampling ambient aerosol during June 2012. The sampling site was located approximately 10 km from the city center. Simultaneously, a high-resolution aerosol mass spectrometer (HR-AMS) was continuously monitoring non-refractory organic and inorganic mass in PM_1 particles.

A $PM_{2.5}$ cyclone (URG) was placed in front of the sampler's inlet. An activated carbon denuder was used after the cyclone to remove organic vapors. The role of the cyclone is to eliminate particles larger than its cut-off point. The URG cyclone used has a nominal

cut-off point at 2.5 μm for 16.7 L min^{-1} sample flow rate. The steam sampler was operating with an average inlet flow rate of 13.6±0.6 L min^{-1} during the measurements, leading to a cut-off point close to 3 μm, according to Figure 3.11. The sample flow rate was measured daily.

The *P* parameter discussed in Chapter 2 which describes the WSOC measurement from filters, expresses the availability of water for the dissolution of the sampled aerosols on filters (Psichoudaki and Pandis, 2013). For the on line measurement, the *P* parameter may be estimated from Equation 3.1:

$$P=V_w/Q \quad (3.1)$$

where V_w is the volume of liquid water ejected as steam per min and *Q* is the sampling flow rate.

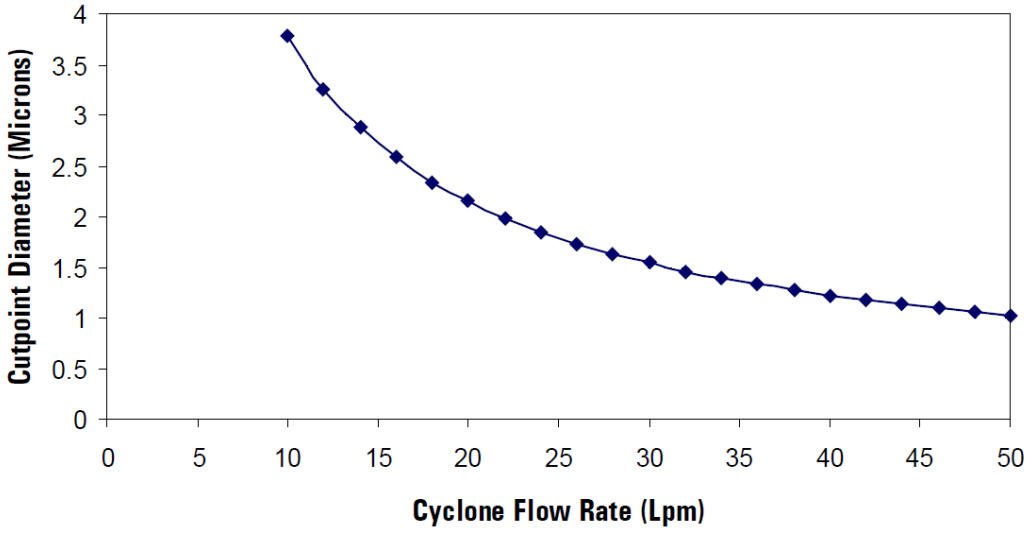

Figure 3.11: Cut-off diameter of URG $PM_{2.5}$ cyclone for different flow rates.

The system vaporizes 0.6 mL of water per minute, which is mixed with the air sample, entering the instrument with an average flow rate of 13.6 L min^{-1}. Thus the *P* parameter of the Steam Sampler is equal to 44.1 cm^3 m^{-3}. This is a rather high *P* parameter value,

however, the order of magnitude of the *P* parameter is determined by the minimum sample volume necessary for TOC measurement which is 0.5 mL and the cyclone which operates with low sample volumes. The "ideal organic solution model" (Chapter 2) predicts that using this *P* parameter in low organic aerosol concentrations (1-10 μg m^{-3}) species with solubility exceeding 10^{-4} g L^{-1} (Figure 3.12). In this case some relatively soluble PAHs will be accounted as WSOC, such as naphthalene, phenanthrene and acenaphthene (See Table 2.2).

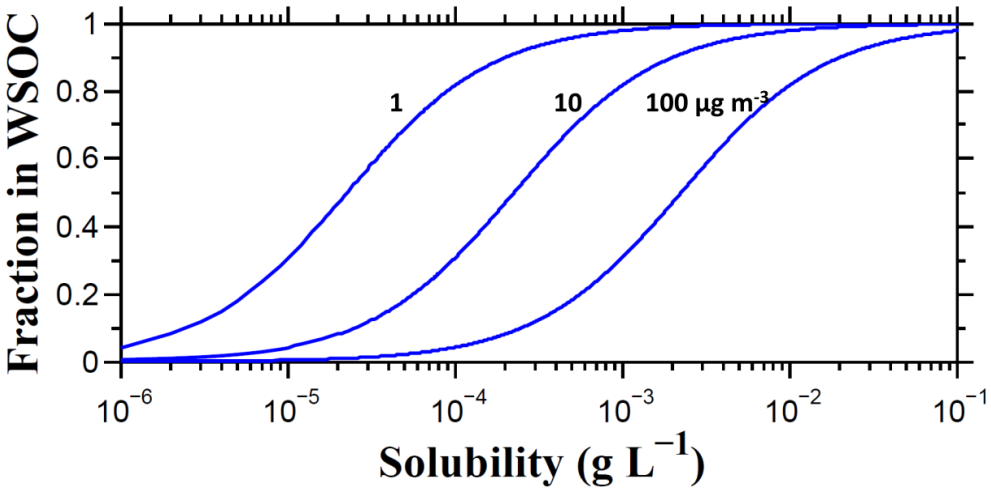

Figure 3.12: Fraction of a compound in WSOC versus its solubility, for different water insoluble organic aerosol concentrations (1, 10, 100 μg m^{-3}) according to the ideal organic solution model.

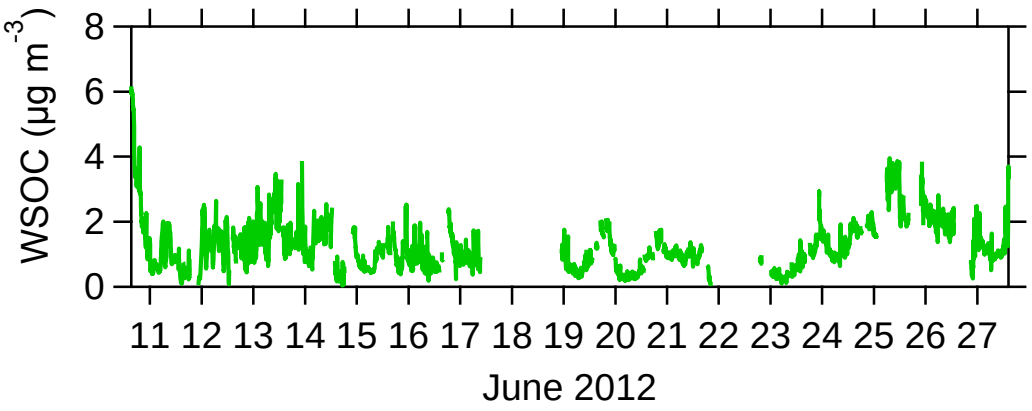

Figure 3.13: Time series of the WSOC concentration measured by the Steam Sampler.

The time series of the WSOC concentration is shown in Figure 3.13. The average WSOC concentration during the sampling period was 1.24 ± 1.4 μg C m^{-3}.

Analysis of the high resolution AMS data allows for the calculation of the organic mass to organic carbon ratio, OM:OC. The organic aerosol (OA) mass may then be calculated, by multiplying the WSOC concentration with the OM:OC ratio assuming that the same ratio applies to both soluble and insoluble OC. This is clearly a zeroth order approximation. The average OM:OC ratio for the total sampling period was 2.0. This ratio was estimated with 2 hour time resolution and was multiplied by the WSOC concentration. The water soluble organic mass (WSOM) time series is shown in Figure 3.14. On average, the WSOC measured was 66% of the total OA in PM_1.

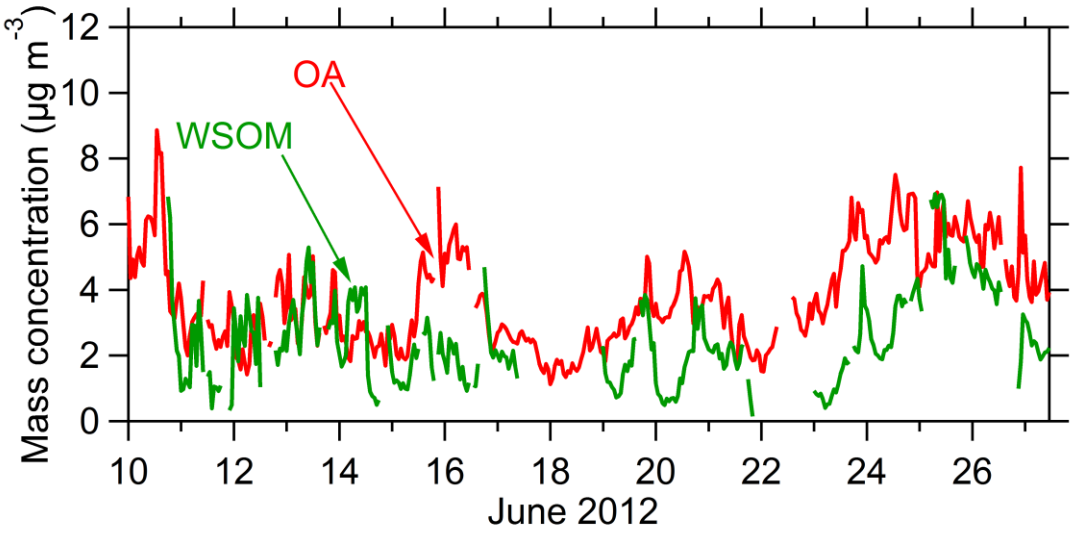

Figure 3.14: Time series of the WSOC concentration measured by the Steam Sampler and the organic aerosol mass (OA) measured by the AMS.

The diurnal profile of OA in PM_1 and the water soluble organic mass (WSOM) of PM_3 are shown in Figure 3.15. OA concentrations presented a peak in the morning (7:00-10:00), dropped in the evening and presented a second sharper peak at night between 20:00-23:00. The WSOM showed a peak in the afternoon (around 16:00) probably due

to photochemistry. The weak correlation found between OA and WSOA (R^2=0.25) was expected as WSOM expresses part of the OA mass, however, WSOM and OA have different sources.

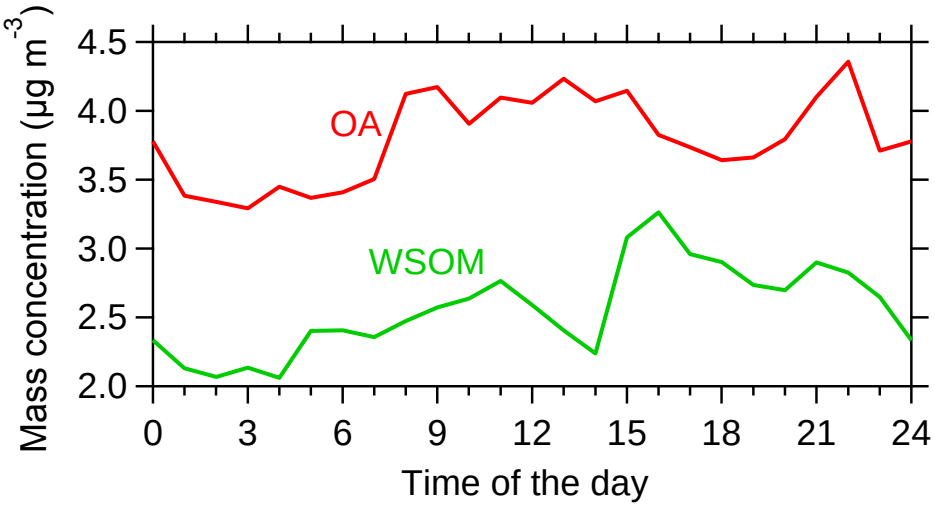

Figure 3.15: Diurnal profiles of the atmospheric organic aerosol (OA) and the water soluble organic aerosol (WSOM).

Applying positive matrix factorization on the high resolution data from the AMS the oxygenated part of the organics (OOA) can be estimated.

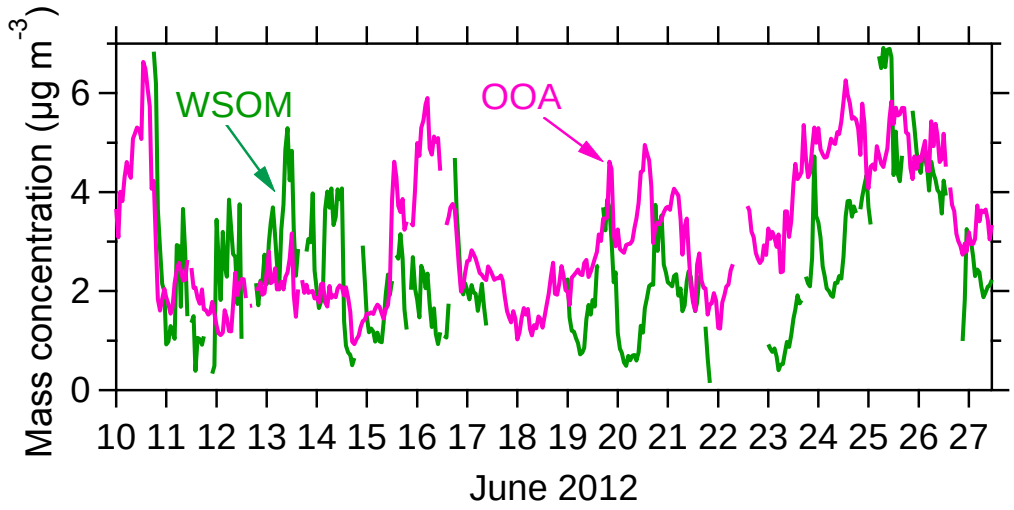

Figure 3.16: Time series of the WSOC concentration measured by the Steam Sampler and the oxygenated organic mass concentration measured by the AMS.

According to Figure 3.16, from 10 to 15 of June the water soluble organic mass in PM_3 was higher than the oxygenated fraction in PM_1, while the opposite happens for the rest of the sampling period. During the same time period WSOM concentrations correlate significantly (R^2=0.50) with OA (Figure 3.14), indicating that less water soluble species compared with OOA can be measured by the Steam Sampler-TOC.

3.6 Conclusions

We developed a new system for the continuous measurement of the water soluble organic carbon of the atmospheric aerosols. The system provides measurements of the WSOC concentrations every 4 minutes and collects particles with diameter less than 3 μm. The *P* parameter of this WSOC measurement method was estimated to be 44.1 cm^3 m^{-3}. Evaluation experiments have been conducted in order to test the efficiency of the system to sample water soluble species. Sucrose particles were measured by the Steam Sampler and an SMPS. The corresponding measurements were in agreement (within 10%).

The instrument was also tested in field measurements in a background site outside of Patras. The Steam Sampler measurements showed that WSOC concentration was on average 1.2 μg C m^{-3} during June 2012. This concentration corresponds to 2.46 μg m^{-3} of organic mass. The WSOM measured in PM_3 corresponds to 66% of the organic mass measured by the AMS in PM_1 particles, which was on average 3.7 μg m^{-3}. Since the measurements were conducted during summer, a significant fraction of the organic mass is expected to be water soluble and this percentage is reasonable. However, an accurate estimation of the water soluble fraction was impossible since the two instruments measure in different size ranges. The correlation between the WSOM and the OOA was

poor (R^2=0.17) and this can be partially attributed to the different cut-off point of each system. Another reason could be the high *P* parameter of the system which may have allowed the collection of low-solubility organics. However, the decrease of the *P* parameter of the on-line techniques is challenging because of the relatively high minimum liquid sample volume necessary for TOC analysis as well as the low air sampling rate.

3.8 References

Anderson, C., Dibb, J.E., Griffin, R.J., Bergin, M.H. Simultaneous measurements of particulate and gas-phase water-soluble organic carbon concentrations at remote and urban-influenced locations. *Geophys. Res. Lett*., **2008**, *35*, L13706, doi:10.1020/2008GL033966.

Khlystov, A., Wyers, G.P., Slanina, J. The steam-jet aerosol collector. *Atmos. Environ*., **1995**, 29, No 17, 229-234.

Kondo, Y., Miyazaki, Y., Takegawa, N., Miyakawa, T., Weber, R.J., Jimenez, J.L., Zhang, Q., Worsnop, D.R. Oxygenated and water-soluble organic aerosols in Tokyo. *J. Geophys. Res.*, **2007**, 112, D01203, doi:10.1029/2006JD007056.

Kostenidou E., Thesis. Usage of aerosol mass spectrometry for the measurement of physical and chemical properties of atmospheric nanoparticles, University of Patras, **2010**.

Miyazaki, Y., Kondo, Y., Takegawa, N., Komazaki, Y., Fukuda, M., Kawamura, K., Mochida, M., Okozawa, K., Weber, R.J. Time-resolved measurements of water-soluble organic carbon in Tokyo. *J. Geophys. Res.* **2006**, *111*, D23206, doi:10.1029/2006JD007125

Psichoudaki M., Pandis, S.N. Atmospheric aerosol water soluble organic carbon: A theoretical analysis. *Environ. Sci. Technol*., **2013**, 47, 9791-9798.

Sievers 900 portable total organic carbon analyzer. Operation and maintenance manual, GE Analytical Instruments, **2008**.

Sullivan, A.P., Peltier R.E., Brock, C.A., De Gouw, J.A., Holloway, J.S., Warneke, C., Wollny, A.G., Weber, R.J. Airborne measurements of carbonaceous aerosol soluble in water over northeastern United States: Method development and an investigation

into water-soluble organic carbon sources. *J. Geophys. Res.*, **2006**, *111*, doi: 10.1029/2006JD007072.

Sullivan, A.P., Weber, R.J., Clements, A.L., Turner, J.R., Bae, M.S., Schauer, J.J. A method for on-line measurement of water-soluble organic carbon in ambient aerosol particles: Results from an urban site. *Geophys. Res. Lett.,* **2004**, *31*, L13105, doi:10.1029/2004GL019681.

Weber, R J., Orsini, D., Duan, Y., Lee, Y.-N., Klotz, P. J., and Brechtel, F. A particle-into-liquid collector for rapid measurement of aerosol bulk chemical composition. *Aerosol Sci. and Technol.,* **2001**, 35, 718-727.

Chapter 4

Hygroscopic properties of biomass burning organic aerosol in Athens during winter

4.1 Introduction

Atmospheric aerosols play an important role in the Earth's atmosphere, affecting the local and global climate (Vestin et al. 2007). Aerosol particles can affect the global radiation budget by scattering solar radiation and thus have a direct cooling effect on the planet. On the other hand, depending on their physical and chemical properties, aerosols can serve as cloud droplet condensation nuclei (CCN) becoming cloud droplets at water vapor supersaturation conditions and can indirectly affect climate by modifying the cloud reflectivity (Kaufman et al., 2002; Cerully et al., 2011 and references therein). The indirect effect of atmospheric particles on climate depends on their size and hygroscopic properties (Fors et al., 2010). Increased concentrations of CCN result in the formation of more but smaller cloud droplets (Rose et al., 2005; Vestin et al., 2007) which can lead to the suppression of precipitation and the increase of cloud lifetimes and cloud cover (Vestin et al., 2007; Rosenfeld et al., 2008; Fors et al., 2010).

Biomass burning emissions are a major source of fine atmospheric particles on a global scale (Andreae and Rosenfeld, 2008). Main sources include forest fires and domestic wood burning for heating and cooking (Martin et al., 2013). These particles represent a significant fraction of global CCN. Some of the highest CCN concentrations have been observed in biomass burning influenced areas (Hennigan et al., 2012). Biomass burning particles consist mainly of organic species and black carbon. They also contain low concentrations of inorganic species, representing less than 15% of the particle mass. The extent of the contribution of inorganic components depends on fuel composition and the efficiency of the burning process (Reid et al., 2005). The chemical composition of aerosols originating from biomass burning is in general related to the conditions of the combustion of the fuel (Vestin et al., 2007).

Biomass burning organic aerosols (BBOA) can be both primarily emitted, but also can be formed by the oxidation of gaseous organic emissions and subsequent condensation, leading to the formation of secondary aerosol. The chemical aging process of BBOA also includes heterogeneous oxidation of the organic aerosol, condensed-phase reactions and cloud-processing. While primary combustion emissions are in general hydrophobic, the BBOA is relatively hygroscopic and can serve as CCN (Semeniuk et al., 2007). Atmospheric aging of combustion emissions can lead to the increase of their hygroscopicity. In general, the hygroscopicity of organic aerosol increases as it is oxidized in the atmosphere. The organic aerosol O:C (atomic oxygen to carbon) ratio is an indicator of its oxidation state. Water soluble organic carbon (WSOC) represents a large fraction of the BBOA emitted in poor combustion conditions. WSOC is quite hygroscopic and increases the CCN ability of the particles (Vestin et al. 2007).

Biomass burning emissions have also important impacts on regional air quality. The presence of an inversion layer often leads to the trapping of the particles in the lower atmosphere where they can remain for extended periods of time. The contribution of biomass burning to the concentration of the organic aerosols during air pollution episodes was found to be around 40% in Beijing and 70% in a rural site in Austria (Duan et al., 2004; Caseiro et al., 2009). BBOA was also found to be a significant contributor to organic aerosol concentrations in Paris, with a contribution up to 15%, while its contribution in the southeastern US close to 30% during winter (Zhang et al., 2010; Crippa et al., 2013).

In order to understand the impact of biomass burning emissions on climate, the hygroscopic properties of the corresponding particles must be known. The evaluation of

the hygroscopic and CCN properties of BBOA is necessary to further understand the role of such particles in cloud formation processes. In this work, we investigate the hygroscopic properties of fresh and aged biomass burning particle emissions in an urban environment, the center of Athens, during winter of 2013, when wood burning in fireplaces for domestic heating was a dominant source.

4.2 Sampling site

Athens is a city of around 4 million residents. The city is surrounded by mountains to the north, west and east. It has significant air quality problems due to its population density, the meteorology and the morphology of the area (Andreou and Rapsomanikis, 2009). Sampling was conducted at the National Observatory of Athens (NOA site, 37°58′23.99″N 23°43′12″E) located on a hill, at the center of Athens, from 12 January to 7 February of 2013. The data from an almost continuously rainy week were excluded from the following data processing in order to focus mainly on the effect of biomass burning in the urban atmosphere of Athens. The following results are based on the data collected during 10-15 January and 23 January to 7 February of 2013.

4.3 Experimental Setup

The hygroscopic properties of the aerosols were measured using a Cloud Condensation Nuclei Counter (CCNC, DMT Technologies, Roberts and Nenes, 2005). Simultaneously, a High-Resolution Time-of-Flight Aerosol Mass Spectrometer (HR-ToF-AMS, Aerodyne Research Inc, De Carlo et al., 2006) was continuously monitoring the chemical composition of PM_1 particles. The AMS also provides the size distribution of the particles.

4.3.1 CCN counter description

The CCN counter used is based on the principle that the diffusion of heat is slower than the diffusion of water vapors in air media. The basic part of the DMT CCN counter is its column (Figure 4.1).

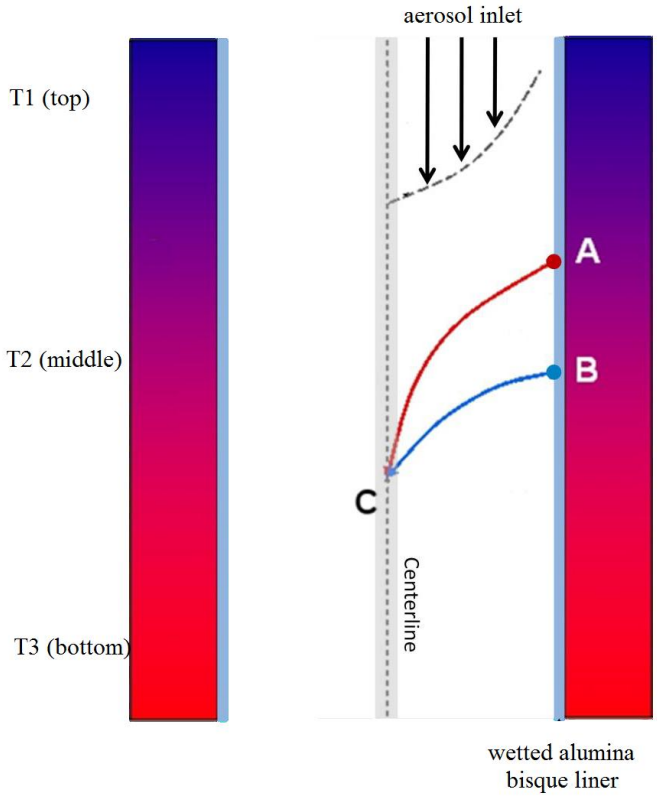

Figure 4.1: Illustration of the DMT CCN counter column.

The column is designed in a way that a well-controlled and relatively uniform centerline supersaturation is achieved. The aerosol sample is driven through the centerline of the column and sheath air flows close to the column walls. The inside of the CCN column is constructed of alumina bisque, is temperature controlled and wetted. The temperature of the walls is lower close to the inlet of the column and increases towards the exit.

Water vapor diffuses from the warm wetted surface of the walls towards the centerline (Figure 4.1) faster than heat does (Roberts and Nenes, 2005). In Figure 4.1, the diffusing

vapor mass originating from point B reaches C faster than the diffusing heat originating from point A. Assuming that the column walls are saturated with water at all points and the temperature at point A is lower than that at point B, the water vapor partial pressure is also greater at point B compared to point A. The water vapor partial pressure at point C is equal to the partial pressure at point B. However, the temperature at point C is lower than the temperature at point B, so more water vapor is present at point B than thermodynamically allowed. Supersaturated water vapor condenses on cloud condensation nuclei as the air sample travels through the column to form droplets. Based on a size-scattering technology an optical particle counter records the counts and the size of the activated droplets.

The column is placed vertically in the instrument and the aerosol sample enters the column from the top. As column walls temperature increases from top to the bottom, aerosol particles are exposed gradually to supersaturation. The sample stream travels through the centerline where the supersaturation is highest as filtered humidified air (sheath flow) flows around the sample. A total flow of 0.5 L min^{-1} of air is sampled, part of which is used to produce the sheath flow after filtration and humidification.

Roberts and Nenes (2005) showed that the centerline supersaturation depends on the temperature difference between the top and the bottom of the column, the flow rate and the pressure inside the column. Three temperature controllers are used to control temperature so that it increases from the top zone to the bottom zone. This allows supersaturation conditions to occur as well as to alter fast between different supersaturations. In general, 30 sec are required for a supersaturation shift. The Optical Particle Sizer (OPC) measures the number and the size of the activated droplets formed

in the column. A diode laser emitting at 660 nm is used as a light source and the OPC measures the number of droplets of a size range between 0.75 and 10 μm and classifies their size in 20 size bins.

4.3.2 Scanning Mobility CCN Analysis (SMCA)

The CCN counter was coupled with a Differential Mobility Analyzer (DMA) and a Condensation Particle Counter (CPC) to provide additional information about the CCN activity of ambient particles. Ambient air was dried by passing through a diffusion drier (RH<5%) and afterwards was introduced in the DMA (TSI 3080). The size-classified aerosol exiting the DMA was split in two, to the CPC (TSI 3787) measuring the total number concentration of particles or Condensation Nuclei (CN) and to the CCN counter (DMT Technologies) which measured the CCN number concentration (Figure 4.2).

The classifier and the CPC are parts of the Scanning Mobility Particle Sizer (SMPS). The supersaturation in the column of the CCNC was stepped in increments of ~0.2%, ranging from 0.19 to 0.91% and changed every 12 min, enabling the data collection of at least 4 SMPS scans (total duration 135 sec each) for each supersaturation. The deviation of the CFSTG flow chamber temperature from the nominal was checked for each scan and scans with temperature deviation more than 15% were discarded.

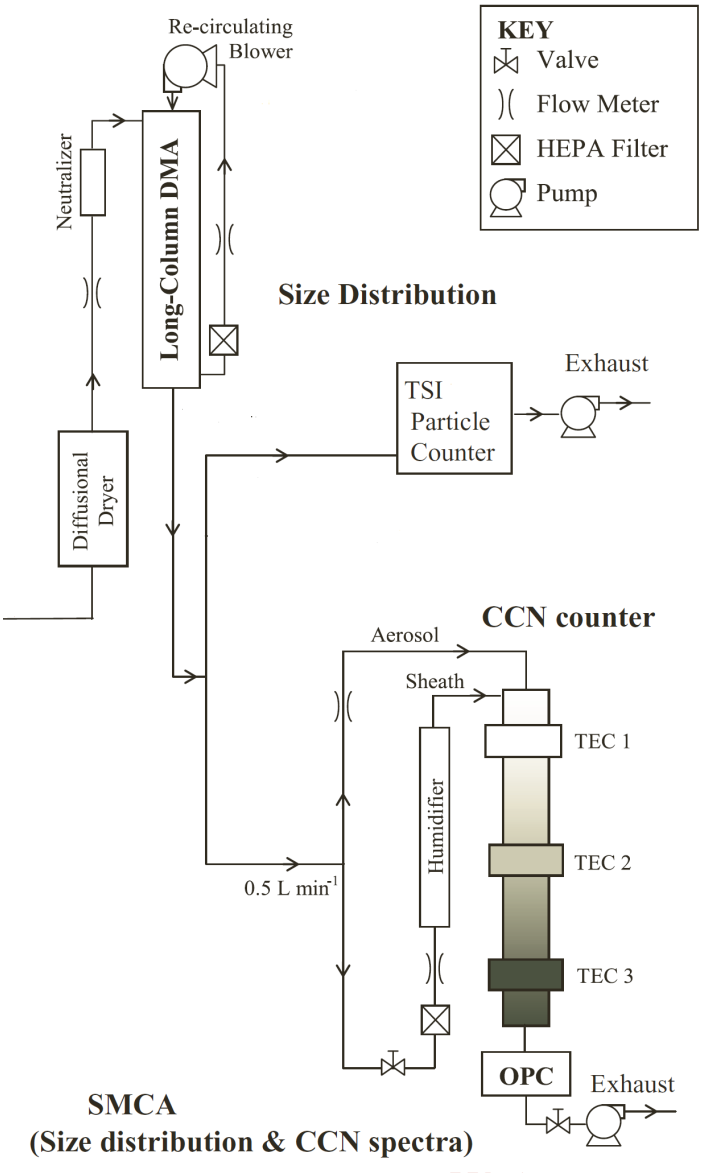

Figure 4.2: Schematic of the SMCA experimental set-up.

4.3.3 Chemical composition measurements – AMS

A High-Resolution Time-of-Flight Aerosol Mass Spectrometer (HR-ToF-AMS) was used in Athens 2013 campaign to measure the concentration of non-refractory species of PM_1: sulfate, nitrate, chloride anions, ammonium and potassium anions and organic species (De Carlo et al., 2006). This instrument provides the mass concentration time series of the above species, as well as the organic aerosol mass spectra, offering extra

information about the "age" and the oxidation state of organic species. This additional information include the atomic oxygen or hydrogen to carbon (O:C or H:C) ratios. Positive Matrix Factorization was used to categorize the data in order to estimate different particle sources (Ulbrich et al., 2009). The AMS also measured the size/composition distribution of the aerosol. During the campaign, the AMS provided 6-minute resolution measurements.

4.3.4 Analysis of SMCA data

The DMA was running from low to high voltages, enabling a monodisperse aerosol flow to exit the DMA column each time. During a scan (135 sec) the DMA selected particle sizes from 10 to 500 nm. The total number concentration of each size bin was recorded by the CPC and the CCN concentration by the CCNC, thus the total number concentration (CN) and CCN distributions were obtained. Afterwards the two distributions were carefully aligned (Figure 4.3).

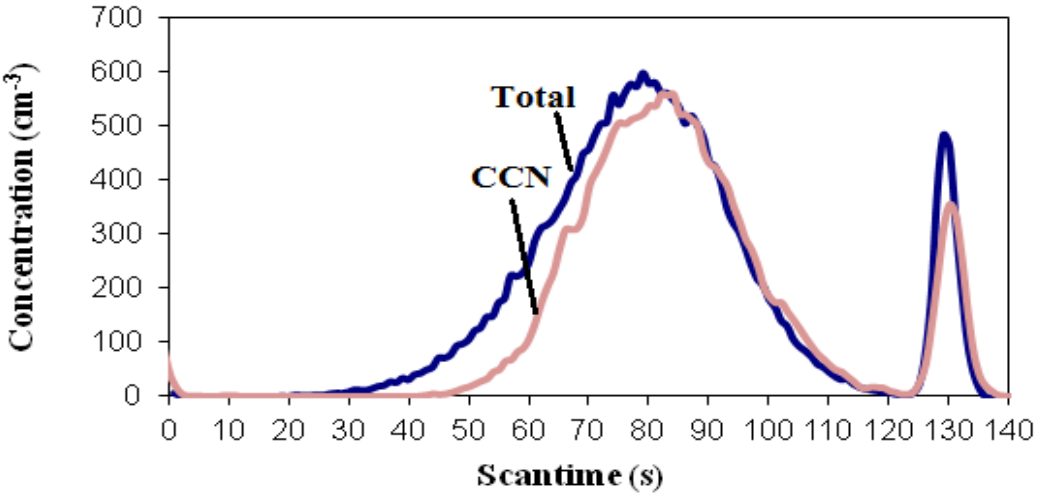

Figure 4.3: Example of aligned SMPS and CCN measurements during the same scan. The blue curve measured by the CPC represents the total number concentration and the pink measured by the CCN counter the CCN number concentration.

The Aerosol Instrument Manager (AIM) software (TSI, Inc) was used to convert the particle number measurements to size distribution. The same inversion technique was applied to the CCN time series to obtain the CCN size distribution. For constant supersaturation of the instrument and by dividing the CCN number concentration by the total number concentration of particles for each diameter d_p, the corresponding activation fraction CCN/CN versus d_p was obtained (Figure 4.4).

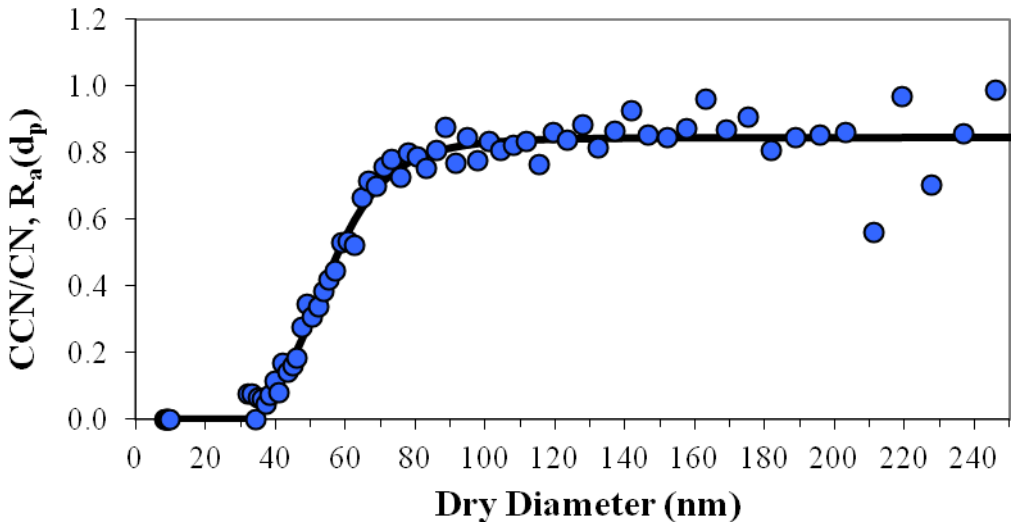

Figure 4.4: Example of activation ratio CCN/CN (blue dots and sigmoid fit (black line) versus particles dry diameter at a supersaturation of 0.8%.

The activation ratio function $R_a(d_p)$ was fit to a sigmoidal function:

$$R_a(d_p) = \frac{CCN(d_p)}{CN(d_p)} = \frac{E}{1+(\frac{d_{p50}}{d_p})^C} \quad (4.1)$$

where E corresponds to the asymptote of $R_a(d_p)$, d_p is the particle diameter, d_{p50} is the characteristic dry diameter for which 50% of the particles activate (activation diameter) and C an empirical coefficient. A similar fitting can be performed for the measurements at a specific particle size using the supersaturation S as an independent variable. The corresponding activated fraction $R_a(S)$ is expressed by Equation 4.2:

$$R_a(S) = \frac{CCN(S, d_p = const)}{CN(d_p = const)} = \frac{E^*}{1 + (\frac{S}{S^*})^{C^*}} \tag{4.2}$$

where E^* refers to the asymptote of the sigmoid and expresses the maximum fraction of particles that activate at high supersaturations, S is the instrument supersaturation, S^* is the critical supersaturation, at which half of the particles activate. C^* is a fitting constant which is proportional to the slope of the sigmoid function and expresses the chemical heterogeneity of the activated particles. An example of the CCN ratio versus the supersaturation is shown in Figure 4.5.

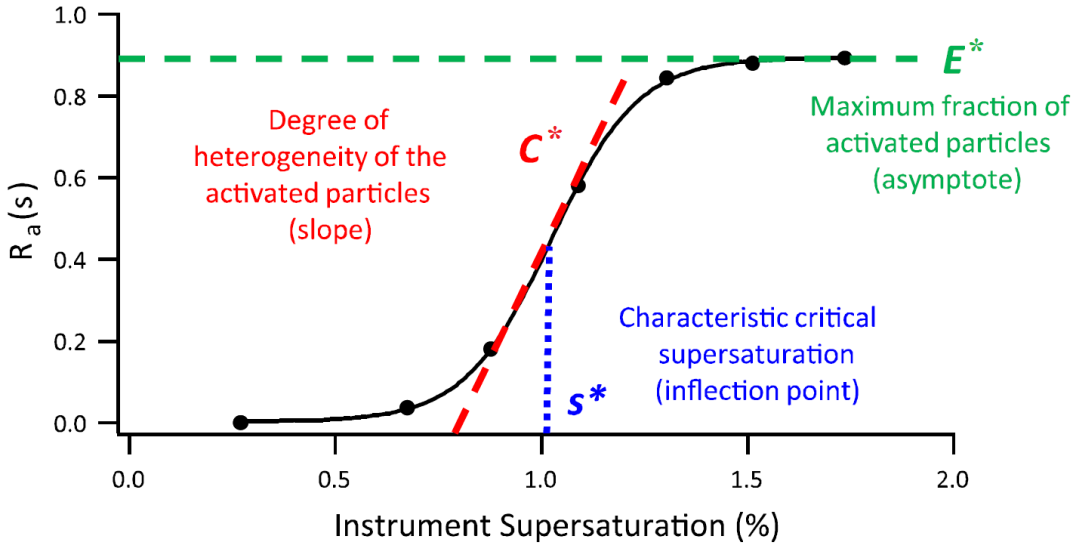

Figure 4.5: Example of activation ratio function versus the instrument supersaturation. The slope of the sigmoid C*, the critical supersaturation S* and the asymptote E* are shown (Cerully et al., 2011).

The activation ratio function, $R_a(s)$ represents the cumulative distribution of critical supersaturation of particles with a specific dry diameter d_p.

Petters and Kreidenweis (2007) introduced as a measure of the hygroscopicity of the material of an aerosol a hygroscopicity factor, κ:

$$\kappa = \frac{4A^3}{27 d_p^3 S^2} \tag{4.3}$$

where $A=4M_w\sigma_w/(RT\rho_w)$, M_w, σ_w, ρ_w is the molecular weight, surface tension and density of water, R the universal gas constant and T the average temperature in the CCNC column. Equations 4.2 and 4.3 can be combined to provide the hygroscopicity-dependent activation ratio function:

$$R_a(\kappa) = \frac{CCN(\kappa, d_p)}{CN(\kappa, d_p)} \frac{E^*}{1+(\kappa^*/\kappa)^{C^*/2}} \tag{4.4}$$

The probability distribution function of κ, p(κ), can be estimated by differentiating and normalizing Equation 4.4 (Cerully et al. 2011; Bougiatioti et al. 2011):

$$p(\kappa) = \frac{1}{E}\frac{dR_a(\kappa)}{d\kappa} = -\frac{\frac{C}{2\kappa^*}(\kappa/\kappa^*)^{\frac{C}{2}-1}}{(1+(\kappa/\kappa^*)^{C/2})^2} \tag{4.5}$$

The standard variation of κ, *σ(κ)*, is also calculated for the same set of measurements. The dispersion of the hygroscopicity parameter expresses the degree of heterogeneity (chemical dispersion) of particles with a diameter dp and is calculated as the square root of the variance of the hygroscopicity around κ* (Lance et al. 2007). One value of κ*±σ(κ) every one hour (5 different supersaturations x 12 min each) is obtained.

$$\sigma^2(\kappa) = \frac{\int_0^\infty (\kappa-\kappa^*)^2 p(\kappa) d\kappa}{\int_0^\infty p(\kappa) d\kappa} \tag{4.6}$$

4.3.5 Calibration of the CCN counter

The basic part of a CCN counter is its column, where the supersaturation is achieved. The calibration of the instrument supersaturation was done by the determination of the critical diameter D_{pc} of $(NH_4)_2SO_4$ particles that activate at the nominal supersaturation of the instrument.

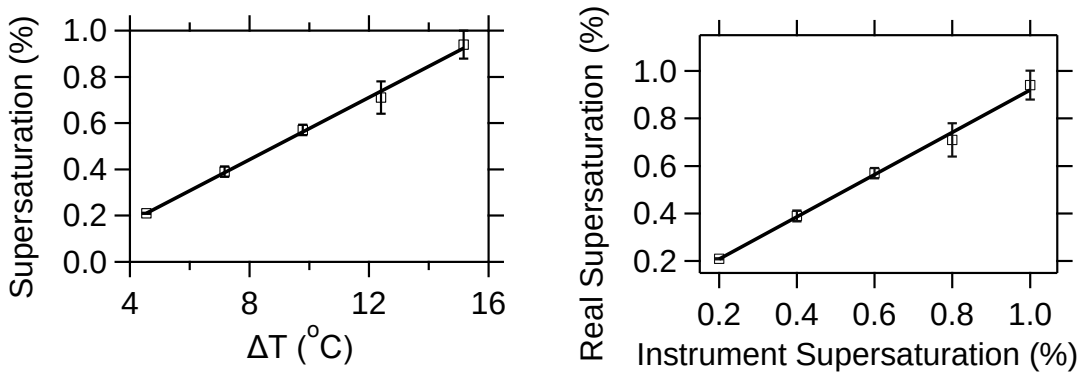

Figure 4.6: (a) CCN-column supersaturation versus ΔT and (b) nominal supersaturation versus real supersaturation in the column. Error bars show the standard deviation of the supersaturation which corresponds to 4 or 5 measurements.

A dilute ammonium sulfate solution was prepared and used in a syringe pump. The syringe pump provided continuously with the solution an atomizer, which produced wet ammonium sulfate particles. The air stream containing the particles afterwards passed through the diffusion drier so that dried particles exited the drier and were introduced to the classifier (Figure 4.2). As in the measurement mode (see section 4.3.2), total (CN) and activated (CCN) particles were simultaneously measured as the nominal supersaturation of the instrument was changing every 12 minutes, from 0.2 to 1% in increments of 0.2. The activated fraction CCN/CN was then calculated. Repeating the procedure for a wide range of sizes, from 10 to 460 nm, the sigmoidal activation curve was obtained. This curve can provide the characteristic, critical diameter D_{pc} which can be used in the Köhler equation (see Chapter 1) in order to estimate the corresponding supersaturation in the instrument. For the calculation of the supersaturation an $(NH_4)_2SO_4$ density of 1770 kg m^{-3}, surface tension of eater solution of 0.0706 N m^{-1}, molar mass of water 0.018 g mol^{-1} and Van't Hoff factor ν equal to 2.5 were used (Brechtel and Kreidenweis, 2000).

4.4 Results and discussion

The chemical composition and the CCN properties of the aerosols in Athens during the winter 2013 campaign are discussed in the following sections.

4.4.1 Particle composition

Organic compounds dominated the PM_1 composition during the campaign representing 58% of the PM_1 mass followed by black carbon (BC) with 20.4% (Figure 4.7). Sulfate ions contributed with 10% to the total PM_1 mass, nitrates 5.1%, ammonium 4.2% and potassium and chloride ions each 1.1%.

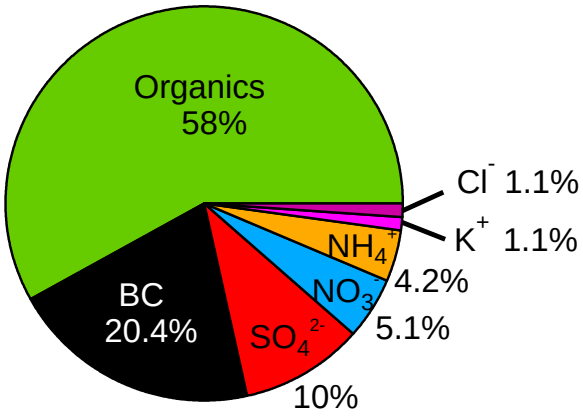

Figure 4.7: Pie chart of the PM_1 mass fractions of major PM_1 components measured by the AMS plus the BC during the whole sampling period.

Their corresponding average composition was 6.5 μg m^{-3} for organic species, 2.3 μg m^{-3} BC, 1.1 μg m^{-3} sulfate ions, 0.6 μg m^{-3} nitrates, 0.5 μg m^{-3} ammonium and potassium and chloride 0.1 μg m^{-3} each.

The average diurnal variations of organics and sulphate measured by the AMS, are shown in Figure 4.8. Organic aerosol concentrations increase after 16:00-17:00

continuously until 23:00 peaking a little before midnight. On the other hand, sulfate had an almost constant average profile with an average concentration around 1 μg m^{-3}. This constant profile is characteristic of species that are not produced locally but are transported to the site.

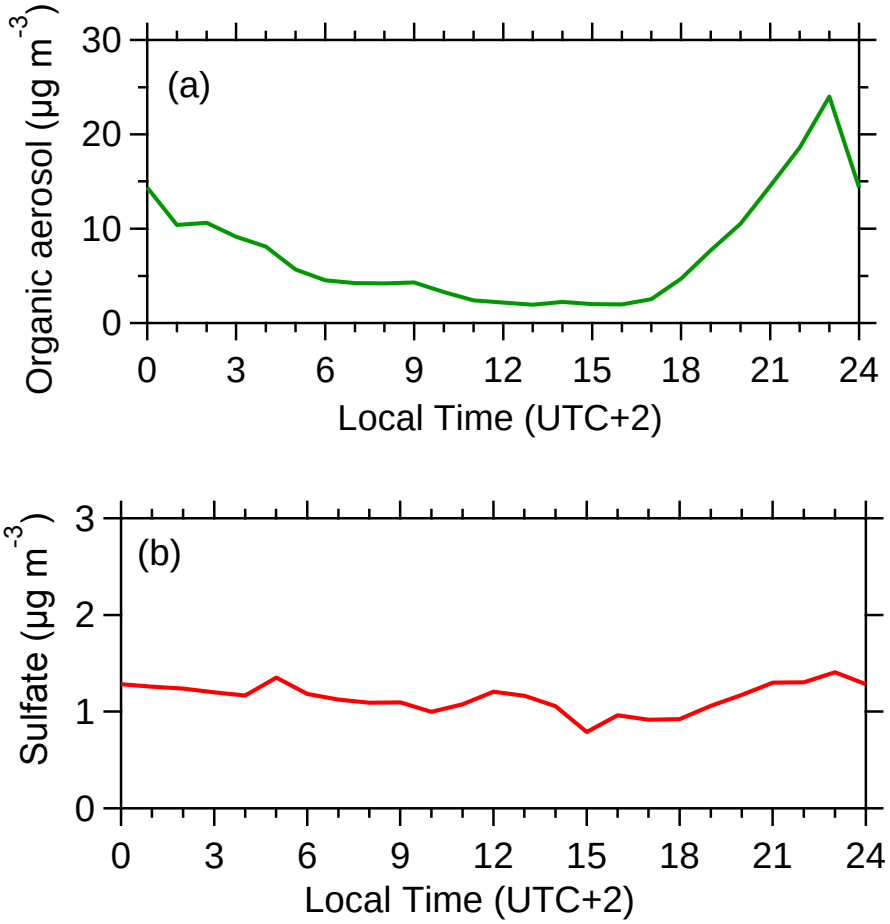

Figure 4.8: Diurnal profile of (a) organic aerosol and (b) sulfate ions in PM_1 particles in Athens during the winter campaign of 2013.

Figure 4.9 represents the organic aerosol fraction in the total PM_1 mass. The organic compounds dominate PM_1 mass composition throughout the day. A peak is observed in the morning between 7:00-10:00 due to the traffic emissions, a smaller one in the afternoon (14:00-16:00) and a major peak is at night with the organic average contribution reaching 80% at 22:00.

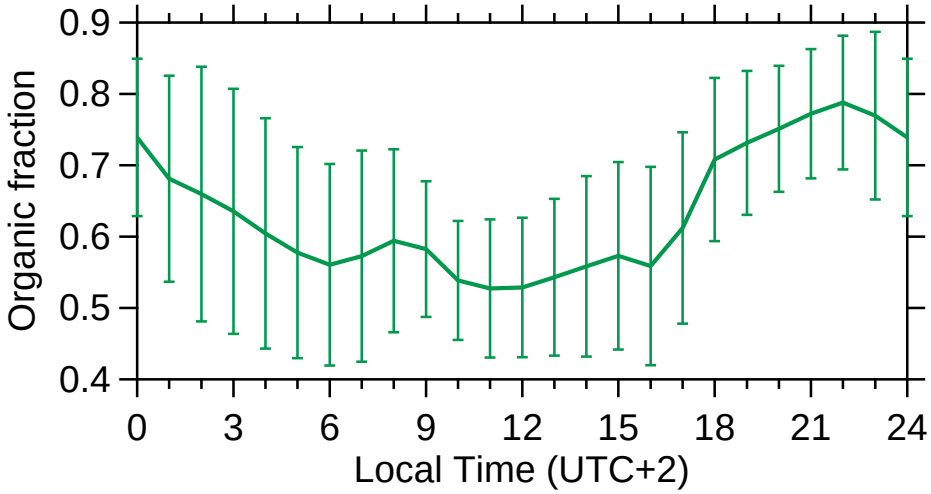

Figure 4.9: Average mass fraction of organic aerosol in PM_1 particles. The error bars represent ±1σ of the corresponding fractions.

PMF analysis revealed 4 organic factors (Florou et al., 2014): biomass burning organic aerosol (BBOA), cooking aerosol (COA), hydrocarbon-like organic aerosol (HOA) and oxygenated organic aerosol (OOA). The average diurnal variations of the factors are shown in Figure 4.10. Biomass burning particle concentrations were found to increase after 16:00 until 23:00 when a peak of 10 μg m^{-3} was reached. BBOA remained at high levels during all night and dropped to almost zero at noon. HOA concentrations peaked in the morning between 18:00-23:00, then remained low increasing again from 6:00-11:00. The oxygenated organics which represent aged aerosol transported to the area had an almost constant average diurnal profile. Corresponding to Greek eating periods, cooking organic aerosol was observed from 13-16 pm and also increased from 18:00 to 23:00.

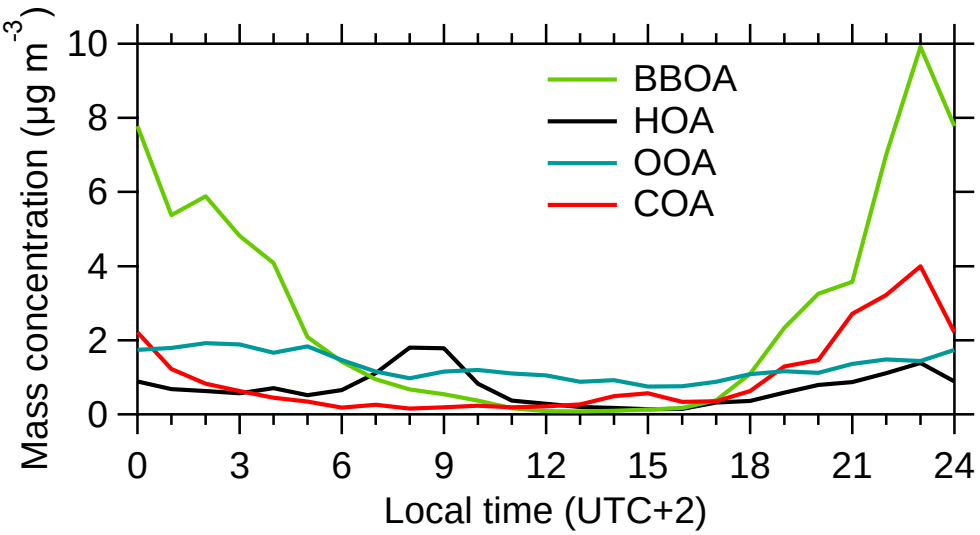

Figure 4.10: Diurnal variation of the concentration of the four factors: biomass burning (BBOA), traffic (HOA), oxygenated (aged) organics (OOA) and cooking (COA).

4.4.2 Particle CCN activity

The average diurnal variability of the critical supersaturation S_c is shown in Figure 4.11. The critical supersaturation expresses the necessary supersaturation for the activation of particles. Same particle sizes may have different chemical composition throughout the day. Particles of 40 nm have been discarded from the following analysis since their S_c was found to be higher than the instrument's maximum supersaturation (0.91%). Smaller particles activate at higher supersaturation values, as expected from Köhler theory.

The main characteristic of the average diurnal profile of particles S_c is a sharp increase in the morning, between 7:00 and 10:00. During this period there is a significant contribution of HOA traffic emissions to the organic aerosol mass (Figure 4.10).

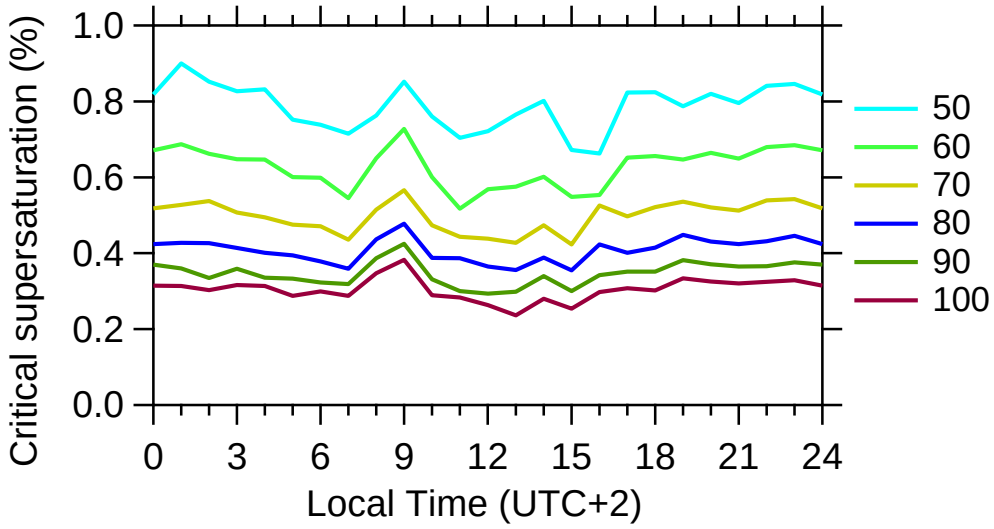

Figure 4.11: Average variation of critical supersaturation for different particle diameters from 50 to 100 nm.

The critical supersaturations of larger particles of diameters in the 70 to 100 nm range were similar. Smaller particles had larger variations of their S_c during the day compared to larger particles (70-100 nm). Such discrepancies of small particles with larger ones could be due to differences in their sources and chemical composition. Consequently, the CCN properties of the small particles do not represent the bulk composition of PM_1 and vice versa.

The size distribution of the chemical components provided by the AMS showed chemical composition differences in the diameter range targeted by the CCN counter. Figure 4.12 represents the diurnal variations of the inorganic and the organic fraction estimated for the time period 23 to 25 January for different particle sizes, ranging from 50 to 100 nm. The size distribution of the AMS was rather noisy, especially for the smaller particle diameters. In accordance to Figure 4.11, smaller particles show a different diurnal behavior compared with the larger sizes. Particles of 50 and 60 nm consisted mainly by inorganic compounds during all hours of the day on average. Their

average inorganic mass fraction was found to be 65% for the 50 nm and 56% for the 60 nm particles.

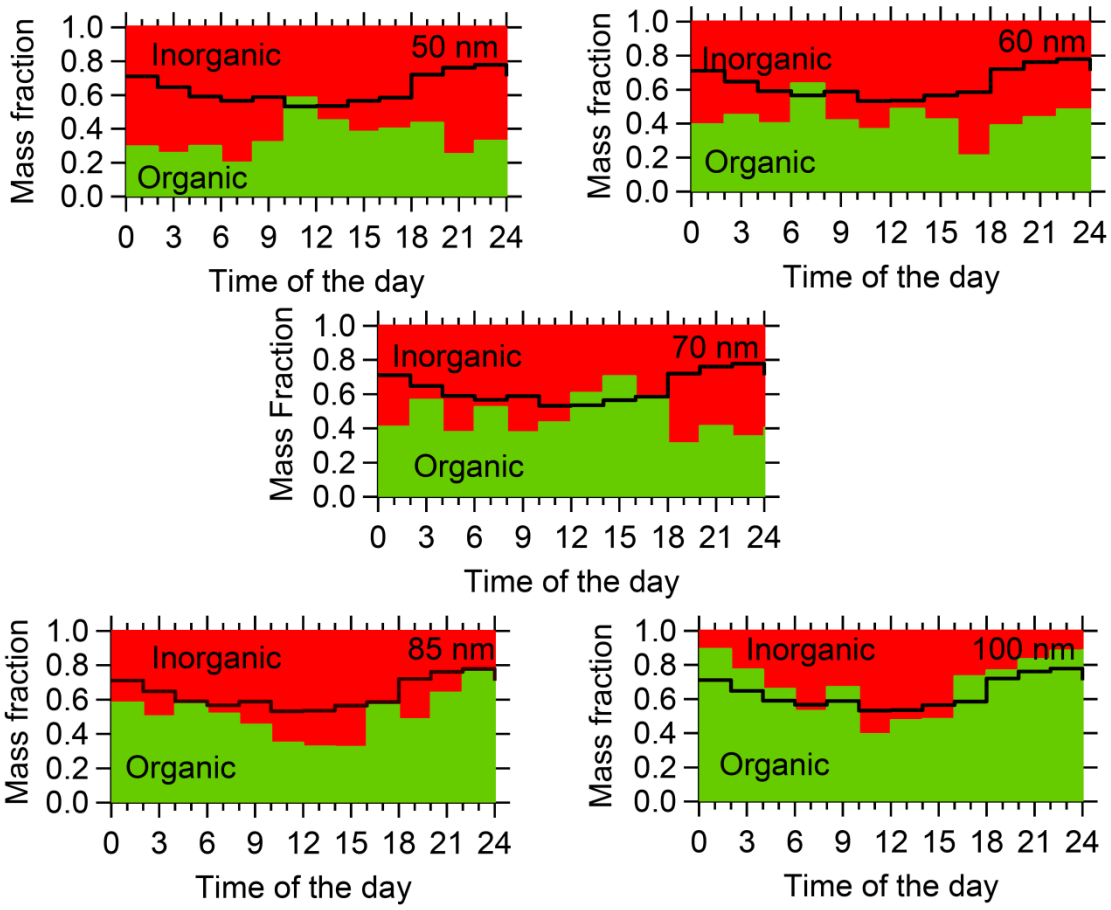

Figure 4.12: Diurnal profiles of organic and inorganic mass fractions for selected particle sizes. The black line indicates the total fraction of organic aerosols in PM_1.

As particle diameter increases, the diurnal cycle of the organic fraction becomes more similar with the cycle of the total organic fraction (Figure 4.12). Particles with dry diameters 85 and 100 nm are dominated by organics (52 and 68% respectively) and both organic fractions follow the diurnal pattern of the total organic fraction in PM_1.

The hygroscopic properties of the particles are strongly affected by the presence of inorganic compounds which are much more hygroscopic compared to the organics. According to Figure 4.12, 85 and 100 nm dry particles follow the diurnal trend of OA in

PM_1 and also have similar composition as the bulk PM_1. For this reason, the averaged hygroscopic properties of 80, 90 and 100 nm in diameter particles will be used here to approximate the properties of PM_1.

The average diurnal profile of the estimated hygroscopicity factor κ for different particle diameters is shown in Figure 4.13. The profile of an average κ, (κ_{av}), of 80 to 100 nm particles was also estimated. The total particle hygroscopicity depends both on the hygroscopicity of the corresponding organic components and on the contribution of the inorganic species to the particle mass.

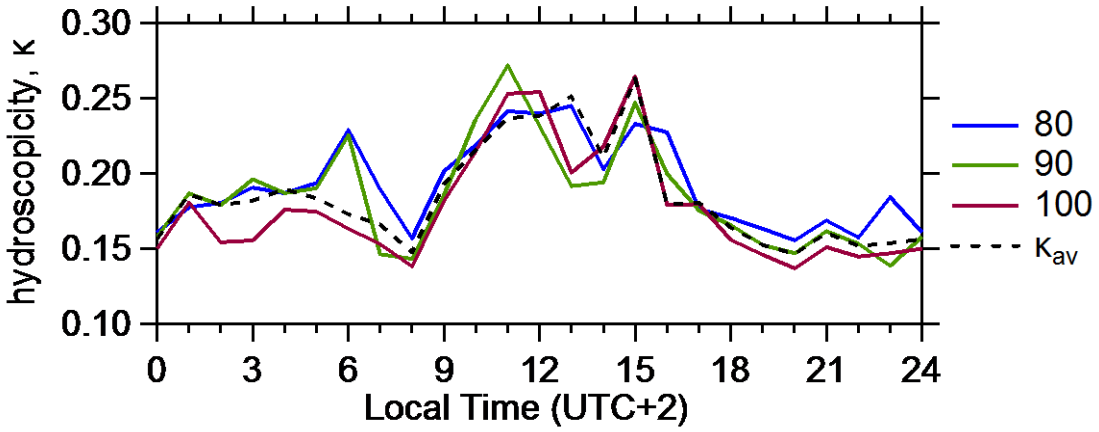

Figure 4.13: Diurnal profile of hygroscopicity κ of 80, 90 and 100 nm particle diameter. The dashed line indicates the averaged hygroscopicity of 80-100 nm particles.

Biomass burning emissions started increasing around 18:00 (Figure 4.10) and dominated the number and mass concentration of the aerosols until midnight. During that period, the average hygroscopicity has a steady profile with a κ value around 0.15. After midnight κ increased and it started to sharply decrease around 6:00, when the contribution of traffic emissions started becoming significant, according to the HOA diurnal profile. Due to the hydrophobic nature of the HOA particles emitted from traffic, hygroscopicity drops, increasing again due to dilution of these particles and

photochemistry to values close to 0.25 after 12:00. The decrease of κ_{av} from around 0.25 to 0.2 between 13:00-14:00 can be attributed to the presence of HOA particles, together with the relatively hydrophobic cooking emissions that peak at the same time. The κ_{av} values remained high (between 0.2 and 0.25) from noon till the beginning of biomass burning early in the evening (around 17:00) when residents go back to their homes and start using their fireplaces.

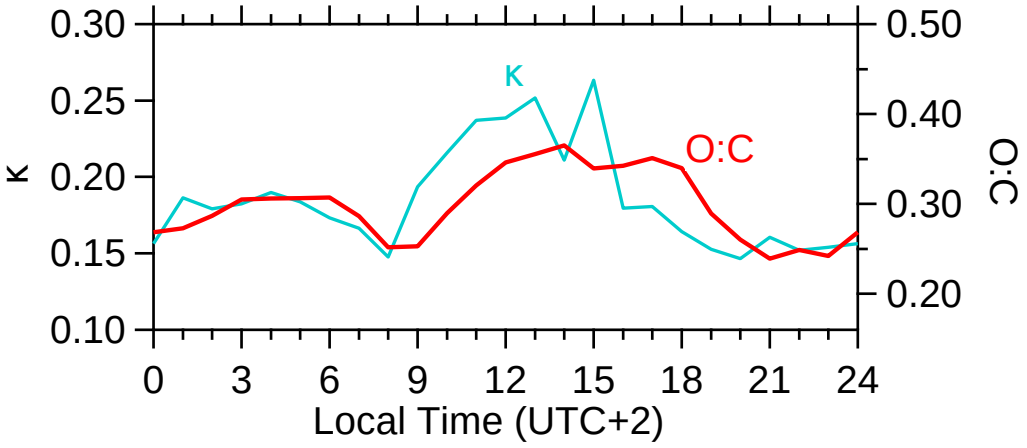

Figure 4.14: Diurnal profile of averaged hygroscopicity and O:C ratio.

The 80-100 nm average hygroscopicity factor κ presented similar diurnal profile as the O:C ratio (Figure 4.14). However, the total time series of κ and O:C had a weak correlation (R^2=0.17). This can be explained by the fact that other factors (e.g. inorganic PM_1 contribution) are more important than the organic O:C in determining the average hygroscopicity of particles. Previous work (Massoli et al., 2010; Martin et al., 2012; Lathem et al., 2013) has also suggested that organic hygroscopicity may not be especially sensitive to O:C for values less than 0.5 encountered in this study.

The degree of heterogeneity of the particles can be expressed by the ratio of the standard deviation (chemical dispersion) of the hygroscopicity, $\sigma(\kappa)$ divided by κ. The diurnal

profile of the chemical dispersion $\sigma(\kappa)/\kappa$ is shown in Figure 4.15. This parameter was found to peak between 7:00 and 11:00, around the same time when average hygroscopicity drops. This can be attributed to the increase of HOA-like traffic contribution to the total aerosol concentration during this period.

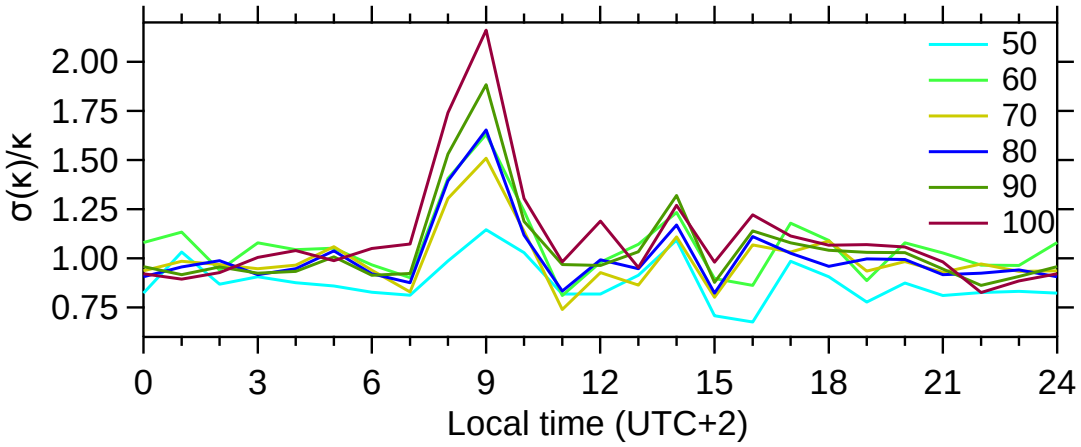

Figure 4.15: Diurnal profile of the dispersion, σ(κ)/κ, around κ of 50, 60, 70, 80, 90 and 100 nm diameter particles and average hygroscopicity for all particle diameters.

This behavior is more pronounced for particles larger than 60 nm while the diurnal profile of the smaller particles presents less variability. The smaller particles were dominated by inorganic species and apparently had more consistent behavior than the larger ones. Figure 4.16 presents the maximum activated fraction E^* (see Equation 4.2) of particles of different diameters. In general, the smaller the particle size, the lower the corresponding maximum activated fraction. This is consistent with Köhler theory predictions that bigger particles activate easier. This trend is opposite to that suggested by the particle composition with organic fraction increasing with particle size in the range of interest.

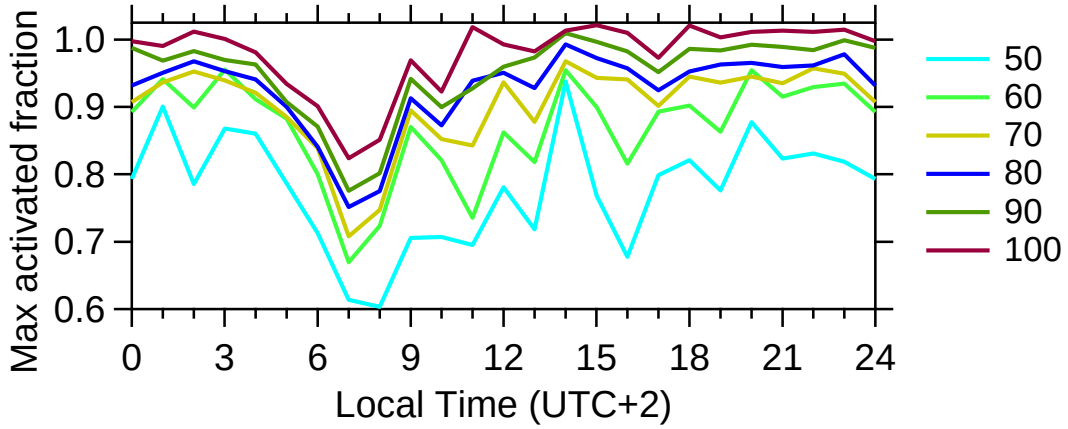

Figure 4.16: Diurnal profile of the maximum activated fraction E* of 50, 60, 70, 80, 90 and 100 nm diameter particles.

4.4.3 Organic aerosol hygroscopicity

The particle hygroscopicity is equal to the sum of the hygroscopicities of all components multiplied by their volume fraction (Petters and Kreidenweis, 2007). Despite the low fraction of the inorganic species compared to the organics which dominate, the former significantly affects the average hygroscopicity of the particles. In order to explore the hygroscopic properties of the organic components of the aerosols, the hygroscopicity of organics, κ_{org} was estimated.

The model ISORROPIA II (Fountoukis and Nenes, 2007) was used in order to estimate chemical composition of the inorganic fraction. This model requires as input the concentrations of the inorganic ions (NH_4^+, SO_4^{2-}, NO_3^-, Cl^-, K^+) relative humidity and temperature conditions and can provide the concentration of the inorganic salts in the aerosol phase (Fountoukis and Nenes, 2007). By dividing the corresponding salt mass concentration by its density, the volume fractions of the inorganic components can be calculated. According to Petters and Kreidenweis, (2007):

$$\Sigma \varepsilon_i \kappa_i = \kappa \qquad (4.7)$$

where ε_i are the volume fractions of all particle components, κ_i their hygroscopicity and κ the total hygroscopicity measured. By using κ_{av} for κ, and assuming that black carbon (BC) has a κ=0, the hygroscopicity of the organic compounds, κ_{org} was estimated. The average diurnal profile of κ_{org} is presented in Figure 4.17.

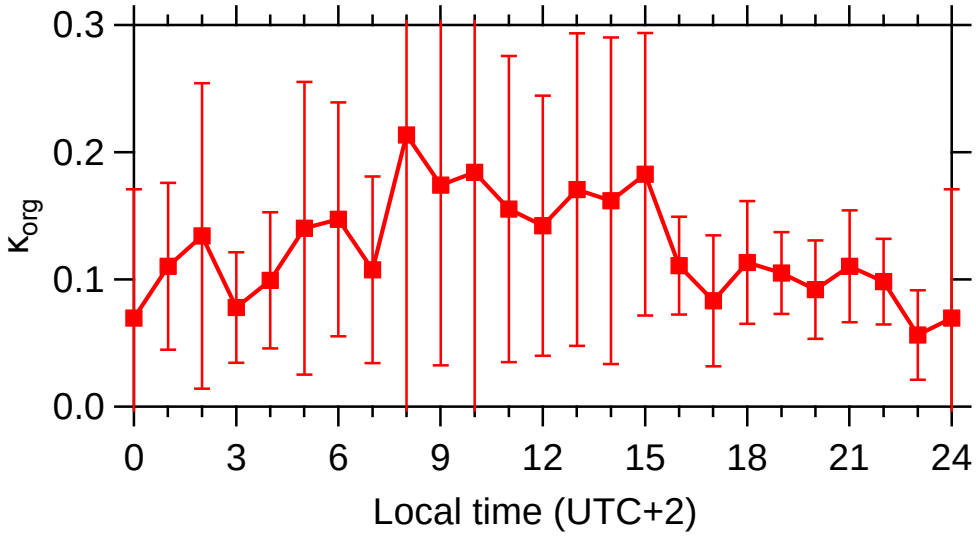

Figure 4.17: Diurnal profile of the average organic hygroscopicity κ_{org}. The error bars represent ±1σ of the corresponding hygroscopicity.

The estimated κ_{org} varies from 0.06 to 0.21. During the night biomass burning emissions dominate and the corresponding κ is around 0.09. After 3:00 OOA becomes an important OA component so κ_{org} increases. OOA dominated the organic aerosol composition between 10:00-17:00 and is expected to be quite hygroscopic. Its κ values reported in literature are around 0.25-0.3 (Kreidenweis et al., 2008; Chang et al., 2010) justifying the increase of the organic aerosol hygroscopicity at that time. Estimations of κ_{org} from open fires and lab measurements (Jimenez, 2009; Moore et al., 2011; Lathem et al., 2013) also leaded to values around 0.1 for biomass burning organics.

4.5 Conclusions

The composition and hygroscopic properties of atmospheric aerosol in Athens during the winter of 2013 were studied. The PM_1 was dominated by organic species during all the sampling period, with an average organic mass fraction of 0.58, followed by black carbon with a corresponding fraction of 0.2. The PMF analysis revealed that the most important contributor to the organic aerosol concentrations was biomass burning which started in the evening and peaked during the night. HOA from traffic peaked during the morning rush hour, affecting the total hygroscopic properties of organic aerosols. During the HOA peak, the critical supersaturation of the particles studied here (50 nm$\leq d_p \leq$100 nm) was lower due to the hydrophobic nature of HOA. The maximum chemical dispersion of the particles is also observed during this period.

Size-resolved chemical composition data provided by the HR-AMS revealed discrepancies on the composition of smaller (50-70 nm) and bigger particles (80-100 nm) and showed that the properties of the PM_1 bulk composition can be represented by the properties of bigger particles. These particles were found to be quite hygroscopic, with the maximum activated fraction reaching almost 1 during most of the day, except for the morning traffic period. The average hygroscopicity of these particles, κ_{av}, ranged roughly from 0.15 to 0.25. The lowest values are observed during the HOA peak, as expected, while the highest were observed between 11:00-16:00 when oxygenated organics dominated the organic mass. The average hygroscopicity κ_{av} of the mixed (organic/inorganic) particles during the night when biomass burning particles prevailed was around 0.15. The diurnal profile of κ_{av} was very similar with the profile of the O:C ratio but no correlation was observed.

Using a thermodynamic model to predict the inorganic chemical composition of the inorganic fraction, the hygroscopicity of the 80-100 nm organic particles was estimated. The organic particles hygroscopicity κ_{org} was on average 0.12 while during the biomass burning period was on average 0.09.

4.6 References

Andreae, M.O. and Rosenfeld, D. Aerosol-cloud precipitation interactions. Part 1. The nature and sources of cloud-active aerosols. *Earth-Science Reviews,***2008**, 89, 13-41.

Bougiatioti, A., Nenes, A., Fountoukis, C., Kalivitis, N., Pandis, S.N., Mihalopoulos, N. Size-resolved CCN distributions and activation kinetics of aged continental and marine aerosol. *Atmos. Chem. Phys.,* **2011**, 11, 8791-8808.

Brechtel, F.J., Kreidenweis, S.M. Predicting particle critical supersaturation from hygroscopic growth measurements in the humidified TDMA. Part I: Theory and sensitivity studies. *J. Atmos. Sci.,* **2000**, 57, 1854-1871.

Cerully, K.M., Raatikainen, T., Lance, S., Tkacik, D., Tiitta, P., Petaja, T., Ehn, M., Kulmala, M., Worsnop, D.R., Laakosonen, A., Smith, J.N., Nenes, A. Aerosol hygroscopicity and CCN activation kinetics in a boreal forest environment during the 2007 EUCAARI campaign. Atmos. Chem. Phys., **2011**, 11, 12369-12386.

Chang, R.Y.-W., Slowik, J.G., Shantz, N.C., Vlasenko, A., Liggio, J., Sjostedt, S.J., Leaitch, W.R., Abbat, J.P.D. The hygroscopicity parameter (κ) of ambient organic aerosol at a field site subject to biogenic and antrhropogenic influences: relationship to degree of aerosol oxidation. *Atmos. Chem. Phys.,* **2010**, 10, 5047-5064.

M. Crippa, De Carlo, P. F., Slowik, J. G., Mohr, C., Heringa, M.F., Chirico, R., Poulain, L., Freutel, F., Sciare, J., Cozic, J., Di Marco, C.F., Elsasser, M., Nicolas, J.B., Marchand, N., Abidi, E., Wiedensohler, A., Drewnick, F., Schneider, J., Borrmann, S., Nemitz, E., Zimmermann, R., Jaffrezo, J.-L., Prevôt, A.S.H., Baltensperger, U. Wintertime aerosol chemical composition and source

apportionment of the organic fraction in the Metropolitan area of Paris.*Atmos. Chem. Phys.*, **2013**, 13, 961-981.

De Carlo, P.F., J.R. Kimmel, J.R., Trimborn, A., Northway, M.J. Jayne, J.T. Aiken, A.C. Gonin, M. Fuhrer, K. Horvath, T. Docherty, K. Worsnop, D.R. Jimenez, J.L. Field-Deployable, High-Resolution, Time-of-Flight Aerosol Mass Spectrometer, *Analytical Chemistry*, **2006**, 78: 8281-8289.

Florou, K., Pikridas, M., Papanastasiou, D.K. Papanastasiou, Louvaris, E.E., Gkatzelis, G.I., Pandis, S.N. Air pollution from airborne particulate matter during wintertime in two Greek cities. In preparation.

Fors, E.O., Rissler, J., Massling, A., Svenningsson, B., Andrae, M.O., Dusek, U., Frank, G.P., Hoffer, A., Bilde, M., Kiss, G., Janitsek, S., Henning, S., Facchini, M.C., Decesari, S., Swietlicki, E. Hygroscopic properties of Amazonian biomass burning and European background HULIS and investigation of thei effects on surface tensxeion with two models linking H-TDMA to CCNC data. *Atmos. Chem. Phys.*, 2010, 10, 5625-5639.

Fountoukis, C., Nenes, A. A computationally efficient thermodynamic equilibrium model for K^+-Ca^{2+}-Mg^{2+}-NH_4^+-SO_4^{2-}-NO_3^--Cl^--H_2O aerosols. *Atmos. Chem. Phys.*, **2007**, 4639-4659.

Hennigan, C.J., Westervelt, D.M., Riipinen, I., Engelhart, G.J., Lee, T., Collet Jr., J.L., Pandis, S.N., Adams, P.J., Robinson, A.L. New particle formation and growth in biomass burning plumes: An important source of cloud condensation nuclei. *Geophys. Res. Let.*, **2012**, 39, L09805, doi:10.1029/2012GL050930.

Kaufman, Y. J., Tanre, D., and Boucher, O. A satellite view of aerosols in the climate system. *Nature*, **2002**, 419, 6903, 215–223.

Lance, S., Raatikainen, T., Onasch, T., Worsnop, D.R., Yu, X.-Y., Alexander, M.L., Stolzenburg, M.R., McMurry, P.H., Smith, J.N., Nenes, A. Aerosol mixing-state, hygroscopic growth and cloud activation efficiency during MIRAGE 2006. *Atmos. Chem. Phys*. **2012**, 12, 15709-15742.

Lathem, T.L., Beyersdorf, A.J., Thornhill, K.L., Winstead, E.L., Cubison, M.L., Hecobian, A., Jimenez, J.L., Weber, R.J., Anderson, B.E., Nenes, A. Analysis of CCN activity of Arctic aerosol and Canadian biomass burning during summer 2008. *Atmos. Chem. Phys.*, **2013**, 13, 2735-2756.

Lide, D.R. CRC Handbook of chemistry and physics. *CRC Press*, Ann Arbor, MI.

Martin, M., Tritscher, T., Jurányi, Z., Heringa, M.F., Sierau, B., Weingartner, E., Chirico, R., Gyzel, M., Prévôt, A.S.H., Baltensperger, U., Lohmann, U. Hygroscopic properties of fresh and aged wood burning particles. *J. Aerosol Sci.*, **2013**, 56, 15-29.

Massoli, P., Lambe, A.T., Ahern, A.T., Williams, L.R., Ehn, M., Mikkilä, J., Canagaratna, M.R., Brune, W.H., Onasch, T.B., Jayne, J.T., Petäjä, T., Kulmala, M., Laaksonen, A., C. E. Kolb, C.E., Davidovits, P., Worsnop, D.R. Relationship between aerosol oxidation level and hygroscopic properties of laboratory generated secondary organic aerosol (SOA) particles. *Geophys. Res.Lett.*, **2010**, 37, L24801.

Moore, R. H., Nenes, A., Medina, J. Scanning mobility CCN analysis - A method for fast measurements of size-resolved CCN distributions and activation kinetics. *Aerosol. Sci. Technol.*, **2010**, 44:861-871.

Petters, M.D., Kreidenweis, S.M. A single parameter representation of hyroscopic growth and cloud condensation nucleus activity. *Atmos. Chem. Phys.*, **2007**, 7, 1961-1971.

Reid, J. S., Koppmann, R., Eck, T. F., and Eleuterio, D. P. A review of biomass burning emissions part II: Intensive physical properties of biomass burning particles, *Atmos. Chem. Phys*., 5, 799–825, 2005.

Roberts, G.C., Nenes, A. A continuous-flow streamwise thermal-gradient CCN chamber for atmospheric measurements. *Aeros. Sci. Technol.*, **2005**, 39, 206-221.

Rose, D., Novak, A., Achtert, P., Wiedensohler, A., Hu, M., Shao, M., Zhang, Y., Andreae, M.O, Pöschl, U. Cloud condensation nuclei in polluted air and biomass burning smoke near the mega-city Guangzhou, China - Part 1: Size-resolved measurements and implications for the modeling of the aerosol particle hygroscopicity and CCN activity. *Atmos. Chem. Phys.*, **2010**, 10, 3365-3383.

Semeniuk, T. A., Wise, M. E., Martin, S. T., Russell, L. M., Buseck, P. R. Hygroscopic behavior of aerosol particles from biomass burning using environmental transmission electron microscopy. J. Atmos. Chem., **2007**, 56:259-273.

Slowik, J.G., Staiken, K., Davidovits, P., Williams, L.R., Jayne, J.T., Kolb, C.E., Worsnop, D.R., rudich, Y., DeCarlo, P.F., Jimenez, J.L. Particle morphology and density chatacterization by combined mobility and aerodynamic diameter measurements. Part 2: Application to combustion-generated soot aerosols as a function of fuel equivalence ratio. *Aerosol Sc. Technol.*, **2004**, 38, 1206-1222.

Ulbrich, I.M., Canagaratna, M.R., Zhang, Q., Worsnop, D.R., Jimenez, J.L. Interpretation of organic components from Positive Matrix Factorization of aerosol mass spectrometric data. *Atmos. Chem. Phys.*, 9, **2009**, 2891-2918.

Vestin, A., Rissler, J., Swietlicki, E., Frank, G. P., Andreae, M. O. Cloud-nucleating properties of Amazonian biomass burning aerosol: Cloud condensation nuclei measurements and modeling. *J. Geophys. Res.*, **2007**, Vol. 112, D14201, doi:10.1029/2006JD008104.

Zhang, X., Hecobian, A., Zheng, M., Frank, N.H., Weber, R.J. Biomass burning impact on PM2.5 over the southeastern US during 2007: integrating chemically speciated FRM filter measurements, MODIS fire counts and PMF analysis. *Atmos. Chem. Phys*, **2010**, 10, 6839-6853.

Zuberi, B., Johnson, K.S., Aleks, G.K., Molina, L.T., Molina, M.J., Laskin, A. Hydrophilic properties of aged soot. *Geophys. Res. Let.*, **2005**, 32, L01807.

Chapter 5

Hygroscopic properties of SOA formed via ozonolysis and chemical aging of α-pinene

5.1 Introduction

Atmospheric aerosols strongly affect Earth's climate by scattering solar radiation (direct effect) and by serving as cloud condensation nuclei (indirect effect). Organic aerosol has been found to contribute to the CCN concentrations (Novakov and Penner, 1993; Hegg et al., 1995). The oxidation of VOCs in the atmosphere leads to the formation of secondary organic aerosols (SOA). SOA gaseous precursors are both biogenic and anthropogenic, with biogenic VOCs dominating on a global scale (Seinfeld and Pankow, 2003; Singh and Zimmerman, 1992). Biogenic emissions depend on temperature, light intensity and vegetation type (Sun and Ariya, 2006) and are estimated to be around 800 TgC yr^{-1} on a global scale which is about 5.5 times higher than the anthropogenic VOC emissions (Tsigaridis et al., 2005). The most important biogenic VOCs (BVOCs) are monoterpenes ($C_{10}H_{16}$), sesquiterpenes ($C_{15}H_{24}$), and isoprene (Chung and Seinfeld, 2002). Terpenes are major precursors of biogenic SOA.

A-pinene (Figure 5.1), b-pinene, limonene and sabinene account for 40 to 80% of the global monoterpene emissions (Kanakidou et al., 2005) with α-pinene having the highest contribution, 25%, among the terpenes. A-pinene global emissions are estimated to be around 50 Tg yr^{-1} (Guenther et al., 1995; Seinfeld and Pankow, 2003). Ozonolysis is the main reaction pathway of α-pinene. It is estimated that 80% of α-pinene reacts through this pathway (Griffin et al., 1999; Pathak et al., 2007). The α-pinene yield depends on its concentration, the oxidizing agent (O_3, OH, NO_3), the temperature and relative humidity conditions (Yu et al., 1999; Presto et al., 2005; Pathak et al., 2007). This yield varies from a few percent at low SOA concentrations to 70% at high concentrations (Hoffmann et al., 1997).

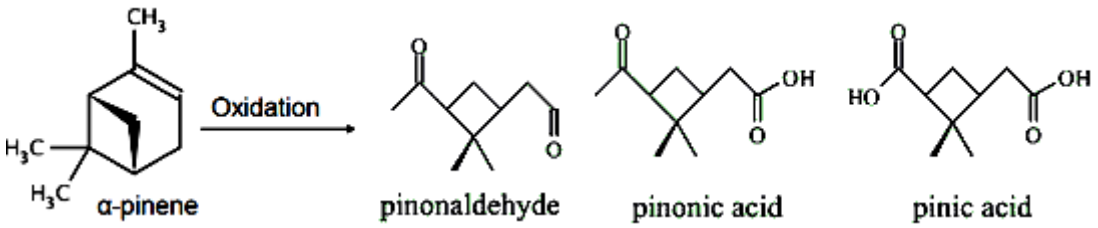

Figure 5.1: A-pinene and main oxidation products.

The ozonolysis reaction of α-pinene starts with the cycloaddition of O_3 on the double bond, leading to the formation of an ozonide which consequently decomposes to an aldehyde or ketone and a Criegee intermediate which either decomposes in the gas phase or continues to react (Criegee, 1975; Johnson and Marston, 2008). Typical α-pinene oxidation products shown in Figure 5.1 include pinonaldehyde, cis-pinonic and pinic acid (Donahue et al., 2012). Freshly formed SOA can undergo further chemical aging in the atmosphere under the effect of oxidants and solar radiation. Aging can include heterogeneous reactions of the condensed-phase with oxidants, repartitioning of semivolatile species produced by gas-phase oxidation, and oligomerization within the particle (Ellison et al., 1999; Ziemann, 2005; Robinson et al., 2007). Such physicochemical processing drives alterations in the chemical composition, hygroscopicity, optical properties and even the toxicity of the SOA (Asad et al., 2004; Mmereki et al., 2004; Rudich et al., 2007). In this work, the hygroscopic properties of the SOA formed from the ozonolysis and the chemical aging of α-pinene are investigated.

5.2 Experimental method

The experiments were carried out in the Institute of Chemical Engineering environmental smog chamber facility using a 10 m^3 Teflon reactor. The reactor was suspended in a temperature-controlled room whose walls are covered by UV lamps.

Table 5.1: A-pinene and initial O_3 mixing ratios used in each experiment. The type of experiment (seeded or non-seeded), the use of n-butanol (d9) and the existence of WSOC measurement is also indicated. The shaded line indicates the blank experiment.

N°	α-pinene (ppb)	Initial O_3 (ppb)	n-butanol (d9) (OH scavenger)	$(NH_4)_2SO_4$ seeds	WSOC
0	0	490	no	yes	no
1	5.3	550	no	yes	no
2	19.3	500	no	yes	no
3	8.2	550	no	yes	no
4	8.2	530	no	yes	no
5	9.7	520	no	yes	no
6	6.1	390	no	no	no
7	16.5	460	no	no	no
8	17.5	410	no	no	no
9	15.7	400	no	no	no
10	11.7	580	yes	no	yes

Before each experiment, the chamber was cleaned and filled with dry, clean air. Clean air was created by passing compressed ambient air through high-efficiency particulate air (HEPA) and activated carbon filters to remove particles and organic vapors and also through silica gel to remove moisture. In each experiment, a volume of α-pinene (Aldrich, >99% purity) was directly injected in the chamber via a septum. Purified air was used to evaporate and flush α-pinene from the line. After 30 min, a volume of O_3 was added to start the ozonolysis. O_3 was produced by an ozone generator (Azcozon, - Azco Industries) which uses a supply of pure air or O_2 and a high voltage to produce O_3 molecules. The experiments were conducted with an excess of O_3, ranging from 370 to 580 ppb. The SOA produced was then chemically aged using OH radicals which were produced by photolysis of HONO. Nitrous acid was formed in a bubbler, using the reaction:

$$NaNO_2 + H_2SO_4 \rightarrow HONO + NaHSO_4 \quad (5.1)$$

Clean air was passed through the bubbler thus injecting the HONO into the chamber. The UV lights were consequently turned on, in order to photolyze HONO forming OH radicals.

Two types of experiments were conducted: Seeded and non-seeded. In the first case, dry $(NH_4)_2SO_4$ particles were produced by atomization (see Chapter 3) and were initially introduced in the chamber in order to offer a surface for the SOA to condense. This procedure simulates atmospheric conditions.

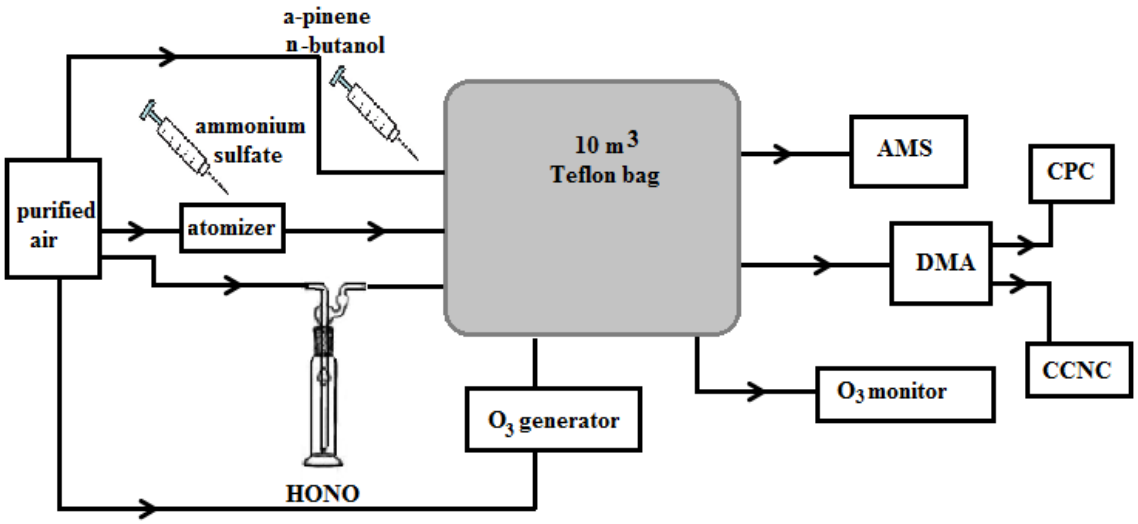

Figure 5.2: Experimental set-up used for the oxidation of α-pinene.

The ammonium sulphate particles were produced using a 1 g L^{-1} $(NH_4)_2SO_4$ solution driven to an atomizer. In the non-seeded experiments the particles were created through nucleation. N-butanol (d9) was used in selected experiments as OH scavenger, in order to focus on the ozonolysis of the α-pinene. This isotopically labelled reagent was selected so that it can be measured without interferences by the proton-transfer reaction

mass spectrometer (PTR-MS) used for the volatile organic compounds measurements. The experimental set-up used is shown in Figure 5.2.

5.2.1 Instrumentation

A CCN counter (DMT Technologies, Roberts and Nenes, 2005) was coupled with an SMPS (DMA, TSI 3080, CPC, TSI 3776) in order to provide size-resolved CCN activity measurements of a wide range of SOA particle size according to the SMCA technique (see section 4.3.3). The details of the measurement are described in section 4.3.3. Briefly, size-classified particles were exposed to different supersaturations within the CCN counter, ranging from 0.2 to 1% (nominal) in steps of 0.2. A HR-ToF-AMS (Aerodyne Research, Inc, De Carlo et al., 2006) was continuously measuring the size-resolved chemical composition of the particles. A Proton-Transfer Reaction Mass Spectrometer (PTR-MS, Ionicon Analytik) was providing continuous measurements of the α-pinene concentration in the gas phase. The concentrations of O_3, NO and NO_2 were measured by gas monitors providing 5-sec measurements. For the last set of 3 non-seeded experiments (Table 5.1), the Steam Sampler-WSOC described in Chapter 3 was also employed for the measurement of the water soluble fraction of α-pinene SOA.

5.2.2 CCN counter calibration

The calibration procedure is the same as that described in section 4.3.5. The critical diameter of size selected $(NH_4)_2SO_4$ particles was determined in order to calculate the corresponding real supersaturation of the instrument. The CCN counter was calibrated during the experiments twice.

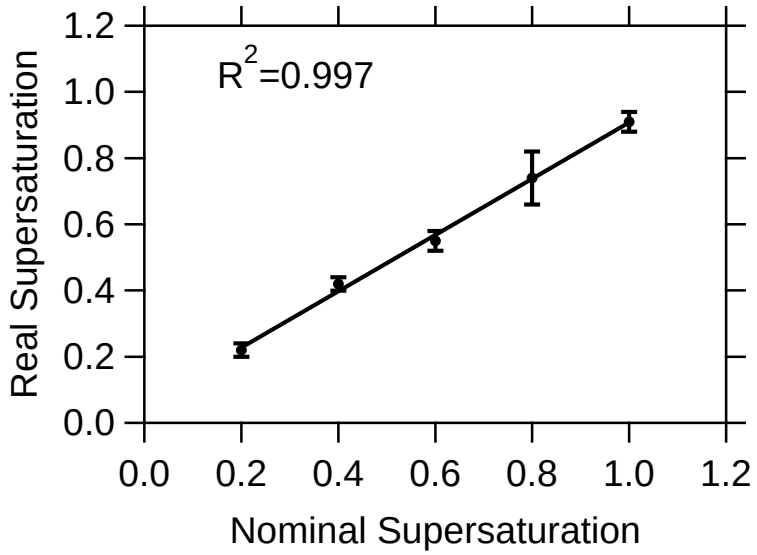

Figure 5.3: Real supersaturation of the instrument versus the nominal supersaturation.

The variability among calibrations did not exceed 5% for all saturations except for 0.2%, where it reached 10%. The relationship between the nominal supersaturation of the instrument and the real supersaturation is shown in Figure 5.3. The error bars correspond to the standard deviation of the calibration measurements.

5.3 Results and discussion

In this series of experiments α-pinene was initially injected in the chamber. It was allowed to stabilize and after 30 to 60 min ozone was introduced continuously for 2 min in order to achieve a mixing ratio close to 500 ppb. The α-pinene was consumed and SOA products were allowed to chemically evolve. After 2 hours a constant volume of HONO was introduced in the chamber and UV lights were turned on in order to promote photochemical aging. The HONO injection step was repeated after 2 hours. For the seeded experiments, initially an $(NH_4)_2SO_4$ solution was supplied to an atomizer in order to produce ammonium sulphate particles. This particle stream was dried and was driven into the smog chamber to offer a surface for α-pinene oxidation products to condense on.

5.3.1 Seeded experiments

The typical evolution of the concentrations of the main species in the particle phase during the experiments where ammonium sulphate seeds were used is shown in Figure 5.4. The injection of the ozone and the initiation of the SOA production correspond to time zero.

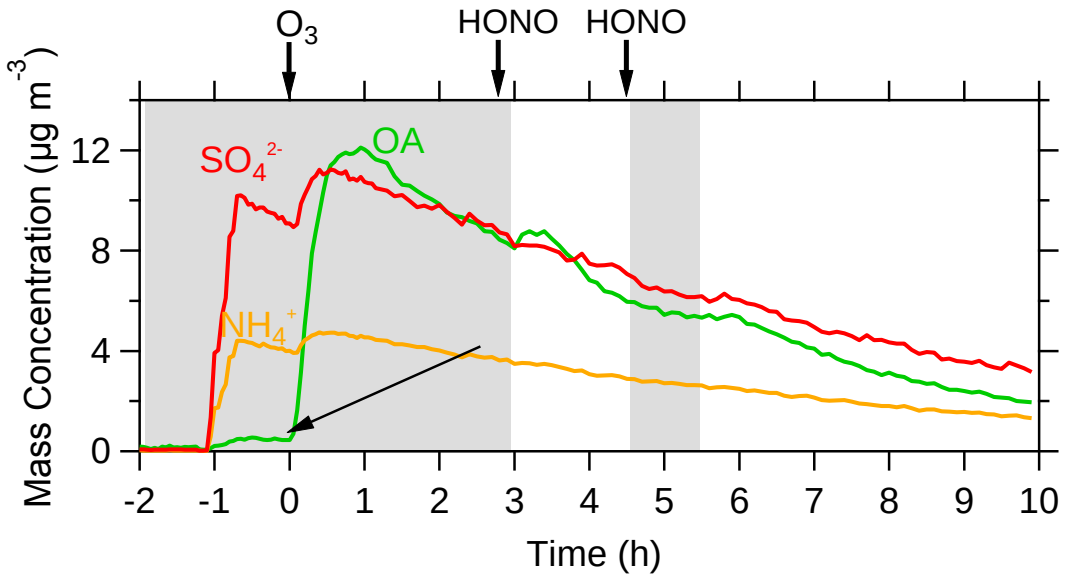

Figure 5.4: Time series of organic aerosol (OA) produced by the α-pinene ozonolysis, ammonium and sulphate concentrations for Experiment 5. The times of ozone and HONO injections are also indicated. The shaded regions correspond to periods during which the chamber was dark. During the rest experiment the lights were on. Time zero corresponds to O_3 addition and initiation of ozonolysis.

The initial decrease of the ammonium sulphate concentrations before the start of the reaction is due to wall losses of the seed particles. The AMS data were not corrected for the collection efficiency. This results in an apparent increase of the ammonium sulphate levels which is actually due to an increase of the collection efficiency when particles are coated by SOA. As SOA is formed the mean diameter of the particles increases. The evolution of the mean diameter of the particles throughout the experiment obtained from the SMPS is shown in Figure 5.5. The initial mean diameter of ammonium sulphate

particles 15 min before the SOA formation is around 85 nm. Organic coating of the inorganic seeds leads to rapid increase of the particle mean size to 110 nm. After the sharp increase of the mean diameter which takes place during the first hour of the ozonolysis, the mean diameter increases from 110 to 114 nm within the next two hours of the ozonolysis. This is due to coagulation but also differences in the loss rates of particles of different sizes on the walls. The first HONO injection causes a 4 nm increase of the aerosol mean diameter while the second one another 3 nm (Figure 5.5).

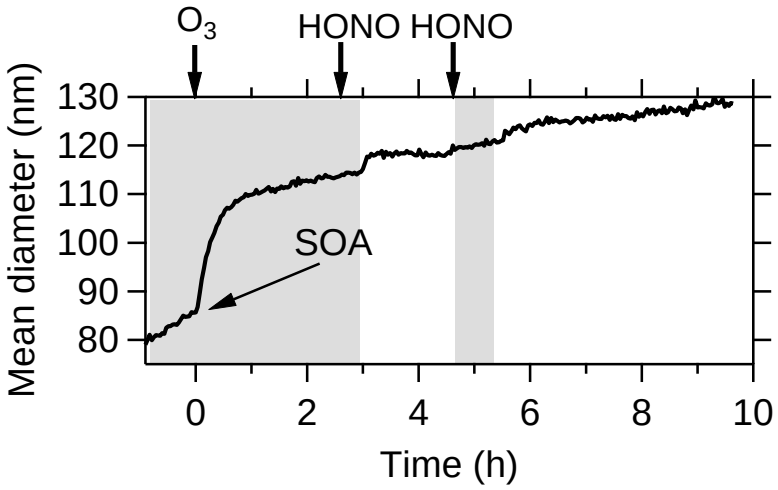

Figure 5.5: Time series of the mean diameter of the particles in the chamber during Experiment 5. Time zero corresponds to O_3 addition and initiation of ozonolysis.

Figure 5.6 presents the typical corresponding evolution of the mixing ratios of the main gas species: α-pinene, O_3 and NO_x (NO plus NO_2) present in the smog chamber. In Experiment 5, a volume of 0.4 μL of α-pinene corresponding to 9.7 ppb in the gas phase was injected in the chamber and after a few minutes ozone was added for 2 min in order to achieve an excess concentration close to 500 ppb. The concentration of initially formed SOA was around 12 μg m^{-3}.

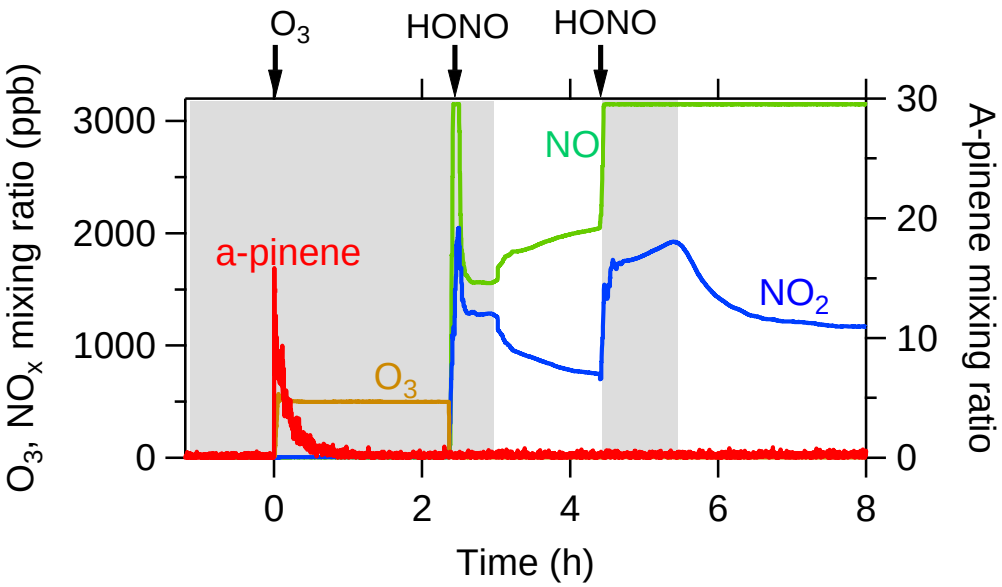

Figure 5.6: O_3, NO_x and α-pinene mixing ratio evolution during Experiment 5. Dark shaded areas correspond to dark conditions during the experiment, non-shaded areas correspond to period when the UV lights were on. Time zero corresponds to O_3 addition and initiation of ozonolysis.

Right after O_3 is introduced in the chamber its concentration is stabilized within a few minutes and remains constant under dark conditions. A-pinene was consumed within an hour. The first products in the particle phase, indicated in Figure 5.4 as OA are formed within a few minutes. After 2.4 hours, HONO was injected in the chamber and the UV lights were turned on after another half an hour. The HONO injection was repeated after 2 hours. Under dark conditions HONO is quite unstable and NO_x is produced (Finlayson-Pitts and Pitts, 2000):

$$2\ HONO \leftrightarrow NO + NO_2 + H_2O \qquad (5.2)$$

HONO is then photolyzed to form OH and NO and the NO can react with O_3:

$$NO + O_3 \rightarrow NO_2 + O_2 \qquad (5.3)$$

By turning UV lights on, after almost half an hour, NO concentrations increase while NO_2 decrease, according to:

$$HONO \xrightarrow{h\nu} OH + NO \quad (5.4)$$

$$NO_2 \xrightarrow{h\nu} NO + O \quad (5.5)$$

5.3.1.1 Blank experiment

The evolution of the concentration of the main aerosol components during the blank experiment is shown in Figure 5.7. In this test, we followed all steps of the rest of the experiments including addition of O_3 and two HONO injections except for the α-pinene addition. This is a test of the degree of cleanliness of the set-up.

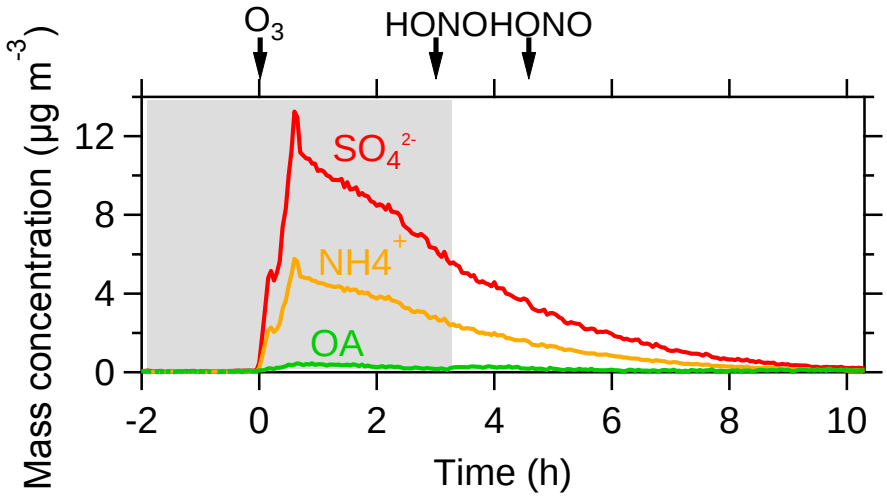

Figure 5.7: Time series of main species in the particle phase during the blank experiment (Experiment 0). Time zero corresponds to O_3 addition and initiation of ozonolysis.

The initial OA concentrations found was 0.4 µg m^{-3}. These low levels of organic contaminants present in the particles together with the ammonium sulphate are probably due to the injection system. The OA concentration did not exceed 3% of the total mass. After the addition of HONO and its photolysis another 0.3 µg m^{-3} were formed. These

low levels of contamination are acceptable for experiments with more than 10 μg m^{-3} of OA like ours and did not influence the rest of the study.

5.3.1.2 CCN activity of seeded SOA particles

The evolution of the CCN fraction (CCN/CN) of SOA particles that activated at 0.42, 0.74 and 0.91% supersaturation formed by the ozonolysis and chemical aging of α-pinene for Experiment 5 is shown in Figure 5.8. The low time resolution measurement (6 min) used in this first set of experiments did not allow selected supersaturations to be created in the CCNC column uniformly and this data was discarded.

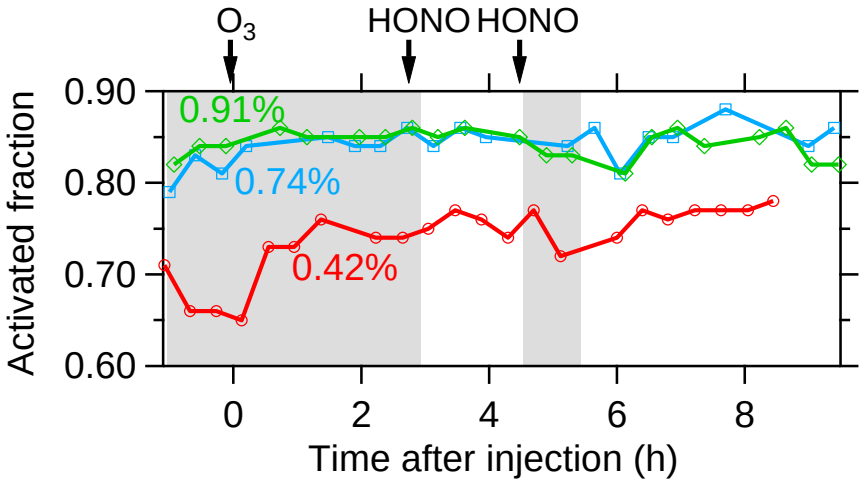

Figure 5.8: Evolution of the activated fraction of SOA particles under 0.42, 0.74 and 0.91% supersaturation during Experiment 5. Time zero corresponds to O_3 addition and initiation of ozonolysis.

Before time zero only ammonium sulphate particles were present in the chamber. The average activated fraction for 0.42% supersaturation was 0.67. At time zero when SOA formation from the ozonolysis of α-pinene started, the activated fraction increased to around 0.75 within the next 2 hours. This initial increase of the activated fraction was observed only for the lowest supersaturation (0.42%). For the other supersaturations where the initial activated fraction was already close to unity no significant differences

were found. This behavior was observed in all the seeded experiments. The activated fraction was calculated for each stage of the experiment (ozonolysis, 1st aging, and 2nd aging) and the results are shown in Table 5.2. For ozonolysis at 0.42% we focus on the final fraction after the initial increase. The t-test revealed no statistically significant differences among supersaturations or among the aging steps.

Table 5.2: Activated fraction (CCN/CN) of SOA particles formed in different steps in all supersaturations for Experiment 5.

	0.42%	**0.74%**	**0.91%**
Ozonolysis	0.73±0.04	0.85±0.01	0.85±0.01
1st aging step	0.76±0.01	0.85±0.01	0.85±0.01
2nd aging step	0.77±0.01	0.85±0.02	0.84±0.02

The corresponding activation diameter of the particles inside the chamber is shown in Figure 5.9. The production of SOA and the formation of an organic coating on the ammonium sulphate particles increased the activation diameter of the particles in all supersaturations as soon as ozonolysis started. The average activation diameter of ammonium sulphate particles before the ozonolysis step for supersaturations 0.42 and 0.74% was 50 and 28 nm respectively and increased to an average of 70 and 50 nm respectively during the ozonolysis.

Similar trends were observed among all seeded experiments. Ammonium sulphate particles are in general more hygroscopic compared to organic particles. The increase of the activation diameter is due to the addition of less hygroscopic substances (SOA) to the $(NH_4)_2SO_4$ particles, making the resulting mixed particles less hygroscopic.

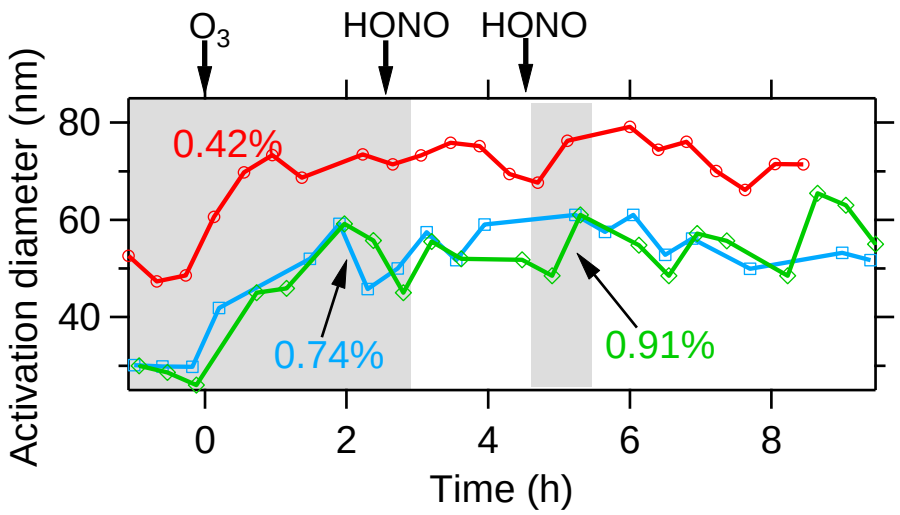

Figure 5.9: Evolution of the activation diameter of SOA particles under 0.42, 0.74 and 0.91% supersaturation for Experiment 5. Time zero corresponds to O_3 addition and initiation of ozonolysis.

On the other hand, the organic film formed on the pre-existing particles increased their size, which according to Köhler theory reduces the necessary supersaturation for their activation, so instead the activation fraction increased or remained stable. The changes of the activation diameter are governed by the changes of particle chemical composition, while the activation fraction behaviour is governed by both the size of the particles and by their composition with the size dominating in these experiments.

5.3.2 Non-seeded experiments

The evolution of the concentrations of main species in the particle phase for a typical experiment without seeds is shown in Figure 5.10.

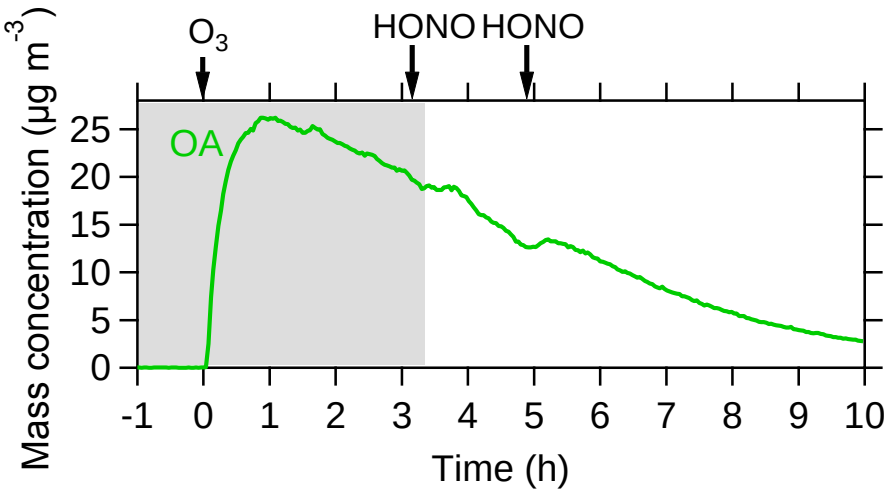

Figure 5.10: Time series of organic aerosol (OA) concentration during Experiment 7. Time zero corresponds to O_3 addition and initiation of ozonolysis.

SOA formation starts as soon as ozone is introduced in the chamber. Similarly to the seeded experiments, SOA concentration reaches a maximum within an hour and then it decreases due to wall losses. The HONO injections lead to the formation of a few additional µg m^{-3} of SOA. Figure 5.11 represents the evolution of the mean diameter of the SOA particles during the same experiment.

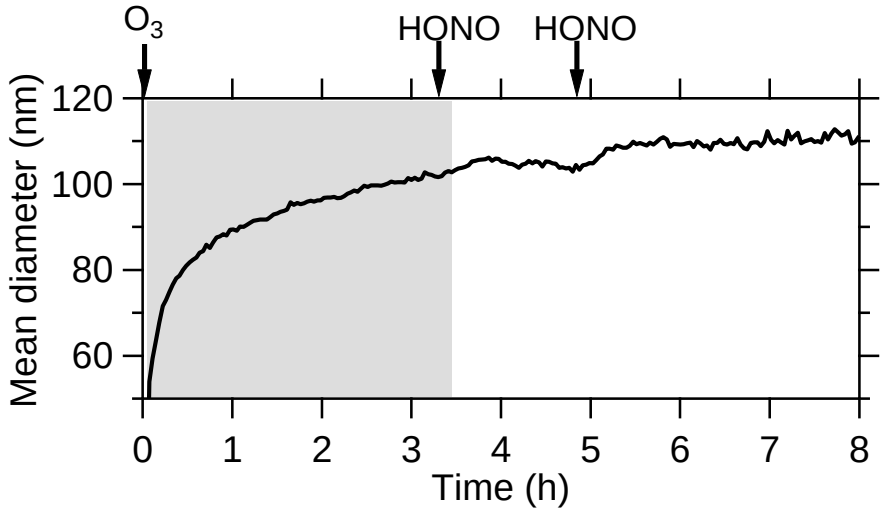

Figure 5.11: Mean diameter of SOA particles during Experiment 7. Time zero corresponds to O_3 addition and initiation of ozonolysis.

The first step of the photochemical aging results in an increase of 3 nm of the mean diameter of the SOA while the second in another 4 nm. This increase is comparable to that observed in the seeded experiments (4 and 3 nm respectively).

Figure 5.12 presents the evolution of the concentrations of the main gas phase species present in the chamber. A volume of 1 μL α-pinene is injected half at time -0.5 h and was allowed to stabilize resulting in a mixing ratio of around 15 ppb. One hour after the ozone injection (time 1 h) all α-pinene had reacted and ozone stabilized to a mixing ratio close to 500 ppb. The first HONO injection which took place in dark conditions led to the formation of NO and NO_2. Exposure to UV light increased NO levels and reduced NO_2 concentrations according to reactions 5.2 to 5.5.

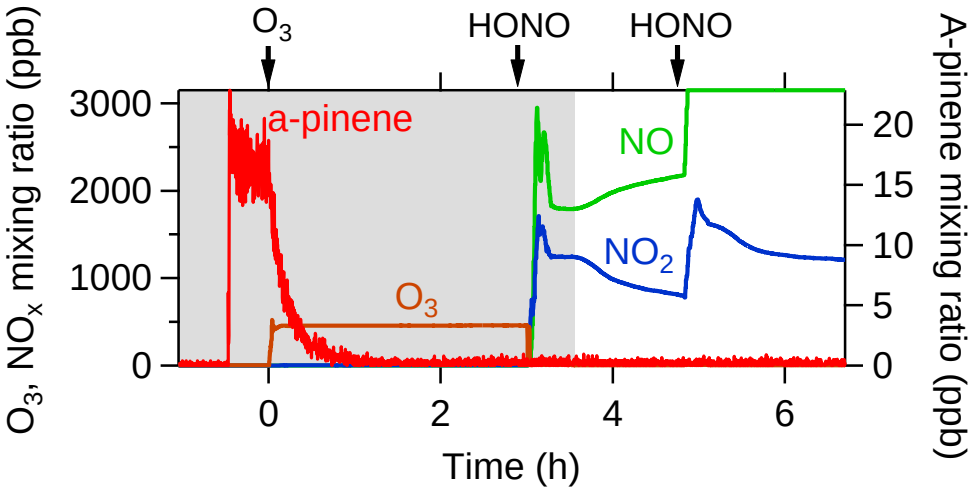

Figure 5.12: Evolution of the mixing ratio of α-pinene (right axis), NO, NO_2 and O_3 (left axis). Time zero corresponds to O_3 addition and initiation of ozonolysis.

5.3.3 Hygroscopic properties of pure SOA particles

For this series of experiments the supersaturation of the CCN counter was changing every 12 min. This allowed 1 to 4 measurements in each supersaturation so that every supersaturation was repeated every one hour. Figure 5.13 illustrates the time series of the activated fraction of pure SOA particles produced by the ozonolysis of α-pinene and two

aging steps using OH radicals produced by HONO photolysis. The UV lights were turned on half an hour after the first HONO. The activated fraction of the SOA particles increased during the first hour of the ozonolysis under all supersaturations. This increase is attributed to the increase of the SOA particles size. During the rest of the ozonolysis phase the activated faction did not significantly change because the change of particle size was a lot smaller. Photochemical aging did not affect the activated faction.

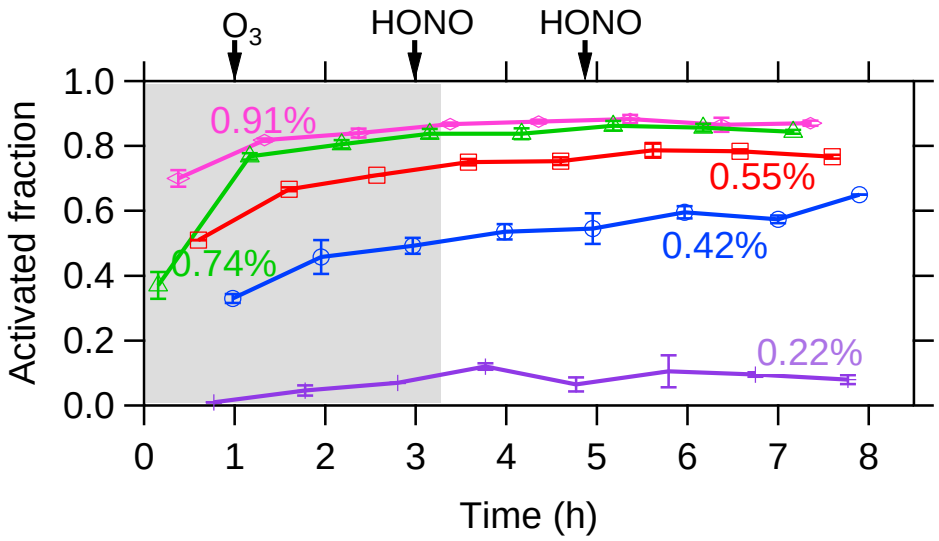

Figure 5.13: Evolution of the activated fraction of α-pinene SOA particles in different supersaturations during Experiment 7. The time of the two HONO injections is also indicated. Time zero corresponds to O_3 addition and initiation of ozonolysis.

Figure 5.14 represents the evolution of the activation diameter of SOA during Experiment 7. The average activation diameter was calculated for each step of the total reaction: ozonolysis (dark reaction), first HONO injection and photo-oxidation step and second HONO injection and photo-oxidation step. The t-test showed that the differences of the averaged activation diameter of each step were not statistically significant at the 95% confidence level, so the activation diameter is not affected by the aging. Photochemical aging had no significant impact on the activation diameter in this experiment.

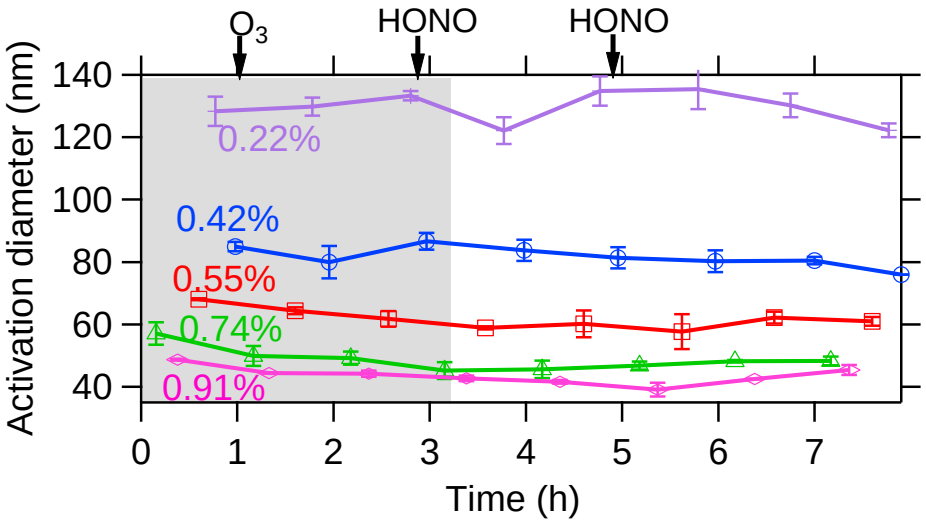

Figure 5.14: Evolution of the activation diameter of pure SOA particles estimated for 5 supersaturations for Experiment 7. Time zero corresponds to O_3 addition and initiation of ozonolysis.

The hygroscopicity parameter κ was calculated for the SOA particles (see also section 4.3.4) for the non-seeded experiments. Similarly to Chapter 4, κ was calculated here for different diameters of SOA particles. In order to estimate the average hygroscopicity of SOA, a weighted κ was calculated. This weighted kappa was estimated by multiplying the number fraction of each size bin with the hygroscopicity of the specific size bin and summing up these contributions.

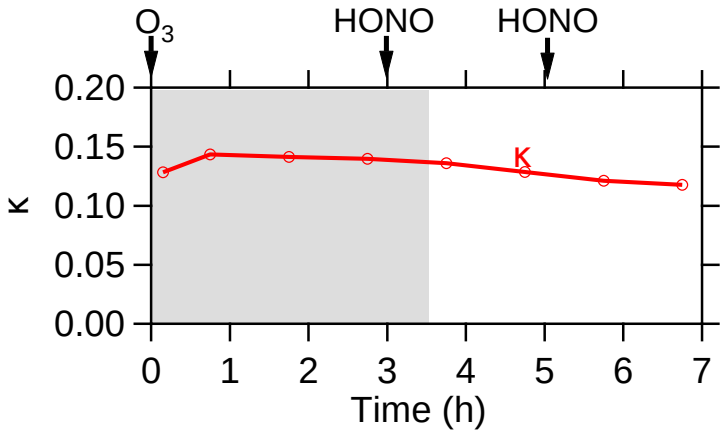

Figure 5.15: Evolution of hygroscopicity κ during Experiment 7. Time zero corresponds to O_3 addition and initiation of ozonolysis.

The hygroscopicity κ was found to be around 0.13 during the experiment. The chemical aging using OH radicals did not appear to induce any statistically significant changes to the hygroscopicity. Similar behavior was observed in all unseeded experiments (experiments 6 to 9). Aging did not affect hygroscopicity while both higher and lower variability of κ value compared to the experiment presented here was found. Table 5.3 summarizes the range of κ measured in experiments 6 to 9.

Table 5.3 Average SOA hygroscopicity values for unseeded experiments

Experiment	κ_{av}
6	0.13±0.02
7	0.13±0.01
8	0.09±0.01
9	0.11±0.00

An average kappa of 0.12±0.02 was calculated for the pure SOA experiments 6 to 9 conducted under similar conditions (ozonolysis, 2 chemical aging steps, no OH scavenger use). The hygroscopicity values estimated here are consistent with previous findings for α-pinene SOA. Frosch et al. (2011) conducted α-pinene ozonolysis and aging in smog chamber under different NO_x conditions. They estimated an average κ value of 0.11±0.02 from CCN measurements and similarly to this work found no effect of the HONO injections. Jurányi et al. (2009) estimated a CCN-derived average κ of 0.09±0.01. Chang et al. (2010) estimated an overall κ of 0.15 for organics from ambient biogenic SOA at a rural site in Canada. Finally, Engelhart et al. (2008) reported a hygroscopicity of 0.15±0.08 for monoterpene SOA and 0.11 for α-pinene SOA formed solely by ozonolysis.

The HR-AMS extracted data are useful to explore the oxidative state of the SOA particles. The ratio of the number of oxygen to the number of carbon atoms of the organic compounds provided by the mass spectra has been extensively used as a measure of the extent of oxidation of the organic aerosol. Figure 5.16 shows the evolution of oxygen to carbon ratio measured during the oxidation of α-pinene SOA in Experiment 7.

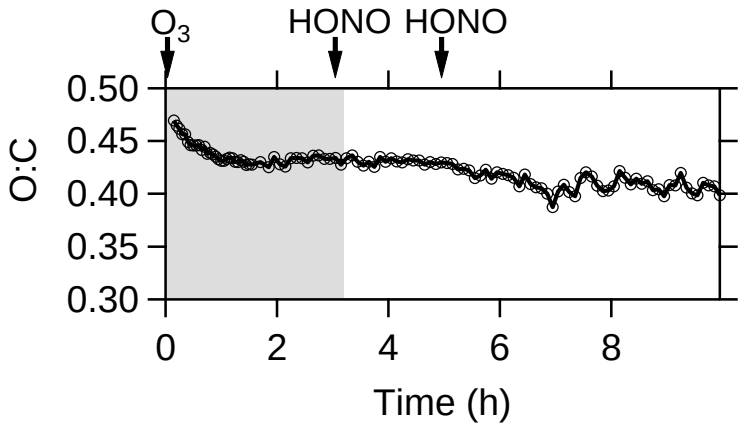

Figure 5.16: Time series of the oxygen to carbon number of atoms ratio during the experiment 7. Time zero corresponds to O_3 addition and initiation of ozonolysis.

The O:C ratio initially decreases and then remains relatively constant throughout the experiment. Similar variations, decreasing or rather steady trend of the O:C ratio has been observed in all experiments. This behaviour is qualitatively consistent with the relatively constant κ values measured. Hygroscopicity κ and O:C time showed an intermediate correlation for Experiment 7 (R^2=0.31, Figure 5.17). Similar correlation has been found in all experiments of this set, ranging from 0.2 to 0.5, except for Experiment 9 where no correlation was observed. However, the O:C ratio was practically constant during this experiment, with average values ranging from 0.38 to 0.39. In Experiment 10, where n-butanol (d9) was injected in the chamber before the initialization of the ozonolysis in order to react with the OH radicals produced during the ozonolysis of α-pinene, the correlation was the strongest with R^2=0.72.

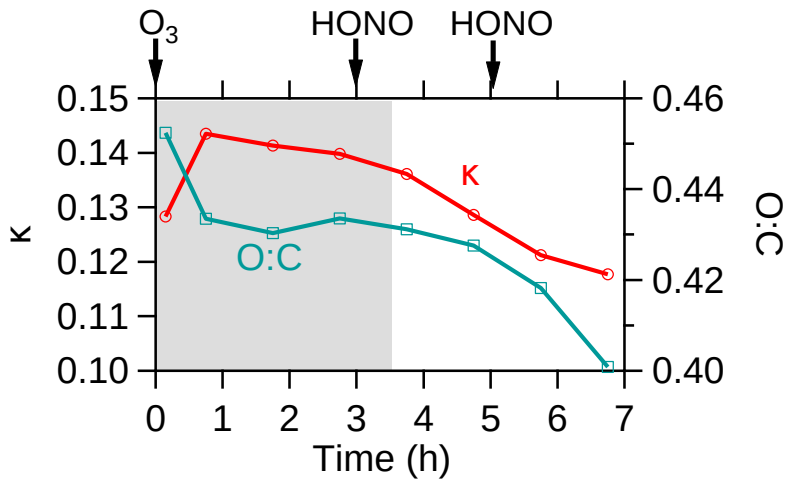

Figure 5.17: Evolution of the hygroscopicity and the oxygen to carbon ratio for Experiment 7. Time zero corresponds to O_3 addition and initiation of ozonolysis.

Figure 5.18 summarizes the relationship of the hygroscopicity parameter κ with the O:C ratio for all non-seeded experiments. The O:C ratio varied from nearly 0.27 to 0.47 while kappa ranged from 0.07 to 0.19.

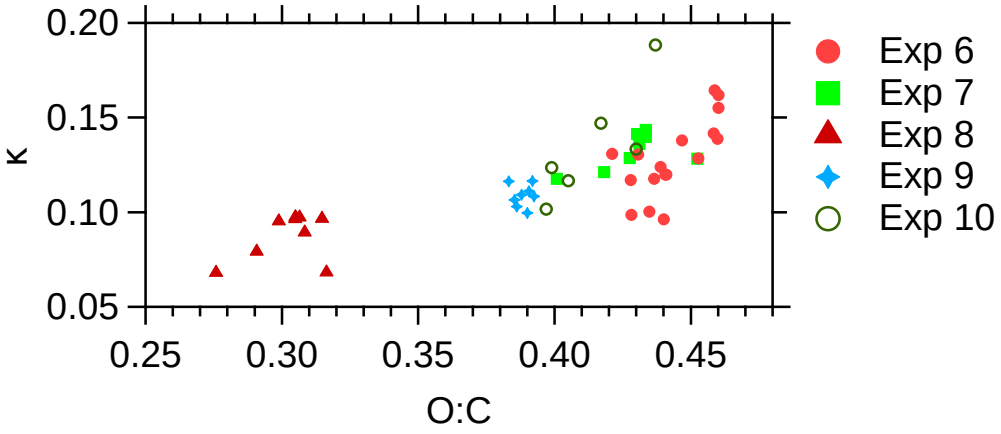

Figure 5.18: Relationship of hygroscopicity κ with the O:C ratio for all non-seeded experiments Each point corresponds to an average of 1 hour.

The hygroscopicity parameter kappa correlates well (R^2=0.53) with the O:C ratio and kappa can be expressed as:

$$\kappa=(0.29\pm0.005)\cdot(O:C) \qquad (5.6)$$

Similar equations have been reported in the literature. Chang et al. (2010) reported exactly the same relationship for field measurements in a forest in Canada. On the other hand Frosch et al. (2011) reported that no relation between κ and O:C ratio could be established in their experiments and found a weak correlation between these two (R^2=0.25). This data was collected by smog chamber ozonolysis and consequent HONO oxidation under low NO_x levels as this work. The agreement with the ambient measurements is encouraging.

5.3.4 WSOC measurements

The Steam Sampler-TOC was used in experiment 10 in order to measure the water soluble fraction of the biogenic SOA formed by the ozonolysis and the impact of chemical aging of α-pinene on the solubility of the final products. In this experiment n-butanol (d9) was also used in the chamber as an OH scavenger in order to remove OH produced by the ozonolysis of α-pinene. Figure 5.19 presents the time series of the water soluble organic aerosol measurement by the Steam Sampler-TOC and the total organic aerosol concentration measured by the SMPS during Experiment 10. The volume distribution of the SMPS was converted to mass distribution using an average density of 1.5 g cm^{-3} for the biogenic SOA which was estimated by Kostenidou et al. (2007) for monoterpene SOA.

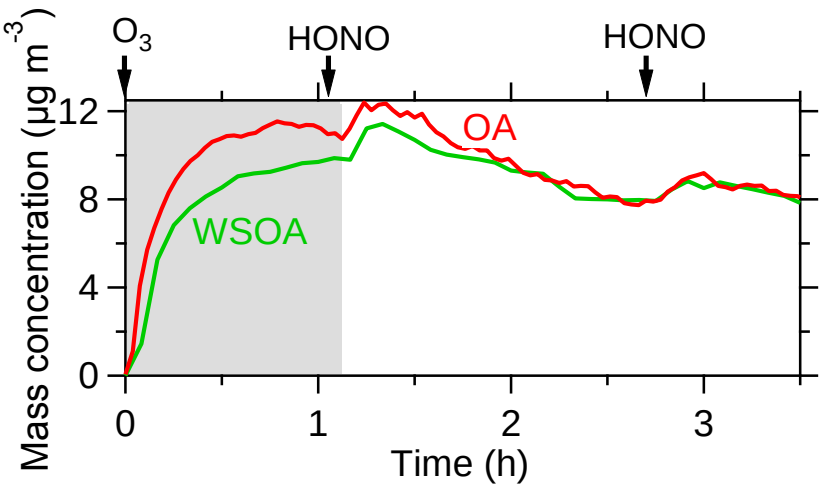

Figure 5.19: Evolution of the water soluble organic aerosol concentration (green line) and total organic aerosol concentration (red line) for Experiment 10. Time zero corresponds to O_3 addition and initiation of ozonolysis.

The initial soluble fraction corresponds to 66% of the total SOA mass but is highly uncertain due to rapidly changing concentrations of both OA and WSOA during this period. The water soluble fraction of the ozonolysis products is around 80%. The first HONO injection which increases significantly the SOA mass (Figure 5.20) results in a further increase of the water soluble fraction of the SOA, reaching practically unity roughly two hours after the initialization of the reaction. The second photo-oxidation induced by the consequent HONO addition does not affect the WSOC fraction of the SOA however the soluble fraction had already reached one and there was no room for improvement. Figure 5.21 presents the evolution of the water soluble faction and the hygroscopicity of the SOA.

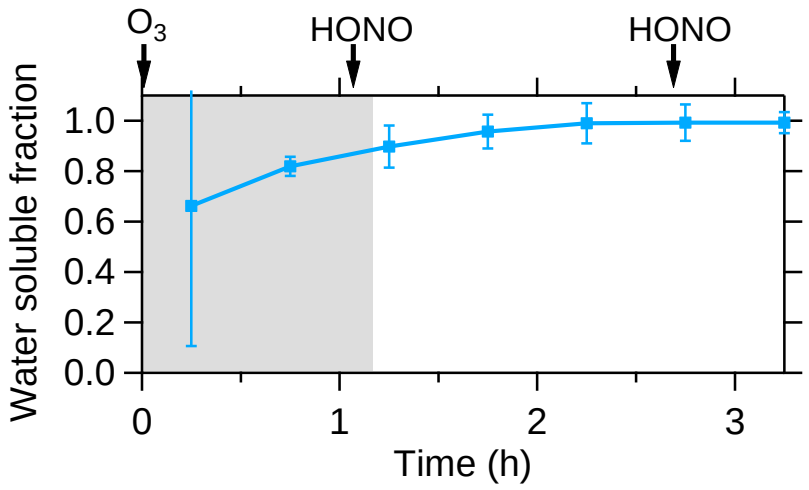

Figure 5.20: Evolution of the 30-min averaged water soluble fraction of α-pinene SOA for Experiment 10. Time zero corresponds to O_3 addition and initiation of ozonolysis.

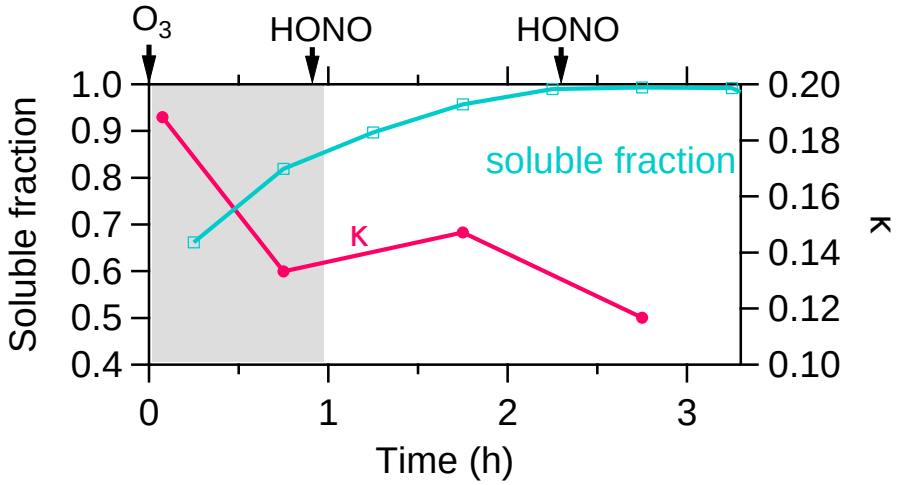

Figure 5.21: Water soluble fraction of α-pinene SOA and their hygroscopicity for Experiment 10. Time zero corresponds to O_3 addition and initiation of ozonolysis.

5.4 Conclusions

In all experiments photochemical aging did not have a significant effect on the ability of the SOA to act as CCN. The activation diameter of pure α-pinene SOA particles remained constant during the ozonolysis and aging reactions.

The hygroscopicity of the particles did not significantly change during each experiment but there was some variability from experiment to experiment. An average hygroscopicity of 0.12±0.02 was estimated for either fresh or aged α-pinene SOA. This value is consistent with other reported in literature estimated for fresh SOA produced by ozonolysis and aged SOA produced in smog chamber studies.

The relation of the hygroscopicity of organic aerosol with the number of oxygen to number of carbon atoms ratio was also estimated based on a series of experiments. The hygroscopicity of pure biogenic organic particles and the O:C ratio correlated well (R^2=0.53) and κ can be expressed as $\kappa=(0.29\pm0.005)\cdot(O:C)$. Previous findings vary from no dependence of hygroscopicity on the O:C ratio to significant dependence as estimated in this work.

The water soluble fraction of the α-pinene SOA was measured using the Steam Sampler-TOC. The soluble fraction of the SOA after one hour of ozonolysis exceeded 0.9 and reached 1 within 2 hours after the initiation of ozonolysis. The photo-oxidation of the SOA with OH radicals did not affect the water soluble fraction of the SOA however the fraction was already close to 1 at the time of HONO injections.

The average parameter κ measured here can be used for the simulation of aerosol cloud interactions in chemical transport models that simulate α-pinene SOA and its chemical aging without keeping track of its chemical composition. Equation (5.6) can be used in the models that simulate also the O:C of the SOA (e.g., 2-D Volatility Basis Set).

5.5 References

Acker, K., Mertes, S., Moller, D., Wieprecht, W., Auel, R., Kalasz, D. Case study of cloud physical and chemical processes in low clouds at Mt. Brocken. *Atmos. Research*, **2002**, 64, 41-51.

Asad, A., Mmereki, B.T., Donaldson, D.J. Enhanced uptake of water byoxidatively processed oleic acid. *Atmos. Chem. and Phys.*, **2004**, 4, 2083-2089.

De Carlo, P.F., Kimmel, J.R., Trimborn, A., Northway, M.J., Jayne, J.T., Aiken, A.C., Gonin, M. Fuhrer, K., Horvath, T., Docherty, K.S., Worsnop, D.R., Jimenez, J.L., 2006. Field-Deployable, High-Resolution, Time-of-Flight Aerosol Mass Spectrometer. *Analytical Chemistry 78*, 8281-8289.

Donahue, N.M., Henry, K.M., Thomas F. Mentel, T.F., Kiendler-Scharr, A., Spindler, C., Bohn, B, Brauers, T., Hans P. Dorn, H.P., Fuchs, H., Tillmann, R., Wahner, A., Saathoff, H., Naumann, K.H.,Möhler, O., Leisner, T., Müller, L., Reinnig, M.-C., Hoffmann, T. Salo, K., Hallquist, M., Frosch, M., Bilde, M., Tritscher, T., Barmet, P., Praplan, A.P., DeCarlo, P.F., Dommen, J., Prévôt, A.S.H., Baltensperger, U. Aging of biogenic secondary organic aerosol via gas-phase OH radical reactions. *PNAS,* **2012**, 109, 34, 13503-13508.

Chang, R., Y.-W., Slowik, J.G., Shantz, N.C., Vlasenko, A., Liggio, J., Sjostedt, S.J., Leaitch, W.R., Abbat, J.P.D. The hygroscopicity parameter (κ)of ambient organic aerosol at a field site subject to biogenic and anthropogenic influences: Relationship to degree of aerosol oxidation. *Atmos. Chem. Phys.*, **2010**, 5047-5064.

Chung S.H. and Seinfeld, J.H. Global distribution and climate forcing of carbonaceous aerosols. *J. Geophys. Res.*, **2002**, 107, 4407.

Engelhart, G.J., Asa-Awuku, A., Nenes, A., Pandis, S.N. CCN activity and droplet growth kinetics of fresh and aged monoterpene secondary organic aerosol. *Atmos. Chem. Phys.*, **2008**, 8, 3937-3940.

Finlaysin-Pitts, B.J., Pitts, J.N. Jr. Chemistry of the upper and lower atmosphere. 2010, Academic Press.

Frosch, M., Bilde, M., DeCarlo, P.F., Jurányi, Z., Tritscher, T., Dommen, J., Donahue, N.M., Gyzel, M., Weingartner, E., Baltensperger, U. Relating cloud condensation nuclei activity and oxidation level of α-pinene secondary organic aerosols. *J. Geophys. Res.*, **2011**, 116, D22212.

Griffin, R.J., Cocker, D.R., Seinfeld, J.H., Dabdub, D. Estimate of global atmospheric organic aerosol from the oxidation of biogenic hydrocarbons. *Geophys. Res. Let.*, **1999**, 26:2721-2724.

Guenther A., Hewitt, C.N., Erickson, D., Fall, R., Geron, C., Graedel, T., Harley, P., Lee Klinger, L., Manuel Lerdau, M., Mckay, W.A., Pierce, T.,Scholes, B., Steinbrecher, R.,Tallamraju, R., John Taylor, J., Zimmerman, P. A global model of natural volatile organic compound emissions. *J. Geophys. Res.*, **1995**, 100, 8873-8892.

Hartz, K.H., Rosenorn, T., Ferchak, S.R., Raymond, T.M., Bilde, M., Donahue, N.M, Pandis, S.N. Cloud condensation nuclei activation of monoterpene and sesquiterpene secondary organic aerosol. *J. Geophy. Res.*, **2005**, 10, D14208.

Hallquist, M. Wenger, J.C., Baltensperger, U., Rudich, Y., Simpson, D., Claeys, M., Dommen, J., Donahue, N.M., George, C., Goldstein, A.H., Hamilton, J.F., Herrmann, H., Hoffmann, T., Iinuma, Y., Jang, M., Jenkin, M.E., Jimenez, J.L., Kiendler-Scharr, A., Maenhaut, W., McFiggans, G., Mentel, T.F., Monod, A., Prévôt, A.S.H., Seinfeld, J.H., Surratt, J.D., Szmigielski, R., and Wildt, J. The formation, properties and impact

of secondary organic aerosol: Current and emerging issues. *Atmos. Chem. Phys.*, **2009**, 10, 5155-5236.

Hegg, D.A., Hobbs, P.V., Ferrek, R.J., Waggoner, A.P. Measurements of some aerosol properties relevant to radiative forcing on the East Coast of the United States. *J. Applied Meteorol.*, **1995**, 34, 2306-2315.

Hoffmann, T., Odum, J.R., Bowman, F.A., Collins, D., Klockow, D., Flagan, R.C., Seinfeld, J.H. Formation of organic aerosol from the oxidation of biogenic hydrocarbon. *J. Atmos. Chem.,* **1997,** 26, 189-222.

Holzinger, H. ,Lee, A., Paw, U.K.T., Goldstein, A.H. Observations of oxidation products above a forest imply biogenic emissions of very reactive compounds. *Atmos. Chem. Phys.Disc.*, **2004**, 4, 5345-5365.

Jurányi, Z., Gyzel, M., Duplissy, J., Weingartner, E., Tritscher, T., Dommen, J., Henning, S., Ziese, M., Kiselev, A., Stratmann, F., George, I., Baltesperger, U. Influence of gas-to-particle partitioning on the hygroscopic and droplet behaviour of α-pinene secondary organic aerosol. *Phys. Chem. Chem. Phys.*, **2009**, 11, 8091-8097.

Kalberer, M., Paulsen, D., Sax, M., Steinbacher, M., Dommen, J., Prevot, A. S. H., Fisseha, R., Weingartner, E., Frankevich, V., Zenobi, R., Baltensperger, U. Identification of polymers as major components of atmospheric organic aerosols. *Science*, **2004**, 303(5664): 1659-1662.

Kanakidou, M., Seinfeld, J.H., Pandis, S.N., Barnes, I., Dentener, F.J., Facchini, M.C., Van Dingenen, R., Ervens, B., Nenes, A., Nielsen, C.J., et al. Organic aerosol and global climate modelling: A review. *Atmos. Chem. Phys,* **2005**, 5, 1053-1123.

Kostenidou, E., Pathak, R., Pandis, S.N. An algorithm for the calculation of secondary organic aerosol density combining AMS and SMPS data. *Aerosol Sci. Technol.*, **2007**, 41, 1002-1010.

Massoli, P., Lambe, A.T., Ahern, A.T., Williams, L.R., Ehn, M., Mikkilä, J., Canagaratna, M.R., Brune, W.H., Onasch, T.B., Jayne, J.T., Petäjä, T., Kulmala, M., Laaksonen, A., C. E. Kolb, C.E., Davidovits, P., Worsnop, D.R. Relationship between aerosol oxidation level and hygroscopic properties of laboratory generated secondary organic aerosol (SOA) particles. *Geophys. Res. Let*, **2010**, 37, L24801.

Matsumoto, K., Tanaka, H., Nagao, I., Ishizaka, Y. Contribution of particulate sulphate and organic carbon to cloud condensation nuclei in the marine atmosphere. Geophys. Res.Lett., 1997, 24, 655-658.

Mmereki, B.T., Donaldson, D.J., Gilman, J.B., Eliason, T.L., Vaida, V.. Kinetics andproducts of the reaction of gas-phase ozone with anthracene adsorbed at theair-aqueous interface. *Atmos. Environ.*, **2004**, 38, 6091-6103.

Novakov, T., Penner, J.E. Large contributions of organic aerosol to cloud-condensation nuclei concentrations. *Nature*, 1993, 365, 823-825.

Pathak R.K., Stanier, C.O., Donahue, N.M., Pandis, S.N. Ozonolysis of α-pinene at atmospherically relevant concentrations: Temperature dependence of aerosol mass fractions (yields). *J. Geophys. Res.*, **2007**, 112, D03201.

Petters, M.D., Kreidenweis, S.M. A single parameter representation of hyroscopic growth and cloud condensation nucleus activity. *Atmos. Chem. Phys.*, **2007,** 7, 1961-1971.

Poulain, L., Wu, Z., Petters, M.D., Wex, H., Hallbauer, E., Wehner, B., Massling, A., Kreidenweis, S.M., Stratmann, F. Towards closing the gap between hygroscopic growth and CCN activation for secondary organic aerosols-Part 3: Influence of the chemical composition on the hygroscopic properties and volatile fractions of aerosols. *Atmos. Chem. Phys.*, **2010**, 10, 3775-3785.

Presto, A.A., Hartz, K.E.H., Donahue, N.M. Secondary organic aerosol production from terpene ozonolysis. 2. Effect of NO_x concentration. *Environ. Sci. Technol.*, **2005**, 39, 7046-7054.

Rudich, Y., Donahue, N.M., Mentel, T.F. Aging of organic aerosol: bridging thegap between laboratory and field studies. *Annual Rev. Phys. Chem*, **2007**, 58, 321-352.

Seinfeld, J.H., and Pankow, J.F. Organic atmospheric particulate matter. *Annu. Rev. Phys. Chem.*, **2003**, 54, 121-140.

Singh, H.B., Zimmerman, P. Atmospheric distribution and sources of non methane hydrocarbons in gaseous pollutants: Characterization and cycling, edited by J.O. Nriagu, **1992**, 177-235, John Wiley, Hoboken, N.J.

Sun, J., Ariya, P.A. Atmospheric organic and bioaerosols as cloud condensation nuclei (CCN): A review. *Atmos. Environ.*, **2006**, 40, 795-820.

Tsigaridis, K., Lathière, J., Kanakidou, M., Hauglustaine, D.A. Naturally driven variability in the global secondary organic aerosol over a decade. *Atmos. Chem. Phys. Disc.*, **2005**, 5, 1845-1852.

Yu, J., cocker, D.R., Griffin, R.J., Flagan, R.C., Seinfeld, J.H. Observation of gaseous and particulate products of mono-terpene oxidation in forest atmospheres. *Geophys. Res. Lett.*,**1999**, 26, 1145-1148.

Chapter 6

Summary
and
Recommendations

6.1 Summary

The measurement of Water Soluble Organic Carbon (WSOC) in atmospheric aerosol is usually carried out by sample collection on filters, extraction in ultrapure water, filtration, and measurement of the total organic carbon. In this wok the role of different conditions of sampling and extraction as well as the range of solubilities of the organic compounds that contribute to the WSOC were investigated. The sampling and extraction of WSOC can be described by a single parameter, *P*, expressing the ratio of water used per volume of air sampled on the analyzed filter. Two cases are examined in order to limit the range of interactions of the various organic aerosol components with each other. In the first we assume that that the organic species form an ideal solution in the particle and in the second that the extraction of a single compound is independent of the presence of the other organics. The ideal organic solution model predicts that species with water solubility as low as 10^{-4} g L^{-1} contribute to the measured WSOC. In the other end, the independent compounds model predicts that low-solubility (as low as 10^{-7} g L^{-1}) compounds are part of the WSOC. Studies of the WSOC composition are consistent with the predictions of the ideal organic solution model. A value of P=0.1 cm^3 m^{-3} is proposed for the extraction of WSOC in typical organic aerosol concentrations (1-10 μg m^{-3}) while higher *P* values should be applied in case of heavier organic aerosol loadings (100-1000 μg m^{-3}).

A new system for the continuous measurement of the water soluble organic carbon of the atmospheric aerosols was also developed. The system provides measurements of the WSOC concentrations every 4 minutes and collects particles with diameter less than 3 μm. The *P* parameter of this WSOC measurement method was estimated to be 44.1 cm^3 m^{-3}. Evaluation experiments have been conducted in order to test the efficiency of the

system to sample water soluble species. Sucrose particles were measured by the Steam Sampler and an SMPS and the corresponding measurements were in agreement within 10%. The instrument was also tested in field measurements in a background site outside of Patras. The Steam Sampler measurements showed that the WSOC average concentration was 1.2 μg C m^{-3} during June 2012. This concentration corresponds to approximately 2.5 μg m^{-3} of organic mass. The WSOM measured in PM_3 represents to 66% of the organic mass measured by the AMS in PM_1, which was on average 3.7 μg m^{-3}. Since the measurements were conducted during summer, a significant fraction of the organic mass is expected to be water soluble and this percentage is reasonable. However, an accurate estimation of the water soluble fraction was impossible since the two instruments measure in different size ranges. The correlation between the WSOM and the OOA was poor (R^2=0.17) and this can only be partially attributed to the different cut-off point of each system. Another reason could be the high *P* parameter of the system which may have allowed the collection of low-solubility organics. However, the decrease of the *P* parameter of the on-line techniques is challenging because of the relatively high minimum liquid sample volume necessary for TOC analysis as well as the low air sampling rate.

The composition and hygroscopic properties of atmospheric aerosol in Athens during winter of 2013 were also studied. The PM_1 was dominated by organic species during all the sampling period, with an average organic mass fraction of 0.58, followed by black carbon with a corresponding fraction of 0.2. The most important contributor to the organic aerosol concentrations was biomass burning which started in the evening and peaked during the night. HOA from traffic peaked during the morning rush hour, affecting the total hygroscopic properties of organic aerosols. During the HOA peak, the

critical supersaturation of the particles studied here (50 nm≤d_p≤100 nm) was lower due to the hydrophobic nature of HOA. The maximum chemical dispersion of the particles is also observed during this period. Size-resolved chemical composition data provided by the HR-AMS revealed discrepancies on the composition of smaller (50-70 nm) and bigger particles (80-100 nm) and showed that the properties of the PM_1 bulk composition can be represented by the properties of bigger particles. These particles were found to be quite hygroscopic, with the maximum activated fraction reaching almost unity during most of the day, except for the morning traffic period. The average hygroscopicity parameter κ of these particles ranged roughly from 0.15 to 0.25. The average hygroscopicity parameter of mixed (organic/inorganic) particles during the night when biomass burning particles prevailed was around 0.15. The diurnal profile of the average hygroscopicity was very similar with the profile of the O:C ratio but no correlation was observed. The organic particles hygroscopicity κ_{org} was on average 0.12 while during the biomass burning period was on average 0.09.

In all experiments photochemical aging did not have a significant effect on the ability of the SOA to act as CCN. The activation diameter of pure α-pinene SOA particles remained constant during the ozonolysis and aging reactions. The hygroscopicity of the particles did not significantly change during each experiment but there was some variability from experiment to experiment. An average hygroscopicity of 0.12±0.02 was estimated for either fresh or aged α-pinene SOA. This value is consistent with other reported in literature estimated for fresh SOA produced by ozonolysis and aged SOA produced in smog chamber studies. The relation of the hygroscopicity of organic aerosol with the number of oxygen to number of carbon atoms ratio was also estimated. The hygroscopicity of pure biogenic organic particles and the O:C ratio correlated well

(R^2=0.53) and κ can be expressed as κ=(0.29±0.005)·(O:C). Previous findings vary from no dependence of hygroscopicity on the O:C ratio to significant dependence as estimated in this work. The average parameter κ measured here can be used for the simulation of aerosol cloud interactions in chemical transport models that simulate α-pinene SOA and its chemical aging without keeping track of its chemical composition. Equation (5.6) can be used in the models that simulate also the O:C of the SOA.

The water soluble fraction of the α-pinene SOA was measured using the Steam Sampler-TOC. The soluble fraction of the SOA after one hour of ozonolysis exceeded 0.9 and reached 1 within 2 hours after the initiation of ozonolysis. The photo-oxidation of the SOA with OH radicals did not affect the water soluble fraction of the SOA however the fraction was already close to 1 at the time of HONO injections.

6.2 Recommendations for Future Work

The current design of the Steam Sampler-TOC allows the air sample to enter the system with an average flow of 13.6 L min^{-1}. Most PM_1 and $PM_{2.5}$ cyclones operate at higher flow rate (16.7 L min^{-1}) to provide their cut-off points. The field tests and the comparisons of WSOC measurements with the AMS data focus on PM_1 in order to facilitate the comparison of data between the instruments. The excess flow necessary to achieve the nominal cut-off point of the cyclone can be obtained using the set-up shown in Figure 6.1.

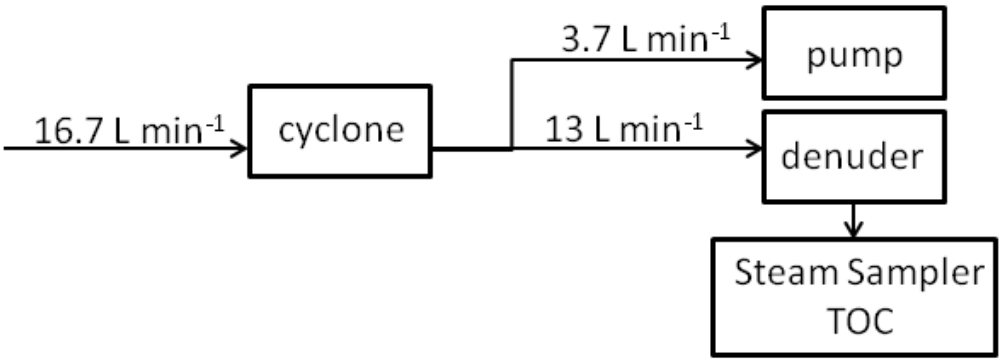

Figure 6.1: Suggested set-up for PM_1 sampling and measurement by the Steam Sampler-TOC.

Using a pump in order to increase the total flow rate passing through the cyclone the appropriate flow rate necessary to achieve the nominal diameter cut-off point can be reached. The set-up of Figure 6.1 allows the determination of the water soluble organic mass present in PM_1 or $PM_{2.5}$, depending on the cyclone used.

The design of the Steam Sampler allows the measurement of OC alternatively with WSOC. Figure 6.2 presents a simply modified version of the Steam Sampler-TOC. Here, line 1 represents the typical pathway of the liquid sample collected in a vial by the Steam Sampler as it is driven for WSOC measurement through a PTFE filter. This filter prevents the entrance of insoluble, suspended species into the TOC analyzer. Line 2 has been added in this set-up in order to bypass the filter so both soluble and insoluble species will be driven to the TOC analyzer and will be measured. An electronically controlled valve enables the transmission of the sample through each line alternatively and the consequent measurement of WSOC (line 1) and total OC (line 2).

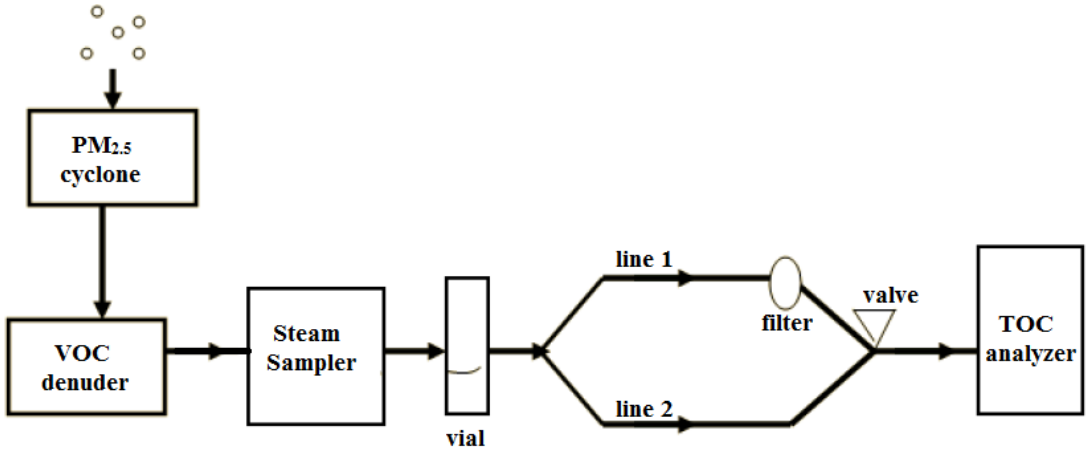

Figure 6.2: Proposed set-up for the measurement of WSOC and OC.

In this work, the CCN properties and the hygroscopicity factor κ of fresh and aged secondary organic aerosol formed ozonolysis and photochemical aging was estimated under low relative humidity conditions (<10%). However, the ozonolysis products may differ as well as their physical properties if water vapor is available (Poulain et al., 2010). In real atmospheric systems the relative humidity is higher than that used here. Similar smog chamber experiments should be carried out under intermediate (~50%) and high (~90%) relative humidity conditions, in order to estimate the hygroscopic properties of the SOA under more realistic conditions.

A two-necked flask on a heating mantle can provide the smog chamber with water vapor. A thermally insulated PTFE tubing should be used to deliver water vapor inside the chamber. The PTFE tubing will eliminate contamination of water vapors while the insulation will prevent condensation of water vapor inside the tubing.

The hygroscopic properties of α-pinene SOA are often used to represent all biogenic emissions. Ozonolysis and photochemical aging experiments can also be carried out

using a different SOA precursor, such as another monoterpene (e.g., caryophylene, limonene) or isoprene, in order to inspect any significant differences on the activation and hygroscopic properties of the SOA.

Appendix

Σύνοψη Διδακτορικής Διατριβής

1. ΠΕΡΙΛΗΨΗ

Τα αιωρούμενα σωματίδια της ατμόσφαιρας επιδρούν σημαντικά στην ανθρώπινη υγεία, την ορατότητα, αλλά και στο κλίμα του πλανήτη. Προκαλούν ψύξη της ατμόσφαιρας σκεδάζοντας την ηλιακή ακτινοβολία πίσω στο διάστημα και δρώντας σαν πυρήνες συμπύκνωσης συννέφων. Τα υδατοδιαλυτά και υγροσκοπικά συστατικά των σωματιδίων είναι κυρίως υπεύθυνα για την έμμεση δράση των σωματιδίων στο κλίμα, λόγω της ικανότητάς τους να προσελκύουν το ατμοσφαιρικά διαθέσιμο νερό. Το μέγεθος αυτών των αλληλεπιδράσεων είναι αρκετά αβέβαιο και περιορίζει την δυνατότητά μας να προβλέψουμε τις μελλοντικές κλιματικές αλλαγές.

Στο πρώτο μέρος αυτής της εργασίας εξετάζονται θεωρητικά οι υπάρχουσες ημιεμπειρικές μέθοδοι μέτρησης των υδατοδιαλυτών οργανικών συστατικών των σωματιδίων. Αναπτύχθηκαν δύο θεωρητικά μοντέλα για να περιγράψουν τη μη συνεχή μέτρηση του υδατοδιαλυτού άνθρακα. Βασιζόμενοι σε μετρήσεις της σύστασης του υδατοδιαλυτού κλάσματος των οργανικών σωματιδίων αλλά και σε πειραματικές και υπολογιστικές εργασίες πάνω στο σχηματισμό φάσεων στα σωματίδια, οδηγηθήκαμε στο συμπέρασμα ότι το μοντέλο του ιδανικού οργανικού διαλύματος μπορεί να περιγράψει ικανοποιητικά τη διαδικασία. Σύμφωνα με αυτό, το κλάσμα μια οργανικής ένωσης στο υδατοδιαλυτό εκχύλισμα εξαρτάται από τη διαλυτότητα του συστατικού, τη συγκέντρωση των μη διαλυτών οργανικών και την παράμετρο P που εισάγεται εδώ για να περιγράψει τη μέθοδο της δειγματοληψίας. Συγκεκριμένες τιμές της P προτείνονται επίσης για την ικανοποιητική εκχύλιση των επιθυμητών ουσιών.

Στη συνέχεια περιγράφεται η ανάπτυξη του Δειγματολήπτη Ατμού για τη μέτρηση των υδατοδιαλυτών οργανικών. Το σύστημα αυτό παράγει ατμό ο οποίος αναμιγνύεται με το

ατμοσφαιρικό δείγμα που φέρει σωματίδια. Ο ατμός συμπυκνώνεται πάνω σε αυτά, δημιουργώντας σταγόνες που συλλέγονται σε κυκλώνες και οδηγούνται προς μέτρηση του οργανικού φορτίου τους σε έναν αναλυτή ολικού οργανικού άνθρακα. Το σύστημα αυτό ελέγχθηκε στο εργαστήριο με σωματίδια γνωστής χημικής σύστασης και διαλυτότητας και χρησιμοποιήθηκε στο πεδίο στην Πάτρα.

Μετρήσεις που διεξήχθησαν στο κέντρο της Αθήνας το χειμώνα του 2013 έδειξαν ότι τα οργανικά σωματίδια επικρατούσαν στην ατμόσφαιρα της πόλης σε όλο το διάστημα των μετρήσεων, ιδιαίτερα κατά τη διάρκεια της νύχτας. Η σημαντικότερη πηγή σωματιδίων ήταν η καύση βιομάζας στα τζάκια, για λόγους οικιακής θέρμανσης, ενώ η κίνηση των αυτοκινήτων αποτέλεσε σημαντική πηγή σωματιδίων κυρίως τις πρωινές ώρες. Τα σωματίδια αυτά είχαν σημαντική υγροσκοπικότητα η οποία ποσοτικοποιήθηκε με την χρήση ενός μετρητή πυρήνων συμπύκνωσης συννέφων.

Πτητικές οργανικές ενώσεις προερχόμενες από βιογενείς εκπομπές οξειδώνονται στην ατμόσφαιρα σχηματίζοντας οργανικά σωματίδια. Τα πειράματα που διεξήχθησαν στον περιβαλλοντικό θάλαμο του Εργαστηρίου Ατμοσφαιρικής Ρύπανσης του ΙΤΕ-ΙΕΧΜΗ έδειξαν ότι η υγροσκοπικότητα των σωματιδίων που προκύπτουν από την οζονόλυση αυτών των βιογενών σωματιδίων είναι υψηλή και δεν μεταβάλλεται με περεταίρω φωτοχημική οξείδωση (χημική γήρανση). Επιπλέον βρέθηκε σημαντική εξάρτηση της υγροσκοπικότητας των σωματιδίων από τον ατομικό λόγο O:C των σωματιδίων και υπολογίστηκε η σχέση μεταξύ τους.

2. ΕΙΣΑΓΩΓΗ

Τα αιωρούμενα σωματίδια της ατμόσφαιρας είναι ικανά να επιδράσουν με διαφορετικούς τρόπους στο κλίμα της Γης, ανάλογα με τη σύστασή τους. Κάποια από τα συστατικά τους (π.χ. ανόργανα άλατα) προκαλούν σκέδαση της προσπίπτουσας ηλιακής ακτινοβολίας ψύχοντας τη γήινη ατμόσφαιρα, ενώ άλλα (π.χ, στοιχειακός άνθρακας) απορροφούν την ακτινοβολία και τελικά προκαλούν αύξηση της θερμοκρασίας[1]. Επιπλέον, τα σωματίδια μπορούν να δράσουν ως πυρήνες συμπύκνωσης συννέφων (CCN), ιδιαίτερα όταν περιέχουν υγροσκοπικές ενώσεις και να σχηματίσουν σταγονίδια τα οποία θα δημιουργήσουν τα σύννεφα.

Η χημική σύσταση των ατμοσφαιρικών σωματιδίων περιλαμβάνει ανόργανα ιόντα (αμμωνιακά, θειικά, νιτρικά, χλωριούχα κ.α.) και χιλιάδες οργανικές ενώσεις. Οι τελευταίες μπορούν είτε να εκπέμπονται στην ατμόσφαιρα πρωτογενώς στη σωματιδιακή φάση είτε να έχουν βρεθεί σε αυτή μετά από οξείδωση πτητικών ενώσεων στην ατμόσφαιρα. Τα πρωτογενή οργανικά αεροζόλ (POA) είναι σχετικά υδρόφοβα και μη-υδατοδιαλυτά, εκτός αν πρόκειται για πρωτογενείς εκπομπές σωματιδίων από καύση βιομάζας, ενώ τα δευτερογενή (SOA) είναι περισσότερο υδρόφιλα και διαλυτά στο νερό. Εκτιμήσεις της υγροσκοπικότητας των σωματιδίων που γίνονται με βάση την ικανότητα των σωματιδίων να λειτουργούν ως CCN χρησιμεύουν στην εκτίμηση της έμμεσης επίδρασής τους στο κλίμα, ενώ η μέτρηση του υδατοδιαλυτού οργανικού περιεχομένου προσφέρει επιπλέον πληροφορίες, περί του κατά πόσο τα σωματίδια είναι φρέσκα ή οξειδωμένα άρα πρωτογενή ή δευτερογενή αντίστοιχα.

3. ΜΗ-ΣΥΝΕΧΗΣ ΜΕΤΡΗΣΗ ΤΟΥ ΥΔΑΤΟΔΙΑΛΥΤΟΥ ΟΡΓΑΝΙΚΟΥ ΑΝΘΡΑΚΑ (WSOC) ΤΩΝ ΑΤΜΟΣΦΑΙΡΙΚΩΝ ΣΩΜΑΤΙΔΙΩΝ – ΜΙΑ ΘΕΩΡΗΤΙΚΗ ΑΝΑΛΥΣΗ

Η μη συνεχής μέτρηση του υδατοδιαλυτού οργανικού άνθρακα (WSOC) γίνεται με συλλογή του δείγματος πάνω σε φίλτρο ινών χαλαζία. Μέρος του ή όλο το φίλτρο εμποτίζεται σε φιάλη με ορισμένο όγκο υπερκάθαρου νερού ώστε να γίνει η εκχύλιση των υδατοδιαλυτών οργανικών ενώσεων. Το λουτρό υπερήχων, η μηχανική ανάδευση και η χειροκίνητη ανακίνηση χρησιμοποιούνται συχνά για να διευκολύνουν την εκχύλιση. Το υδατικό εκχύλισμα στη συνέχεια φιλτράρεται μέσω σύριγγας και αναλύεται σε ένα αναλυτή TOC.[2,3,4,5]

Αναπτύχθηκαν δύο θεωρητικά μοντέλα για να προβλέψουν το εύρος της διαλυτότητας των οργανικών ενώσεων που εκχυλίζονται σαν συνάρτηση των παραμέτρων της εκχύλισης, όπως ό όγκος διαλύτη, η επιφάνεια του φίλτρου που εκχυλίζεται και ο χρόνος της δειγματοληψίας. Στο μοντέλο του *Ιδανικού Οργανικού Διαλύματος* υποθέσαμε ότι οι οργανικές ενώσεις στα σωματίδια σχηματίζουν ένα ιδανικό οργανικό διάλυμα και ότι οι υδατοδιαλυτές οργανικές ενώσεις βρίσκονται διαλυμένες στην υδατική φάση του σωματιδίου. Το κλάσμα της μάζας μιας υποθετικής ουσίας Α στην υδατική φάση που προκύπτει κατά την εκχύλιση υπολογίστηκε ως το γινόμενο του μοριακού κλάσματος της ουσίας Α στην οργανική φάση, πολλαπλασιασμένο με τη συγκέντρωση κορεσμού της ουσίας στην υδατική φάση, που αντιστοιχεί στη διαλυτότητα της. Έτσι βρέθηκε ότι το κλάσμα της ουσίας Α που θα εκχυλιστεί από το σωματίδιο εξαρτάται από τη διαλυτότητά της, S_A, τη συνολική συγκέντρωση των μη υδατοδιαλυτών οργανικών ενώσεων, C_{WIOA} και της παραμέτρου P και ισούται με:

$$f_A = \frac{S_A P}{S_A P + C_{WIOA}},$$

$$P = \frac{V_W}{Q \cdot f \cdot \Delta t} .$$

‘Οπου V_W ο όγκος του νερού που χρησιμοποιείται κατά την εκχύλιση, Q η ροή του δείγματος στον αέριο δειγματολήπτη, f το κλάσμα της επιφάνειας του φίλτρου που χρησιμοποιείται για την εκχύλιση και Δt ο χρόνος της δειγματοληψίας. Η παράμετρος P εκφράζεται σε $cm^3\ m^{-3}$ και πρακτικά περιγράφει τη «διαθεσιμότητα» του διαλύτη (νερό) να εκχυλίσει τις συλλεχθείσες οργανικές ενώσεις. Για τις μεθόδους που χρησιμοποιούνται η παράμετρος αυτή βρέθηκε να έχει εύρος περίπου από 0.01 μέχρι 1 $cm^3\ m^{-3}$. Υψηλές τιμές της παραμέτρου P οδηγούν στην εκχύλιση περισσότερων οργανικών ενώσεων ή και στην αύξηση της συνεισφοράς της κάθε ένωσης. Αξίζει επίσης να σημειωθεί το κλάσμα της μάζας μιας ουσίας στο υδατικό εκχύλισμα δεν εξαρτάται από την αρχική συγκέντρωση της Α. Η Εικόνα 1 συνοψίζει τις προβλέψεις του μοντέλου για τη συνεισφορά μιας ουσίας στο WSOC σαν συνάρτηση της διαλυτότητας της για μια μικρή, μια ενδιάμεση και μια υψηλή τιμή της παραμέτρου P.

Σύμφωνα με την Εικόνα 1, για συνήθεις ατμοσφαιρικές συγκεντρώσεις του WIOA, μεταξύ 1 και 10 $\mu g\ m^{-3}$, η χρήση της τιμής 1 της παραμέτρου P έχει σαν αποτέλεσμα την πλήρη εκχύλιση των οργανικών ενώσεων (συνεισφορά με >90% της μάζας τους στο WSOC) με διαλυτότητα μεγαλύτερη από 0.01 $g\ L^{-1}$. Ακόμα, ενώσεις με διαλυτότητα μεγαλύτερη από 10^{-4} $g\ L^{-1}$ μπορούν επίσης να συνεισφέρουν στο WSOC με συνεισφορά μεγαλύτερη από 10%. Μικρότερες τιμές της P οδηγούν στην εκχύλιση λιγότερων οργανικών ή και μικρότερη συνεισφορά από μια χημική ένωση. Τα αντίστοιχα όρια για πλήρη εκχύλιση για P=0.1 και P=0.01 $cm^3\ m^{-3}$ είναι 0.1 και 1 $g\ L^{-1}$, ενώ ενώσεις με διαλυτότητα πάνω από 10^{-3} και 10^{-2} $g\ L^{-1}$ θα αρχίσουν να συνεισφέρουν στο WSOC για P=0.1 και P=0.01 $cm^3\ m^{-3}$ αντίστοιχα. Να σημειωθεί ότι μια αλλαγή της παραμέτρου P

κατά μια τάξη μεγέθους μεταβάλλει κατά το ίδιο το όριο της διαλυτότητας. Το ίδιο συμβαίνει με αντίστοιχη μεταβολή της συγκέντρωσης του WIOA που επίσης θα μεταβάλλει κατά μια τάξη μεγέθους το όριο διαλυτότητας. Αντίθετα, το κλάσμα της μάζας μιας ουσίας στο WSOC επηρεάζεται σε μικρότερο βαθμό. Έτσι το κλάσμα της συνεισφοράς στο WSOC μιας ουσίας με διαλυτότητα 0.01 g L^{-1} μπορεί να μειωθεί από 60 σε 10% με μια αύξηση της συγκέντρωσης του WIOA από 1 σε 10 μg m^{-3}.

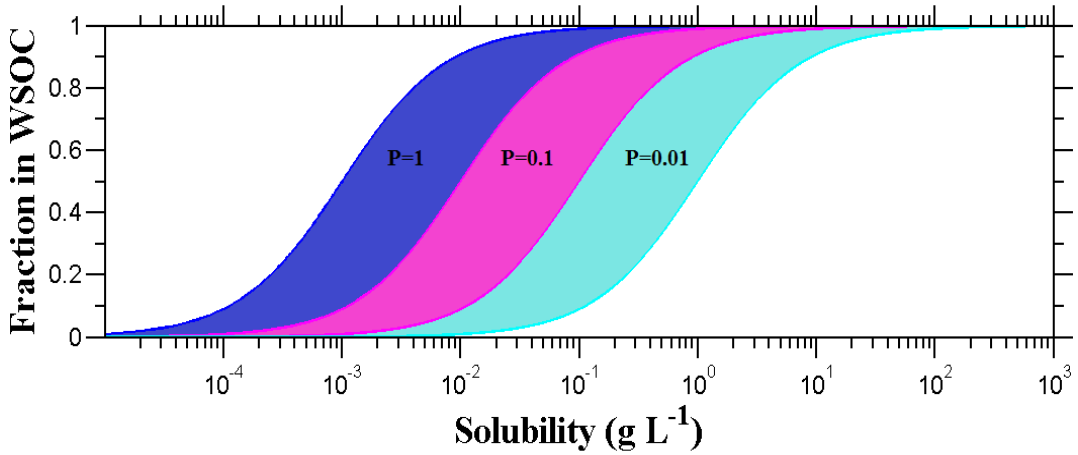

Εικόνα 1: Κλάσμα του συστατικού που θα εκχυλιστεί στο WSOC, σύμφωνα με το μοντέλο Ιδανικού Οργανικού Διαλύματος, για τρεις διαφορετικές τιμές της παραμέτρου P: 1 (μπλε), 0.1 (μωβ) και 0.01 cm^3 m^{-3} (κυανό).Το εύρος για την κάθε τιμή του P αντιστοιχεί σε συγκέντρωση μάζας των αδιάλυτων οργανικών 1 (αριστερό άκρο) μέχρι 10 μg m^{-3} (δεξιό άκρο της σκιασμένης περιοχής).

Στην Εικόνα 2 αναπαριστάται το εύρος της διαλυτότητας διαφόρων κατηγοριών οργανικών ενώσεων που μπορούν να βρεθούν σε ατμοσφαιρικά δείγματα και στο επάνω μέρος οι προβλέψεις του μοντέλου για διαφορετικές τιμές τη παραμέτρου *P*. Για *P*=1 cm^3 m^{-3} το μοντέλο προβλέπει την εκχύλιση σακχάρων, αμινών, φαινολών, HULIS και μια σειρά απλών οργανικών οξέων, δικαρβοξυλικών και κυκλικών οξέων, ενώ ορισμένες πολυκυκλικές ενώσεις (π.χ. πυρένιο) θα συνεισφέρουν μερικώς στο WSOC. Η εφαρμογή της τιμής *P*=0.1 cm^3 m^{-3} οδηγεί στην εκχύλιση όλων των παραπάνω

ενώσεων, ενώ αποφεύγεται η συνεισφορά πολυκυκλικών οργανικών στοWSOC. Η χρήση της ακόμη χαμηλότερης τιμής P=0.01 cm^3 m^{-3} στη μέθοδο της μέτρησης του WSOC περιορίζει τη συνεισφορά αρκετά υδατοδιαλυτών ενώσεων, όπως φαινόλες και οξέα.

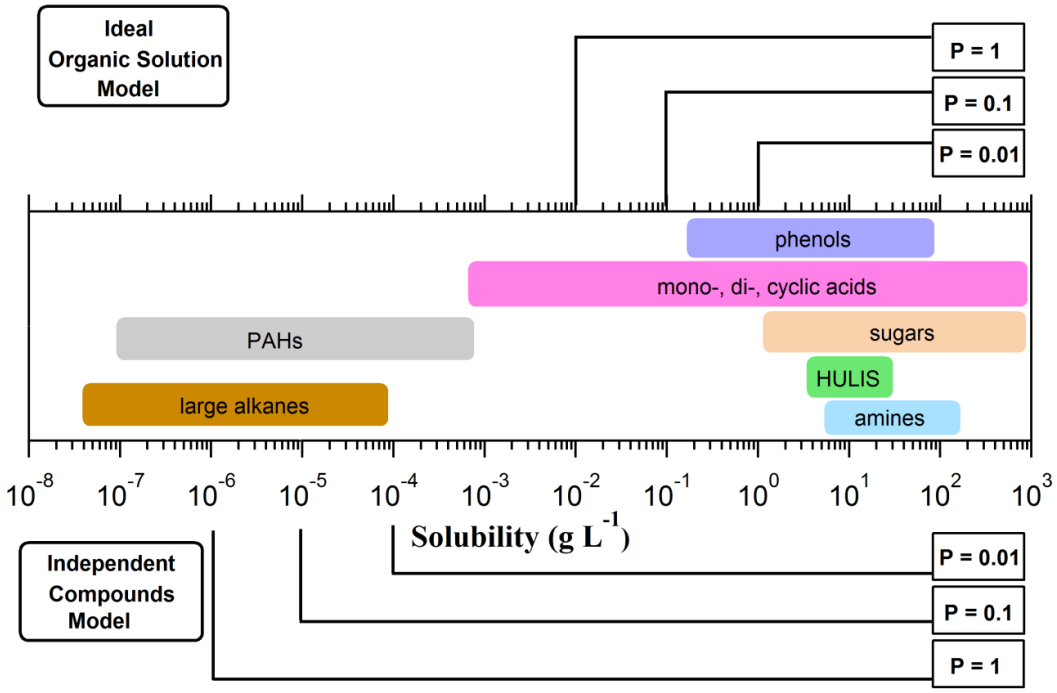

Εικόνα 2: Εύρος διαλυτότητας διαφόρων κατηγοριών οργανικών ενώσεων που μπορεί να βρίσκονται στα ατμοσφαιρικά σωματίδια. Στο επάνω μέρος φαίνονται οι προβλέψεις του μοντέλου Ιδανικού Οργανικού Διαλύματος και κάτω οι αντίστοιχες του μοντέλου Ανεξάρτητων Συστατικών, για διάφορες τιμές της παραμέτρου P. Οι γραμμές πάνω και κάτω υποδεικνύουν το όριο της διαλυτότητας, πάνω από το οποίο οι ενώσεις θα εκχυλίζονται πλήρως στο WSOC.

Η τιμή αυτή εξασφαλίζει πρακτικά την εκχύλιση μόνο των υδατοδιαλυτών οργανικών ενώσεων και αποφεύγει την εκχύλιση υδρόφοβων οργανικών. Γι' αυτό συστήνεται η χρήση της P=0.1 cm^3 m^{-3} για μετρήσεις WSOC σε συνήθεις ατμοσφαιρικές συγκεντρώσεις. Στην περίπτωση όπου η συγκέντρωση των μη υδατοδιαλυτών αεροζόλ είναι πολύ υψηλή (>100 μg m^{-3}) όπως π.χ. στην περίπτωση μέτρησης κοντά σε πηγή, συστήνεται η χρήση μιας υψηλότερης τιμής P, αφού η αύξηση του WIOA περιορίζει το

εύρος της διαλυτότητας που μπορούν να έχουν τα οργανικά που συνεισφέρουν στο WSOC.

Το μοντέλο των *Ανεξάρτητων Συστατικών* ήταν το δεύτερο μοντέλο που αναπτύχθηκε, στην προσπάθεια να εκτιμηθούν οι αλληλεπιδράσεις των οργανικών ενώσεων κατά την εκχύλιση και να υπολογιστεί η συνεισφορά μιας οργανικής ένωσης στο WSOC. Εδώ θεωρήσαμε ότι η διάλυση στο νερό ενός συστατικού των σωματιδίων δεν επηρεάζεται από την παρουσία άλλων συστατικών και ότι το εκχύλισμα που προκύπτει είναι πολύ αραιό. Έτσι υπολογίστηκε ότι το κλάσμα μιας ουσίας Α στο WSOC θα δίνεται από τη σχέση

$$f_A = \frac{P \cdot S_A}{C_A},$$

όπου C_A η συγκέντρωση του συστατικού Α. Σε αυτή την περίπτωση, η συνεισφορά του Α στο WSOC εξαρτάται και πάλι από τη διαλυτότητα της ουσίας και την παράμετρο *P*, αλλά και από τη συγκέντρωση του συστατικού Α. Οι προβλέψεις αυτού του μοντέλου για διαφορετικές τιμές της παραμέτρου *P* φαίνονται στην Εικόνα 3. Η εφαρμογή της τιμής P=0.01 $cm^3\ m^{-3}$ στη μέθοδο ανάλυσης του WSOC σύμφωνα με το μοντέλο, οδηγεί στην πλήρη εκχύλιση (συνεισφορά μεγαλύτερη από το 90% της μάζας) ενώσεων με διαλυτότητα στο νερό μεγαλύτερη από 0.01 g L^{-1}, ανεξάρτητα από τη συγκέντρωσή τους, ενώ ενώσεις με διαλυτότητα μικρότερη των 10^{-5} g L^{-1} δεν εκχυλίζονται. Έτσι αρκετοί PAHs (π.χ. πυρένιο, φενανθρένιο) μπορούν να εκχυλιστούν μερικώς ενώ σάκχαρα, αμίνες, HULIS, οξέα, φαινόλες και πολυυποκατεστημένες ενώσεις αναμένεται να κυριαρχούν στο WSOC. Αύξηση της τιμής του *P* σε 0.1 $cm^3\ m^{-3}$ μετατοπίζει τις αντίστοιχες καμπύλες προς τα αριστερά: ενώσεις με διαλυτότητα που ξεπερνά τα 10^{-6} g L^{-1} μπορούν να εκχυλιστούν μερικώς και να μετρηθούν ως WSOC, όπως μεγάλοι PAHs (α-βενζοανθρακένιο, τριφενυλένιο κ.α.). Η δε εφαρμογή της τιμής 1 $cm^3\ m^{-3}$ στην

παράμετρο *P* επιτρέπει την μερική ή πλήρη εκχύλιση σχεδόν όλων των πολυκυκλικών ενώσεων, ανάλογα με την ατμοσφαιρική τους συγκέντρωση και τη διαλυτότητά τους, ενώ ακόμα και αλκάνια μπορούν να βρεθούν στο WSOC, σύμφωνα με τις εκτιμήσεις του μοντέλου.

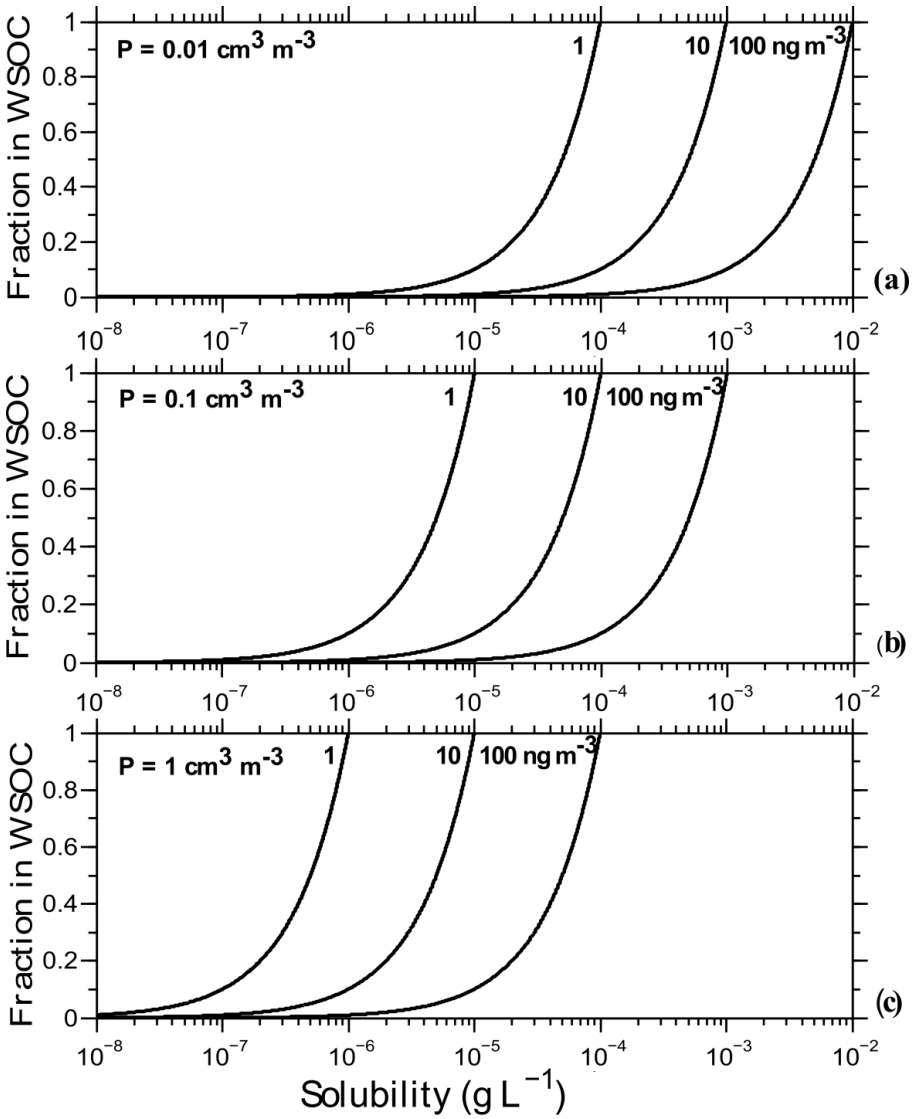

Εικόνα 3: Κλάσμα της μάζας μιας ουσίας στο WSOC, σαν συνάρτηση της διαλυτότητας και της συγκέντρωσής του στην ατμόσφαιρα, όπως προβλέπει το μοντέλο Ανεξάρτητων Συστατικών, για (a) χαμηλή, (b) ενδιάμεση και (c) υψηλή τιμή της παραμέτρου *P*.

Μετρήσεις πεδίου και εργαστηριακά πειράματα έχουν προσφέρει μέχρι στιγμής αρκετές πληροφορίες για τη χημική σύσταση του WSOC. Με χρήση HPLC-UV και GC-MS οι Mayol-Bracero et al. (2002)[6] βρήκαν ότι το WSOC στον Αμαζόνιο περιέχει κυρίως οξέα και πολυόξινα συστατικά, ενώ μετρήθηκαν σάκχαρα και αλκοόλες σακχάρων. Η παρουσία ποικιλίας μονοκαρβοξυλικών και πολυκαρβοξυλικών οξέων και σακχάρων επιβεβαιώνεται επίσης και από τους Decessari et al. (2000)[7] οι οποίοι μέτρησαν και μακρομοριακές ενώσεις (HULIS) στο WSOC. Άλλοι ερευνητές αναφέρουν ότι έχουν μετρήσει οξέα, πολυυποκατεστημένες ενώσεις, φαινόλες, HULIS, αμίνες και σάκχαρα.[8,9,10] Τα παραπάνω ευρήματα συμφωνούν ότι το WSOC μπορεί να περιέχει μονοκαρβοξυλικά και πολυκαρβοξυλικά οξέα, σάκχαρα, αμίνες, φυσικές μακρομοριακές ενώσεις, φαινόλες και πολυυποκατεστημένες ενώσεις.

Η ύπαρξη μιας ή και δύο οργανικών φάσεων επιβεβαιώνεται από πολλές έρευνες. Το μοντέλο πτητικότητας-βαθμού οξείδωσης VBS έδειξε ότι όταν φρέσκα σωματίδια που εκπέμπονται από καύση βιομάζας και δεν είναι ιδιαίτερα οξειδωμένα, αναμιγνύονται με προϋπάρχοντα υδρόφοβα σωματίδια δημιουργώντας μια οργανική φάση. Αντίθετα, αν τα προϋπάρχοντα σωματίδια είναι πολύ οξειδωμένα και άρα περισσότερο υδατοδιαλυτά, δεν αναμιγνύονται και δημιουργούνται δύο οργανικές φάσεις[11]. Θερμοδυναμικοί υπολογισμοί της ελεύθερης ενέργειας Gibbs επίσης έδειξαν ότι ο διαχωρισμός των φάσεων είναι σταθερότερος και ευνοείται η δημιουργία δύο οργανικών φάσεων, μια που περιέχει τα περισσότερο οξειδωμένα και υδατοδιαλυτά συστατικά και μια που περιέχει τις λιγότερο οξειδωμένες και υδρόφοβες ενώσεις[12,13]. Ο διαχωρισμός των φάσεων έχει παρατηρηθεί και πειραματικά σε πειράματα περιβαλλοντικού θαλάμου με υδρόφοβα και υδρόφιλα σωματίδια, αλλά και σε πειράματα υπολογισμού της υδατοδιαλυτότητας ενώσεων σε μείγματα[14,15,16]. Στα τελευταία βρέθηκε ότι η παρουσία των υπόλοιπων

ενώσεων περιορίζει τη διάλυση του κάθε συστατικού, υποστηρίζοντας ότι το Μοντέλο *Ιδανικού Οργανικού Διαλύματος* είναι πιο κοντά στην πραγματικότητα από αυτό των *Ανεξάρτητων Συστατικών*.

4. ΑΝΑΠΤΥΞΗ ΜΕΘΟΔΟΥ ΓΙΑ ΤΗ ΣΥΝΕΧΗ ΜΕΤΡΗΣΗ ΤΟΥ ΥΔΑΤΟΔΙΑΛΥΤΟΥ ΟΡΓΑΝΙΚΟΥ ΑΝΘΡΑΚΑ ΤΩΝ ΑΤΜΟΣΦΑΙΡΙΚΩΝ ΣΩΜΑΤΙΔΙΩΝ

Γενικά η χρήση της τεχνικής τη συλλογής φίλτρων για τη μέτρηση του WSOC έχει αρκετά μειονεκτήματα, όπως ο μεγάλος χρόνος δειγματοληψίας ο οποίος απαιτείται για τη συλλογή ικανοποιητικής ποσότητας δείγματος για τον προσδιορισμό του WSOC. Επιπλέον, η εξάτμιση ημιπτητικών ενώσεων από την επιφάνεια του φίλτρου ή η προσρόφηση αερίων από το φίλτρο μπορεί να έχει ως αποτέλεσμα τη μέτρηση λιγότερης ή περισσότερης μάζας στο WSOC. Στα πλαίσια αυτής της εργασίας αναπτύχθηκε μια νέα τεχνική για τη συνεχή συλλογή και μέτρηση του υδατοδιαλυτού κλάσματος των οργανικών ενώσεων στα ατμοσφαιρικά σωματίδια, που θα μπορούσε να χρησιμοποιηθεί και για τη μέτρηση των συνολικών οργανικών συστατικών των ατμοσφαιρικών σωματιδίων.

Ο Δειγματολήπτης Ατμού (SJAC) είναι μια διάταξη που αναπτύχθηκε και χρησιμοποιήθηκε συζευγμένο με ιοντικό χρωματογράφο για τη συλλογή και τη μέτρηση των ανόργανων υδατοδιαλυτών ιόντων που βρίσκονται στα σωματίδια. Το σύστημα αυτό αποτελείται από ένα σύστημα παραγωγής ατμού, ένα γυάλινο δοχείο ανάμειξης και δυο κυκλώνες. Η ροή του δείγματος συναντά την κάθετη ροή του ατμού μέσα στο δοχείο ανάμειξης όπου δημιουργούνται σταγονίδια.[17] Αυτά οδηγούνται στους κυκλώνες όπου συλλέγεται το υγροποιημένο δείγμα και οδηγείται προς ανάλυση. Μία αντλία αέρα

είναι υπεύθυνη για την εισαγωγή του αέριου δείγματος στο σύστημα και μία περισταλτική αντλία για τη μεταφορά του δείγματος από τους κυκλώνες σε δοχείο από όπου εισροφούν δείγμα οι χρωματογράφοι.

Η ιδέα εδώ ήταν η σύζευξη αυτού του συστήματος με έναν αναλυτή ολικού άνθρακα (TOC) για τη μέτρηση των υδατοδιαλυτών οργανικών που διαλύονται στον ατμό και δημιουργούν σταγόνες. Το συζευγμένο σύστημα κρίθηκε όμως ακατάλληλο για τη μέτρηση του υδατοδιαλυτού οργανικού άνθρακα, λόγω της πολύ υψηλής συγκέντρωσης που μετρούσε ακόμα και για υπερκάθαρο νερό. Παρατηρήθηκε ότι μια σειρά από πλαστικά μέρη στο σύστημα προκαλούσαν αύξηση της μετρούμενης συγκέντρωσης άνθρακα και για το σκοπό αυτό πραγματοποιήθηκαν μια σειρά από τροποποιήσεις. Η τροποποιημένη διάταξη του δειγματολήπτη ατμού φαίνεται στην Εικόνα 4. Στην αρχική διάταξη του δειγματολήπτη υγροποιημένων σταγόνων χρησιμοποιούνταν μια τρίλαιμη φιάλη πάνω σε ένα βραστήρα για την παραγωγή ατμού. Το τμήμα αυτό αντικαταστάθηκε από μια ανοξείδωτη σπείρα συνολικού μήκους 120 cm, τυλιγμένη εξωτερικά από θερμαντική ταινία και τοποθετημένη κάθετα ώστε από το κάτω μέρος να εξάγεται ατμός. Η περισταλτική αντλία, υπεύθυνη για τη μεταφορά του δείγματος από τους κυκλώνες προς το δοχείο συλλογής και την παροχή καθαρού νερού στο σύστημα παραγωγής ατμού αντικαταστάθηκε με αντλίες πιστονιού, όπου το δείγμα έρχεται σε επαφή με γυάλινα μόνο μέρη και PTFE. Δύο αντλίες πιστονιού λειτουργούν συνδιασμένα έτσι ώστε να παρέχουν μια σταθερή ροή ατμού στο σύστημα, ενώ μια τρίτη είναι υπεύθυνη για τη μεταφορά του δείγματος. Επιπλέον προστέθηκε ένας απογυμνωτής οργανικών αερίων στην είσοδο του συστήματος, ώστε να συλλέγεται και να μετράται μόνο η συγκέντρωση στη σωματιδιακή φάση.

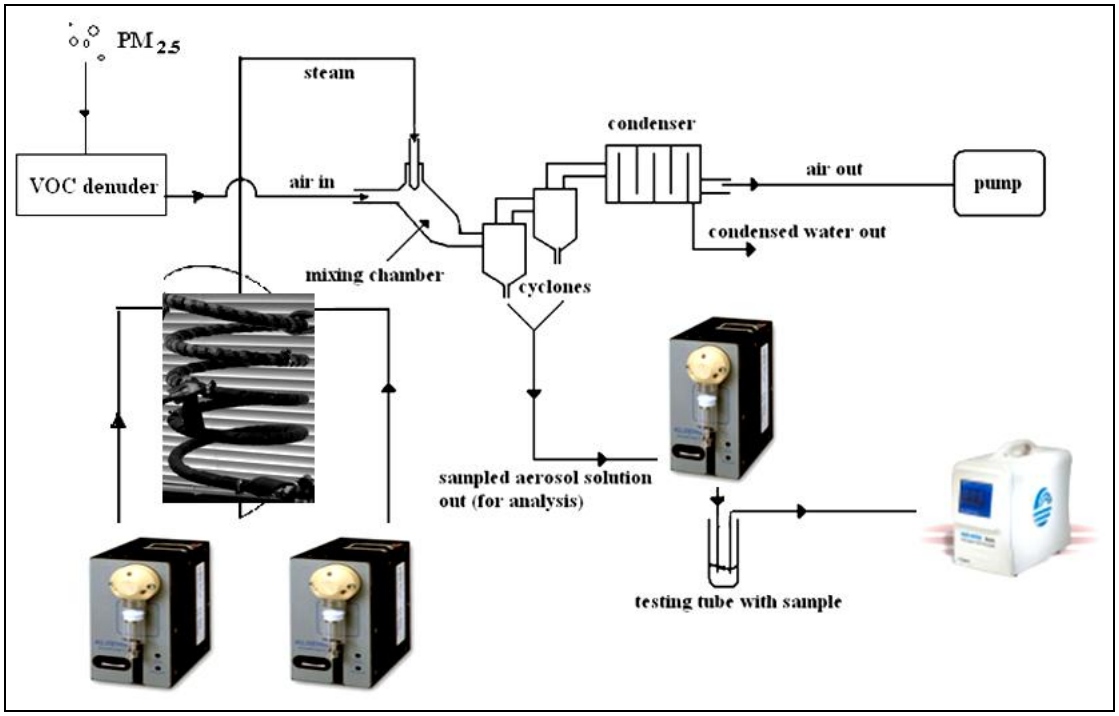

Εικόνα 4: Διάταξη του τροποποιημένου δειγματολήπτη ατμού.

Η μέτρηση του υδατοδιαλυτού οργανικού άνθρακα που περιέχεται στο δείγμα που συλλέγεται με την παραπάνω διάταξη γίνεται με τη βοήθεια ενός μετρητή ολικού οργανικού άνθρακα (TOC). Στο όργανο αυτό, το δείγμα εισάγεται και αμέσως οξινίζεται από H_3PO_4. Στη συνέχεια το δείγμα χωρίζεται σε δύο μέρη: Το ένα οδηγείται κατευθείαν για μέτρηση και παρέχει τη συγκέντρωση του ανόργανου άνθρακα και το δεύτερο οδηγείται σε ένα αντιδραστήρα οξείδωσης. Εκεί υφίσταται τη δράση υπεριώδους ακτινοβολίας παρουσία $(NH_4)_2S_2O_8$ και έτσι παράγονται ρίζες ΟΗ που οξειδώνουν το οργανικό φορτίο πλήρως προς CO_2. Στη συνέχεια οι δυο ροές του δείγματος οδηγούνται η κάθε μια σε ένα σύστημα μέτρησης του περιεχόμενου CO_2. Η αρχική οξίνιση του δείγματος αποτρέπει τη διάσταση του CO_2 και τη μεταφορά του στο σύστημα μέτρησης σε αυτή τη μορφή. Το σύστημα μέτρησης διαθέτει μια ημιπερατή μεμβράνη από την οποία το CO_2 διέρχεται και εισέρχεται σε δοχείο με καθαρό νερό, όπου τελικά μετράται η αύξηση της αγωγιμότητας που προκαλεί η διάσταση του CO_2.Η

συνολική συγκέντρωση του συνολικού οργανικού άνθρακα υπολογίζεται αφαιρώντας τη συγκέντρωση του ανόργανου άνθρακα από τον ολικό που μέτρήθηκε.

4.1 Χαρακτηρισμός Δειγματολήπτη Ατμού

Για το χαρακτηρισμό του δειγματολήπτη ατμού ως προς την ικανότητα του στη συλλογή διαλυτών οργανικών σωματιδίων παράχθηκαν σωματίδια σουκρόζης με τη χρήση ενός ατομοποιητή στον οποίο διοχετεύονταν συνεχώς διάλυμα σουκρόζης 0.01 g L^{-1} και καθαρός πεπιεσμένος αέρας. Τα σωματίδια που παράγονταν συνεχώς με αυτό τον τρόπο στη συνέχεια διέρχονταν από ξηραντήρα πληρωμένο με silica gel και στη συνέχεια το ρεύμα του αέρα που περιείχε τα ξηρά πλέον σωματίδια σουκρόζης μετρούνταν ταυτόχρονα από το δειγματολήπτη υγροποιημένων σταγόνων συζευγμένο με αναλυτή ολικού οργανικού άνθρακα (TOC) και από έναν αναλυτή σάρωσης κινητικότητας (SMPS). Έτσι το πρώτο σύστημα συνέλλεγε και μετρούσε τη συγκέντρωση μάζας των υδατοδιαλυτών σωματιδίων και το δεύτερο τη συνολική συγκέντρωση σωματιδίων, που στην περίπτωση αυτή ταυτίζονται. Τα αποτελέσματα της σύγκρισης αυτής ήταν ιδιαίτερα ενθαρυντικά, με τη συμφωνία των δυο οργάνων να παρουσιάζεται σε ένα αρκετά μεγάλο εύρος συγκεντρώσεων (Εικόνα 5).

Στη συνέχεια το σύστημα του τροποποιημένου αναλυτή WSOC χρησιμοποιήθηκε σε μετρήσεις πεδίου, που διεξήχθησαν τον Ιούνιο του 2012 στην περιοχή της Πάτρας. Ένας κυκλώνας (URG), ο οποίος είναι υπεύθυνος για τον αποκλεισμό σωματιδίων από μια διάμετρο και πάνω, τοποθετήθηκε μπροστά από την είσοδο του συστήματος. Το σύστημα του τροποποιημένου δειγματολήπτη λειτουργούσε με ροή δείγματος 13.6±0.6 L min^{-1}, η οποία επιτρέπει τη διέλευση από τον κυκλώνα σωματιδίων με διάμετρο κάτω από 3 μm.

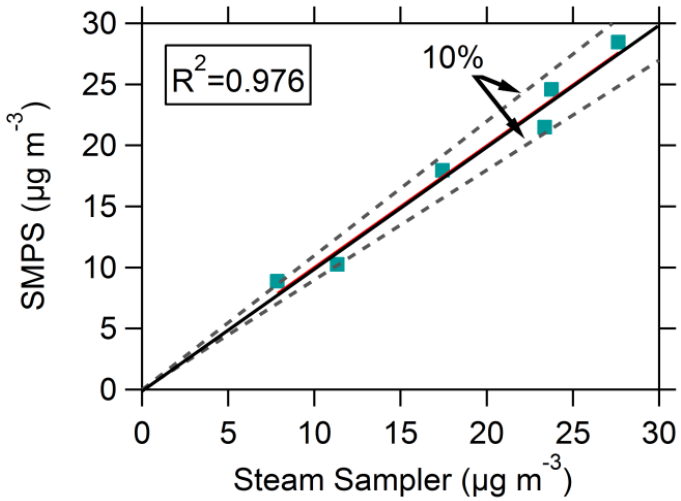

Εικόνα 5: Σύγκριση μεταξύ της συγκέντρωσης οργανικών σωματιδίων (μέσοι όροι 30 λεπτών) που μετρήθηκαν ταυτόχρονα από τον τροποποιημένο δειγματολήπτη υγροποιημένων σταγόνων και τον αναλυτή σάρωσης κινητικότητας (SMPS).

Η παράμετρος P για τις μεθόδους μέτρησης του υδατοδιαλυτού οργανικού άνθρακα, στην περίπτωση της συνεχούς μέτρησης όπως εδώ, μπορεί να υπολογιστεί από τη σχέση $P=V_w/Q$, όπου V_W είναι ο όγκος του νερού που υγροποιείται ανά λεπτό (mL) και Q η ροή του αερίου δείγματος στον δειγματολήπτη (L min^{-1}). Έτσι υπολογίστηκε ότι στην τεχνική αυτή η παράμετρος P είναι ίση με 44.1 cm^3 m^{-3}. Αυτή η τιμή είναι αρκετά υψηλή, όμως η τάξη μεγέθους της P πρακτικά καθορίζεται αφενός από τον ελάχιστο όγκο που απαιτεί το TOC (0.5 mL) και αφετέρου από τη χαμηλή ροή του αερίου δείγματος. Σύμφωνα με το μοντέλο Ιδανικού Οργανικού Διαλύματος (Κεφάλαιο 2), σε συνήθεις ατμοσφαιρικές συγκεντρώσεις (1-10 μg m^{-3}), στο WSOC μπορούν να συμμετέχουν ενώσεις με διαλυτότητα πάνω από 10^{-4} g L^{-1} ενώ εκχυλίζονται πλήρως ενώσεις με S>0.001 g L^{-1} (Εικόνα 6). Αυτό πρακτικά σημαίνει ότι ακόμη και ορισμένοι σχετικά υδατοδιαλυτοί πολυκυκλικοί υδρογονάνθρακες (π.χ. ναφθαλένιο, φενανθρένιο) μπορεί να συνεισφέρουν ή να μετέχουν ποσοτικά στο WSOC.

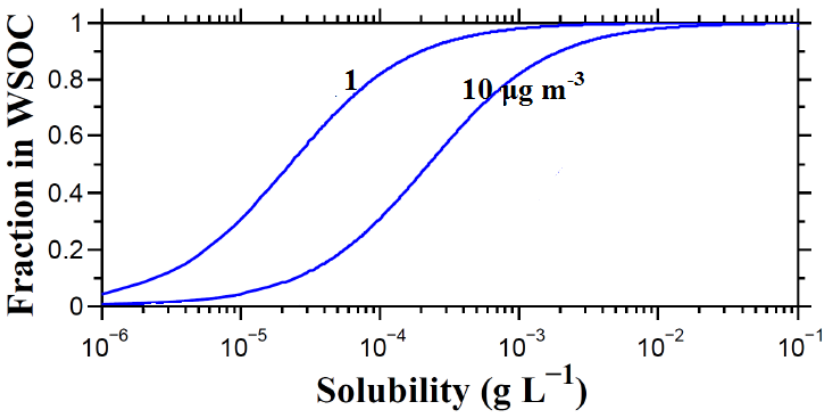

Εικόνα 6: Κλάσμα ενός συστατικού στο WSOC ως προς τη διαλυτότητά του, για διαφορετικές συγκεντρώσεις αδιάλυτων οργανικών αεροζόλ (1, 10, 100 μg m^{-3}) σύμφωνα με το μοντέλο *Ιδανικού Οργανικού Διαλύματος* για *P*=44.1 cm^3 m^{-3} που χρησιμοποιήθηκε στις μετρήσεις πεδίου με τον αναλυτή WSOC.

Στην Εικόνα 7 παρουσιάζεται η χρονοσειρά της συγκέντρωσης του WSOC όπως μετρήθηκε από τον τροποποιημένο αναλυτή WSOC. Η μέση συγκέντρωση του υδατοδιαλυτού οργανικού άνθρακα ήταν 1.24 ± 0.8 μg C m^{-3}.

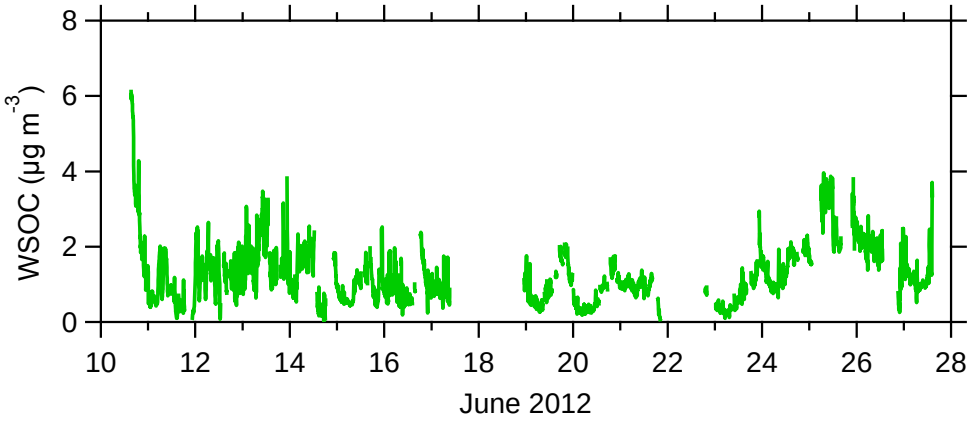

Εικόνα 7: Χρονοσειρά της συγκέντρωσης του WSOC όπως μετρήθηκε με τον τροποποιημένο αναλυτή WSOC στο ITE-IEXMH.

Ένας φασματογράφος μάζας αεροζόλ (AMS) μετρούσε ταυτόχρονα τη χημική σύσταση των σωματιδίων PM_1. Από ανάλυση των φασμάτων του AMS προκύπτει ο λόγος OM:OC (λόγος της οργανικής μάζας προς μάζα οργανικού άνθρακα) ο οποίος χρησιμοποιείται για τη μετατροπή της συγκέντρωσης του WSOC σε μάζα υδατοδιαλυτών οργανικών ενώσεων (WSOM). Στην Εικόνα 8 παρουσιάζεται το μέσο

ημερήσιο προφίλ της συγκέντρωσης των οργανικών (OA) και των υδατοδιαλυτών οργανικών (WSOM).

Τα υδατοδιαλυτά οργανικά ακολουθούν το προφίλ του OA κατά τη διάρκεια της νύχτας, την ημέρα όμως διαφοροποιείται λόγω των διαφορετικών πηγών τους. Το WSOM αυξάνεται το πρωί λόγω της φωτοχημείας που οδηγεί στο σχηματισμό περισσότερο οξειδωμένων και υδατοδιαλυτών ενώσεων, ενώ παρουσιάζει μέγιστο στις 16:00 όπου η φωτοχημεία είναι έντονη. Η συσχέτιση των WSOM και OA ήταν σχετικά ασθενής (R^2=0.25). Μη σημαντική ήταν η συσχέτιση του WSOM με το οξυγονωμένο κλάσμα των οργανικών (OOA), ενώ τις πρώτες μέρες των μετρήσεων (10-15 Ιουνίου) η συγκέντρωση των υδατοδιαλυτών ταυτίζεται σχεδόν με αυτή των συνολικών οργανικών, πιθανότατα λόγω της υψηλής τιμής της παραμέτρου *P*, η οποία επιτρέπει τη μέτρηση και σχετικά μη διαλυτών ενώσεων στο νερό.

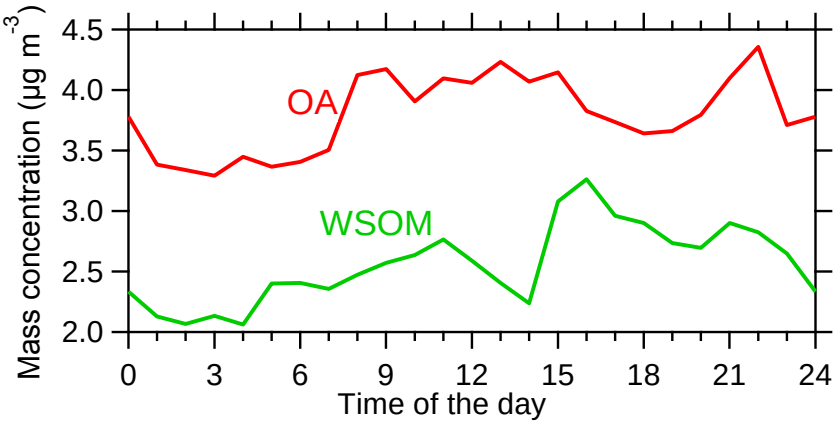

Εικόνα 8: Ημερήσια μεταβολή της συγκέντρωσης των οργανικών (OA) και των υδατοδιαλυτών οργανικών (WSOM).

5. ΜΕΤΡΗΣΕΙΣ ΥΓΡΟΣΚΟΠΙΚΩΝ ΙΔΙΟΤΗΤΩΝ ΤΩΝ ΑΤΜΟΣΦΑΙΡΙΚΩΝ ΣΩΜΑΤΙΔΙΩΝ ΚΑΥΣΗΣ ΒΙΟΜΑΖΑΣ

Η καύση βιομάζας αποτελεί μια πολύ σημαντική πηγή ατμοσφαιρικών σωματιδίων και τη σημαντικότερη πηγή πρωτογενών σωματιδίων σε παγκόσμια κλίμακα. Οι κυριότερες πηγές των σωματιδίων καύσης βιομάζας είναι οι δασικές πυρκαγιές και η καύση ξύλων για θέρμανση και μαγείρεμα[18]. Αυτά τα σωματίδια είναι ικανά να λειτουργήσουν ως πυρήνες συμπύκνωσης συννέφων (CCN) με αβέβαιες επιπτώσεις στο κλίμα, γι' αυτό ο χαρακτηρισμός των υγροσκοπικών τους ιδιοτήτων είναι ιδιαίτερα σημαντικός. Η καύση

ξύλων σε τζάκια για τη θέρμανση των κατοικιών είναι αρκετά διαδεδομένη τα τελευταία χρόνια στην Ελλάδα με αβέβαιες επιπτώσεις στην ανθρώπινη υγεία και το κλίμα. Κατά τη διάρκεια του χειμώνα του 2013, πραγματοποιήθηκαν εντατικές μετρήσεις στην περιοχή του κέντρου της Αθήνας στο διάστημα 10/1-10/2.

5.1 Αποτελέσματα - Συζήτηση

Για την εκτίμηση των υγροσκοπικών ιδιοτήτων των σωματιδίων χρησιμοποιήθηκε ένας μετρητής πυρήνων συμπύκνωσης συννέφων σε συνδυασμό με έναν αναλυτή σάρωσης κινητικότητας, ενώ ένας φασματογράφος μάζας αεροζόλ προσέφερε συνεχείς μετρήσεις χημικής σύστασης και μεγέθους. Οι οργανικές ενώσεις βρέθηκαν να απαρτίζουν το μεγαλύτερο μέρος της μάζας (58%) των σωματιδίων PM_1 καθ' όλη τη διάρκεια της μέρας. Ο στοιχειακός άνθρακας ακολουθούσε με 20% και τα θειικά ιόντα με 10%. Το ημερήσιο προφίλ του μέσου κλάσματος των οργανικών παρουσιάζεται στην Εικόνα 9.

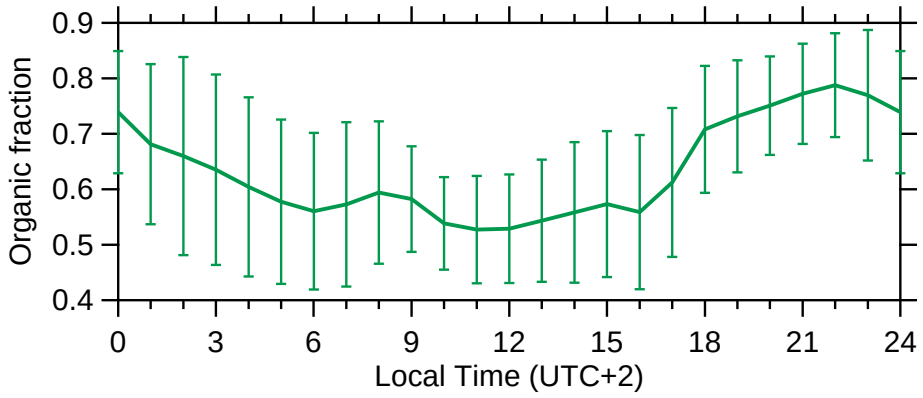

Εικόνα 9: Ημερήσιο προφίλ της μέσης τιμής του κλάσματος των οργανικών στην Αθήνα το χειμώνα το 2013.

Η εφαρμογή *Ανάλυσης Θετικής Μήτρας* (PMF) στα δεδομένα του φασματογράφου μάζας αεροζόλ έδειξε ότι τα οργανικά σωματίδια προέρχονται κυρίως από καύση βιομάζας τα οποία επικρατούν τις βραδινές ώρες μετά τις 18:00 (Εικόνα 10). Η κίνηση των αυτοκινήτων είναι υπεύθυνη για την πρωινή αύξηση του κλάσματος των οργανικών τις πρωινές ώρες μεταξύ 7:00 και 10:00, ενώ σωματίδια που εκπέμπονται από το μαγείρεμα εμφανίζονται το μεσημέρι και το βράδυ μετά τις 18:00. Το προφίλ των οξυγονωμένων οργανικών είναι αρκετά σταθερό κατά τη διάρκεια της μέρας, υποδεικνύοντας ότι τα οξυγονωμένα οργανικά δεν σχηματίζονται από τοπική φωτοχημεία, αλλά έχουν μεταφερθεί από άλλες περιοχές.

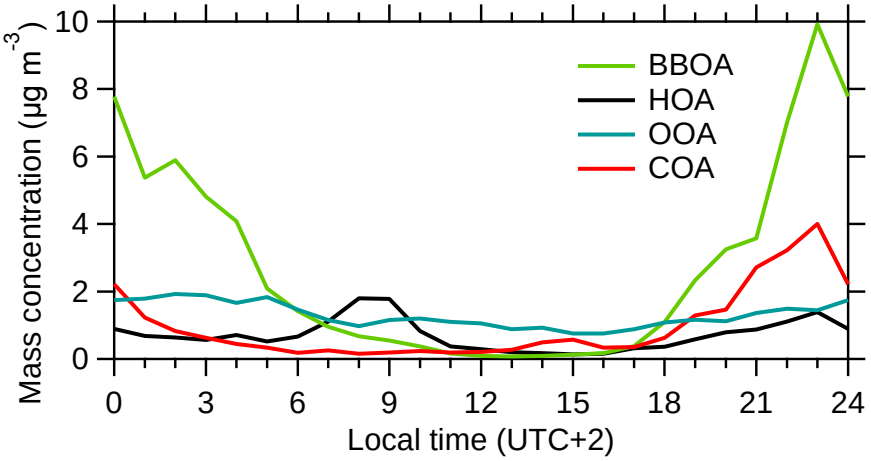

Εικόνα 10: Ημερήσιο προφίλ των μέσων συγκεντρώσεων των 4 παραγόντων που υπολογίστηκαν από το PMF: Καύση βιομάζας (BBOA), υδρόφοβα από την κυκλοφορία αυτοκινήτων (HOA) οξυγονωμένα οργανικά (OOA) και σωματίδια από μαγείρεμα (COA) στην Αθήνα το χειμώνα του 2013.

Το ημερήσιο προφίλ του κρίσιμου υπερκορεσμού υπολογίστηκε για σωματίδια διαφορετικής διαμέτρου (Εικόνα 11). Τα μεγαλύτερα σωματίδια ενεργοποιούνται σε χαμηλότερο υπερκορεσμό, όπως ήταν αναμενόμενο. Αύξηση του κρίσιμου

υπερκορεσμού σε κάθε διάμετρο παρατηρείται μεταξύ 7:00-10:00. Το διάστημα αυτό τα υδρόφοβα οργανικά από την κίνηση των αυτοκινήτων επικρατούν στην ατμόσφαιρα, προκαλώντας την αύξηση του υπερκορεσμού που είναι απαραίτητος για την ενεργοποίησή τους.

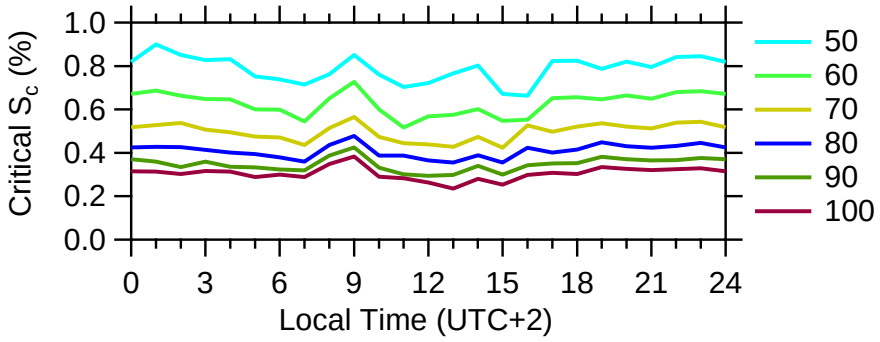

Εικόνα 11: Ημερήσιο προφίλ του κρίσιμου υπερκορεσμού ανά διάμετρο στην Αθήνα το χειμώνα του 2013.

Χρησιμοποιώντας την κατανομή της σύστασης των σωματιδίων PM_1 με τη διάμετρό τους καταλήξαμε ότι οι υγροσκοπικές ιδιότητες που αντιστοιχούν στη μέση χημική σύσταση των PM_1 μπορούν να εξαχθούν από τα σωματίδια 80-100 nm. Το ημερήσιο προφίλ της μέσης υγροσκοπικότητας των σωματιδίων αυτών καθώς και η μέσης τιμής τους παρουσιάζονται στην Εικόνα 12. Η ελάχιστη τιμή της μέσης υγροσκοπικότητας κ_{av} παρατηρείται τις πρωινές ώρες (7:00-10:00) όπου οι υδρόφοβες σωματιδιακές εκπομπές των αυτοκινήτων (HOA) παρουσιάζουν μέγιστο, ενώ το μεσημέρι παρατηρείται αύξηση της μέσης υγροσκοπικότητας. Τα διάστημα αυτό οι οξυγονωμένες οργανικές ενώσεις (OOA) που είναι υγροσκοπικές έχουν μεγαλύτερη συγκέντρωση σε σχέση με τα σωματίδια από τις άλλες πηγές, οδηγώντας στην αύξηση της υγροσκοπικότητας. Από τις 18:00 μέχρι τα μεσάνυχτα, όπου επικρατούν στην ατμόσφαιρα τα σωματίδια καύσης βιομάζας (BBOA) η μέση υγροσκοπικότητα εμφανίζεται αρκετά σταθερή, και κυμαίνεται κοντά στο 0.15. Γενικά, τα σωματίδια ήταν αρκετά υγροσκοπικά και το

μέγιστο κλάσμα ενεργοποίησης που μετρήθηκε πλησίαζε τη μονάδα για τα μεγαλύτερα από αυτά. Μείωση του ενεργοποιημένου κλάσματος των σωματιδίων παρατηρήθηκε και πάλι τις πρωινές ώρες κατά το διάστημα που υπήρχαν υψηλότερες συγκεντρώσεις HOA.

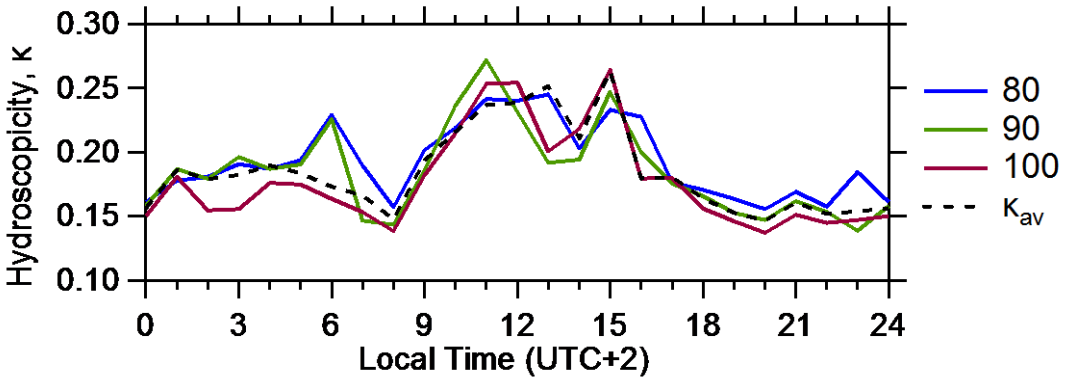

Εικόνα 12: Ημερήσιο προφίλ της υγροσκοπικότητας των σωματιδίων διαμέτρου 80, 90 και 100 nm. Στο ίδιο διάγραμμα με διακεκομμένη γραμμή φαίνεται η μέση τιμή τους στην Αθήνα το χειμώνα του 2013.

Η συνολική υγροσκοπικότητα *κ* ενός σωματιδίου συνδέεται με το κλάσμα του όγκου ε_i του κάθε συστατικού και της υγροσκοπικότητάς του κ_i με την εξίσωση $\Sigma\varepsilon_i \cdot \kappa_i = \kappa$.[19] Για τον υπολογισμό της υγροσκοπικότητας των οργανικών αρχικά χρησιμοποιήθηκε το μοντέλο ISORROPIA II.[20] Το μοντέλο αυτό χρησιμοποιεί τις συγκεντρώσεις των ανόργανων ιόντων που έχουν μετρηθεί (NH_4^+, SO_4^{-2}, NO_3^-, Cl^-, K^+) υπό γνωστή θερμοκρασία και σχετική υγρασία, υπολογίζει τη συγκέντρωση των αλάτων από τα οποία προήλθαν. Υποθέτοντας ότι η υγροσκοπικότητα του στοιχειακού άνθρακα είναι μηδενική, η πυκνότητα των οργανικών[21] είναι 1.5 g cm^{-3} και αφού υπολογιστούν τα αντίστοιχα κλάσματα όγκου των ανόργανων συστατικών, είναι εφικτός ο υπολογισμός της υγροσκοπικότητας των οργανικών.

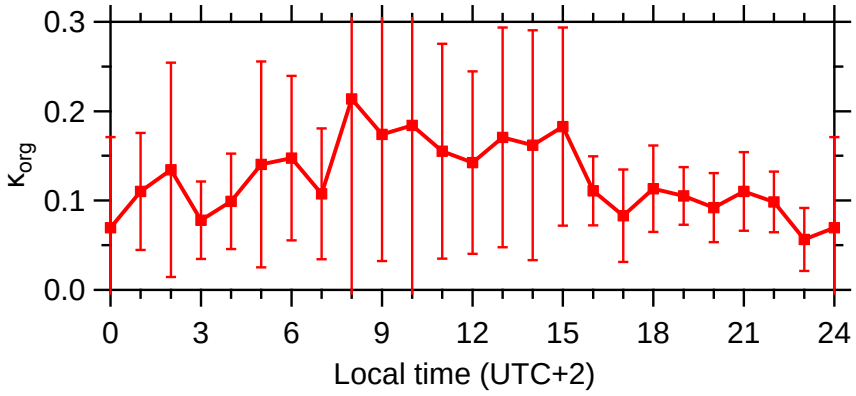

Εικόνα 13: Ημερήσιο προφίλ της υγροσκοπικότητας των οργανικών σωματιδίων.

Η παράμετρος υγροσκοπικότητας *κ* των οργανικών σωματιδίων κυμάνθηκε από 0.06 έως 0.21. Κατά τη διάρκεια της νύχτας όπου τα σωματίδια της καύσης επικρατούν, η υγροσκοπικότητα παρέμεινε αρκετά σταθερή, γύρω στο 0.09. Προηγούμενες μετρήσεις της υγροσκοπικότητας σωματιδίων προερχόμενα από καύση βιομάζας κατέληξαν επίσης σε τιμές κοντά στο 0.1. Η αύξηση του κ_{org} που παρατηρήθηκε μετά τις 3:00 οφείλεται στο γεγονός ότι τα οξυγονωμένα οργανικά αρχίζουν να γίνονται σημαντικά εκείνη την περίοδο.

6. ΜΕΤΡΗΣΕΙΣ ΥΓΡΟΣΚΟΠΙΚΩΝ ΙΔΙΟΤΗΤΩΝ ΔΕΥΤΕΡΟΓΕΝΩΝ ΟΡΓΑΝΑΝΙΚΩΝ ΣΩΜΑΤΙΔΙΩΝ ΠΑΡΑΓΟΜΕΝΩΝ ΑΠΟ ΟΖΟΝΟΛΥΣΗ ΚΑΙ ΦΩΤΟΧΗΜΙΚΗ ΓΗΡΑΝΣΗ ΤΟΥ Α-ΠΙΝΕΝΙΟΥ

Η φωτοχημική οξείδωση πτητικών οργανικών ενώσεων (VOCs) στην ατμόσφαιρα έχει ως αποτέλεσμα το σχηματισμό δευτερογενών οργανικών σωματιδίων (SOA). Οι βιογενείς VOCs αποτελούν τη μεγαλύτερη πηγή SOA σε παγκόσμια κλίμακα και η παραγωγή τους εξαρτάται από πολλούς παράγοντες όπως η ένταση του ηλιακού φωτός, η θερμοκρασία και το είδος της βλάστησης. Τα τερπένια έχουν τη μεγαλύτερη συνεισφορά στις βιογενείς πτητικές οργανικές ενώσεις, με το α-πινένιο να εκπέμπεται

στην ατμόσφαιρα στις υψηλότερες συγκεντρώσεις. Το α-πινένιο αντιδρά στην ατμόσφαιρα κατά κύριο λόγο με το όζον σχηματίζοντας οζονίδιο που διασπάται και συνεχίζει να αντιδρά προς το σχηματισμό λιγότερο πτητικών ενώσεων και σχηματίζουν σωματίδια. Τα σωματίδια αυτά μπορούν να υποστούν περαιτέρω μεταβολές αντιδρώντας με άλλα οξειδωτικά μέσα της ατμόσφαιρας, όπως οι υδροξυλικές ρίζες. Στα πλαίσια αυτής της διατριβής έγινε μια σειρά πειραμάτων αναπαραγωγής αυτής της σειράς αντιδράσεων μέσα σε ένα περιβαλλοντικό θάλαμο. Ο θάλαμος αυτός βρίσκεται στις εγκαταστάσεις του Ινστιτούτου Χημικής Μηχανικής ΙΤΕ-ΙΕΧΜΗ στην Πάτρα μέσα σε ειδικά διαμορφωμένο χώρο καλυμμένο με λάμπες UV.

Συνολικά έγιναν 10 πειράματα και ένα τυφλό. Πριν από κάθε πείραμα, ο θάλαμος καθαριζόταν με αέρα απαλλαγμένο από σωματίδια, υγρασία και οργανικά αέρια. Στο πρώτο σετ πειραμάτων, σωματίδια $(NH_4)_2SO_4$ εισάγονταν στο θάλαμο τα οποία παρασκευάζονταν με τη χρήση ατομοποιητή. Στη συνέχεια περίπου 500 ppb O_3 εισάγονταν στο θάλαμο και 30 λεπτά αργότερα μια ποσότητα α-πινενίου. Τα λιγότερο πτητικά προϊόντα έτσι συμπυκνώνονται πάνω στα προϋπάρχοντα σωματίδια θειικού αμμωνίου. Στη συνέχεια τα σωματίδια αντιδρούσαν με ρίζες OH, οι οποίες παράγονταν από τη φωτόλυση νιτρώδους οξέος κάτω από υπεριώδες φως. Στο δεύτερο σετ πειραμάτων παρακάμφθηκε το στάδιο της παρασκευής και εισαγωγής στο θάλαμο σωματιδίων $(NH_4)_2SO_4$ και τα οργανικά σωματίδια σχηματίστηκαν από πυρηνογέννεση. Σε όλη τη διάρκεια των πειραμάτων ένας φασματογράφος μάζας αεροζόλ παρείχε δεδομένα χημικής σύστασης των σωματιδίων και της κατανομής του μεγέθους τους ενώ ο μετρητής πυρήνων συμπύκνωσης συννέφων (CCNC) σε συνδυασμό με ένα αναλυτή σάρωσης κινητικότητας (SMPS) παρείχαν πληροφορίες για το κλάσμα ενεργοποίησης των σωματιδίων και το μέγεθος τους. Ο δειγματολήπτης ατμού επίσης

χρησιμοποιήθηκε για τη μέτρηση της συγκέντρωσης των υδατοδιαλυτών οργανικών συστατικών των σωματιδίων στο τελευταίο πείραμα.

Παρόλο που τα σωματίδια θειικού αμμωνίου που προϋπάρχουν στο θάλαμο είναι περισσότερο υγροσκοπικά από τις οργανικές ενώσεις, με την προσθήκη δευτερογενών οργανικών στα σωματίδια από την οζονόλυση του πινενίου δεν παρατηρείται κάποια στατιστικά σημαντική μεταβολή του κλάσματος ενεργοποίησης. Επίσης η επίδραση της φωτοχημικής γήρανσης των σωματιδίων δεν επέδρασε στο κλάσμα των σωματιδίων που ενεργοποιούνται. Αντίθετα, η κρίσιμη διάμετρος των σωματιδίων αυξάνεται μετά τη συμπύκνωση οργανικών πάνω στα σωματίδια $(NH_4)_2SO_4$ (Εικόνα 14). Αυτό συμβαίνει γιατί η κρίσιμη διάμετρος εξαρτάται από τη σύσταση των σωματιδίων. Αντίθετα, το ενεργοποιημένο κλάσμα παραμένει αμείωτο λόγω της αύξησης του μεγέθους των σωματιδίων μετά την οζονόλυση, γεγονός που επιτρέπει στα σωματίδια να συνεχίζουν να ενεργοποιούνται.

Μικρή αύξηση του κλάσματος ενεργοποίησης παρατηρείται στην αρχή της οζονόλυσης λόγω αύξησης του μεγέθους των σωματιδίων ενώ δεν παρατηρήθηκε κάποια μεταβολή του CCN κλάσματος των παραγώγων της οζονόλυσης μετά την επίδραση υδροξυλικών ριζών και UV ακτινοβολίας.

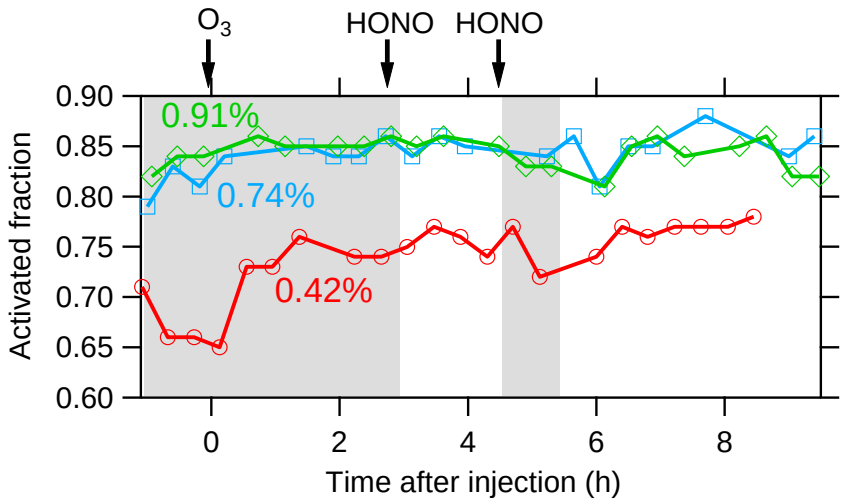

Εικόνα 14: Εξέλιξη του κλάσματος ενεργοποίησης κατά τη διάρκεια πειράματος παρουσία πυρήνων θειικού αμμωνίου. Η σκιασμένη περιοχή αντιστοιχεί σε σβησμένα φώτα UV ενώ η λευκή σε ανοιχτά. Η κόκκινη, μπλε και πράσινη καμπύλη αντιστοιχεί σε υπερκορεσμό 0.42, 0.74 και 0.91% αντίστοιχα. Στην εικόνα φαίνονται επίσης οι χρονικές στιγμές στις οποίες έγινε προσθήκη O_3 για να σχηματιστούν SOA και HONO για φωτοχημική γήρανση.

Στη δεύτερη σειρά πειραμάτων όπου δεν προϋπάρχουν στο θάλαμο σωματίδια θειικού αμμωνίου, παρατηρήθηκε ότι και πάλι το κλάσμα ενεργοποίησης των σωματιδίων δε μεταβάλλεται κατά τη φωτοχημική γήρανση. Τα αντίστοιχα αποτελέσματα παρουσιάζονται στην Εικόνα 15. Η αύξηση που παρουσιάζεται τα πρώτα λεπτά της οζονόλυσης οφείλεται στη ραγδαία αύξηση της διαμέτρου των σωματιδίων που τα καθιστά ενεργά. Η διάμετρος ενεργοποίησης των σωματιδίων επίσης βρέθηκε να μη μεταβάλλεται σημαντικά κατά τη διάρκεια τόσο της οζονόλυσης όσο και της φωτοχημικής οξείδωσης.

Επιπλέον υπολογίστηκε η υγροσκοπικότητα κ των καθαρών οργανικών σωματιδίων από το δεύτερο σετ πειραμάτων. Η παράμετρος υγροσκοπικότητας κ δεν μεταβλήθηκε σημαντικά κατά τη διάρκεια της οζονόλυσης και της φωτοχημικής οξείδωσης ενώ

παρατηρήθηκε καλή συσχέτιση με το λόγο O:C στο σύνολο των πειραμάτων (Εικόνα 16). Η υγροσκοπικότητα μπορεί να εκφραστεί ως συνάρτηση του λόγου O:C με βάση την εξίσωση: κ=(0.29±0.005)·(O:C).

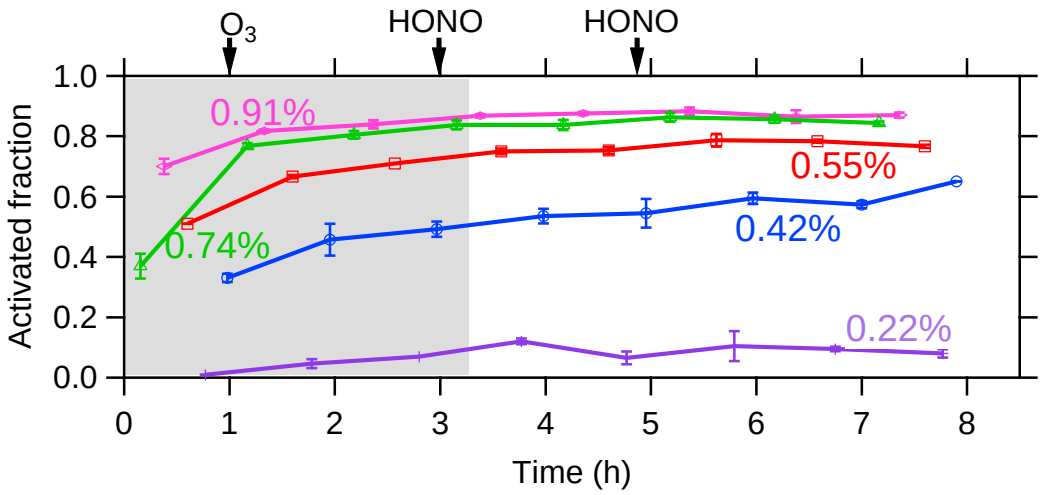

Εικόνα 15: Εξέλιξη του κλάσματος ενεργοποίησης κατά τη διάρκεια πειράματος απουσία πυρήνων θειικού αμμωνίου. Η σκιασμένη περιοχή αντιστοιχεί σε σβησμένα φώτα UV ενώ η λευκή σε ανοιχτά. Η κόκκινη, μπλε και πράσινη καμπύλη αντιστοιχεί σε υπερκορεσμό 0.42, 0.74 και 0.91% αντίστοιχα. Στην εικόνα φαίνονται επίσης οι χρονικές στιγμές στις οποίες έγινε προσθήκη O_3 για να σχηματιστούν SOA και HONO για φωτοχημική γήρανση.

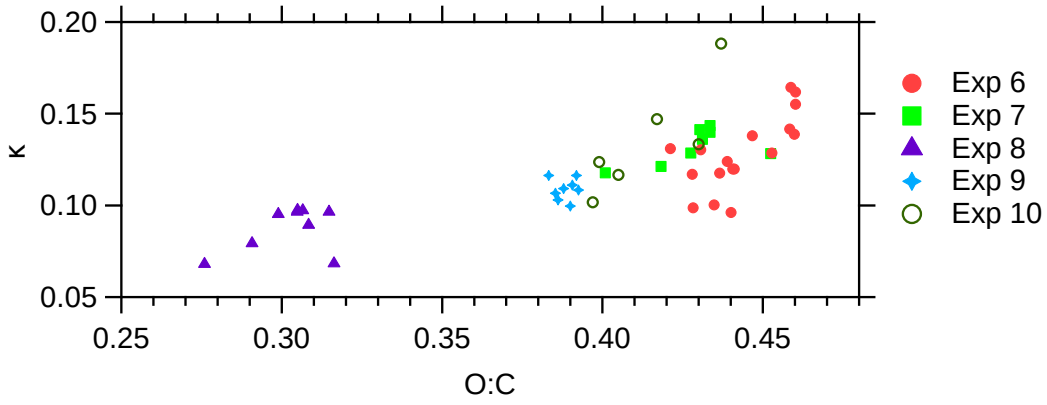

Εικόνα 16: Σχέση της υγροσκοπικότητας με τον ατομικό λόγο O:C για το σύνολο των πειραμάτων όπου ήταν εφικτός ο υπολογισμός της υγροσκοπικότητας. Διαφορετικό χρώμα αντιστοιχεί στο κάθε πείραμα.

Τέλος, με τη βοήθεια του δειγματολήπτη ατμού υπολογίστηκε το υδατοδιαλυτό κλάσμα των οργανικών σωματιδίων. Μετά από μια ώρα από την έναρξη της οζονόλυσης, το υδατοδιαλυτό κλάσμα ξεπερνά το 0.9, ενώ μετά από δύο ώρες και την επίδραση ριζών υδροξυλίου από την πρώτη προσθήκη HONO το υδατοδιαλυτό κλάσμα αγγίζει τη μονάδα. Η εξέλιξη του υδατοδιαλυτού κλάσματος των σωματιδίων κατά τη διάρκεια ενός πειράματος φαίνεται στην Εικόνα 17.

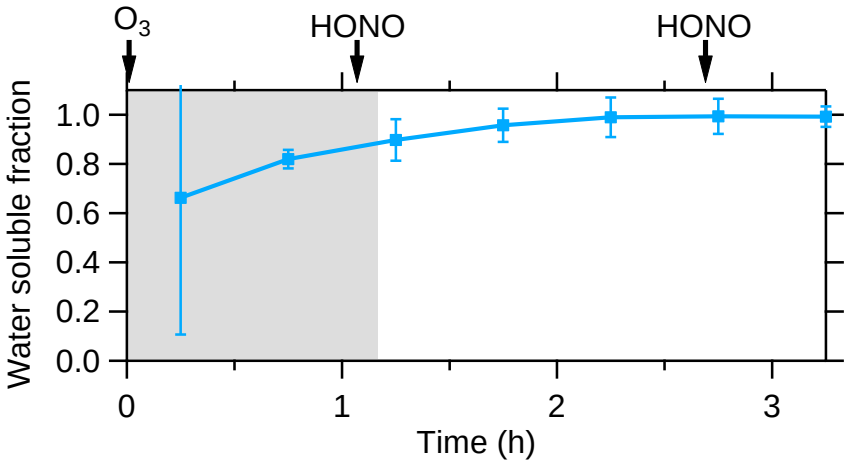

Εικόνα 17: Εξέλιξη του υδατοδιαλυτού οργανικού κλάσματος κατά τη διάρκεια του πειράματος 10. Η σκιασμένη περιοχή αντιστοιχεί σε σβησμένα φώτα UV ενώ η λευκή σε ανοιχτά.

ΒΙΒΛΙΟΓΡΑΦΙΑ

[1]. IPCC, 2007: Summary for policymakers. Intergovernmental Panel on Climate Change **2007**: The physical science basis. Contribution of working group I to the fourth assessment report of the intergovernmental panel on climate change [Solomon, S., Qin, D., Manning, Z., Chen, M., Marquis, M., Averyt, K.B., Tignor, M., Miller, H.L.]. Cambridge University Press, NY, USA. [2]. Facchini, M.C., Fuzzi, S., Zappoli, S., Andracchio, A., Gelencér, A., Kiss, G., Krivácsy, Z., Mészáros, E., Hanson, H.C., Alsberg, T., Zebühr, Y. Partitioning of the organic aerosol component between fog droplets and interstitial air. *J. Geophys. Res.* **1999**, *104*, No D21, 26,821-26,832.

[3]. Hagler, G.H.W., Bergin, M.H., Smith, E.A., Dibb, J.E., Anderson, C., Steig, E.J. Particulate and water-soluble carbon measured in recent snow at Summit, Greenland. *Geophys. Res. Lett.* **2007**, *34*, L16505.

[4]. Huang, X.F., Yu, J.Z., He, L.Y., Yuan, Z. Water-soluble organic carbon and oxalate in aerosols at a coastal urban site in China: Size distribution characteristics, sources, and formation mechanisms. *J. Geophys. Res.* **2006**, *111*, D22212.

[5]. Duvall, R.M., Majestic, B.J., Shafer, M.M., Chuang, P.Y., Simoneit, B.R.T., Schauer, J.J. The water-soluble fraction of carbon, sulphur, and crustal elements in Asian aerosols and Asian soils. *Atmos. Environ.* **2008**, *42*, 5872-5884.

[6]. Mayol-Bracero, O.L., Guyon, P., Graham, B., Roberts, G., Andreae, M.O., Decesari, S., Facchini, M.C., Fuzzi, S., Artaxo, P. Water-soluble organic compounds in biomass burning aerosols over Amazonia 2. Apportionment of the chemical composition and importance of the polyacidic fraction. *J. Geophys. Res.* **2002**, *107*, No D20, 8091.

[7]. Decesari, S., Facchini, M.C., Fuzzi, S., Tagliavini, E. Characterization of water-soluble organic compounds in atmospheric aerosol: A new approach. *J. Geophys. Res.* **2000**, *105*, D1, 1481-1489.

[8]. Kiss, G., Varga, B., Galambos, I., Ganszky, I. Characterization of water-soluble organic matter isolated from atmospheric fine aerosol. *J. Geophys. Res.* **2002**,*107*, D21,8339.

[9]. Krivászcy Z., Gelencsér, Kiss, G., Mészáros, T., Sárvári, Z., Temesi, D., Varga, B., Baltensperger, U., Nyeki, S., Weingartner, E. Study of the chemical character of water soluble organic compounds in fine atmospheric aerosol at Jungfraujoch. *J. Atmos. Chem.* **2001**, *39*, 235-259.

[10]. Sullivan, A.P., Peltier R.E., Brock, C.A., de Gouw, J.A., Holloway, J.S., Warneke, C., Wollny, A.G., Weber, R.J. Airborne measurements of carbonaceous aerosol soluble in water over northeastern United States: Method development and an investigation into water-soluble organic carbon sources. *J. Geophys. Res.* **2006**, *111*, doi: 10.1029/2006JD007072. Zuend A., Marcolli., C., Peter, T., Seinfeld, J.H. Computation of liquid-liquid equilibria and phase stabilities: implications for RH-dependent gas/particle partitioning of organic-inorganic aerosols. *Atmos. Chem. Phys.* **2010**, 7795-7820.

[11]. Donahue, N.M., Epstein, S.A., Pandis S.N., Robinson, A.L. A two-dimensional volatility basis set: 1. organic aerosol mixing thermodynamics. *Atmos. Chem. and Phys*. **2011**, *11*, 3303-3318.

[12]. Zuend A., Marcolli., C., Peter, T., Seinfeld, J.H. Computation of liquid-liquid equilibria and phase stabilities: implications for RH-dependent gas/particle partitioning of organic-inorganic aerosols. *Atmos. Chem. Phys.* **2010**, 7795-7820.

[13]. Zuend, A., Seinfeld J.H. Modelling the gas-particle partitioning of secondary organic aerosol: the importance of liquid-liquid phase separation. *Atmos. Chem. Phys.* **2012**, *12*, 3857-3882.

[14]. Asa-Awuku, A., Miracolo, M.A., Kroll, J.H., Robinson, A.L., Donahue, N.M. Mixing and phase partitioning of primary and secondary organic aerosols, *Geophys. Res. Lett*. **2009**, *36*, L15827, doi:10.1029/2009GL039301.

[15]. Banerjee, S. Solubility of organic mixtures in water. *Environ. Sci. Technol.* **1984**, 18, 587-591.

[16]. De Hemptine, J.C., Delepine, H., Jose, J.C., Jose, J. Aqueous solubility of hydrocarbon mixtures. *Rev. Inst Fr. Pet.* **1998**, 53(4), 409-419.

[17]. Khlystov, A., Wyers, G.P., Slanina, J. The steam-jet aerosol collector. *Atmos. Environ.*, **1995**, 29, 2229-2234.

[18]. Martin, M., Tritscher, T., Jurányi, Z., Heringa, M.F., Sierau, B., Weingartner, E., Chirico, R., Gyzel, M., Prévôt, A.S.H., Baltensperger, U., Lohmann, U. Hygroscopic properties of fresh and aged wood burning particles. *J. Aerosol Sci.*, **2013**, 56, 15-29.

[19]. Petters, M.D., Kreidenweis, S.M. A single parameter representation of hyroscopic growth and cloud condensation nucleus activity. *Atmos. Chem. Phys.*, **2007,** 7, 1961-1971.

[20]. Fountoukis, C., Nenes, A. A computationally efficient thermodynamic equilibrium model for K^+-Ca^{2+}-Mg^{2+}-NH_4^+-SO_4^{2-}-NO_3^--Cl^--H_2O aerosols. *Atmos. Chem. Phys.*, **2007**, 4639-4659.

[21]. Kostenidou, E., Pathak, R., Pandis, S.N. An algorithm for the calculation of secondary organic aerosol density combining AMS and SMPS data. *Aerosol Sci. Technol.*, **2007**, 41, 1002-1010.

Curriculum Vitae Magda Psichoudaki

Date of Birth 5 September 1981

Current Position Institute of Chemical Engineering (ICE/FORTH)
Stadiou Str, Platani, 26504, Patras

Contact office: (+30)2610965313
mpsichoudaki@chemeng.upatras.gr

Education

3/2008-4/2013	**PhD Candidate**, Chemical Engineering Department, University of Patras. Advised by Prof. Spyros Pandis. PhD thesis title: "***Atmospheric organic aerosol – water interactions***"
11/2005-11/2007	**M.S. on Environmental Analysis,** Chemistry Department, University of Patras.
9/1999-9/2004	**B.S.,** Department of **Chemistry**, University of Patras.

Work Experience

3/2009-6/2009	**Graduate Teaching Assistant** - Laboratory of Polymers, Chemical Engineering Dept., University of Patras.
9/2008-12/2008	**Graduate Teaching Assistant** – Chemical Reaction Engineering, Chemical Engineering Dept., University of Patras.
3/2008-6/2008	**Graduate Teaching Assistant** - Laboratory of Polymers, Chemical Engineering Dept., University of Patras.
3/2007-6/2007	**Graduate Teaching Assistant** - Laboratory of Nuclear Chemistry, Chemistry Dept., University of Patras.
9/2006-12/2006	**Graduate Teaching Assistant** - Laboratory of Chemistry, Biology Dept., University of Patras.
8/2004	**Research Assistant** at Hellenic Public Power Corporation, Coal-Fired Power Plant "AHS Ptolemaidos" Laboratory of Chemistry, Ptolemaida, Greece.

Research Experience

2008-now	University of Patras, Greece, Dept. of Chemical En Laboratory for Air Quality Studies (LAQS), Institute of Chemical Engineering, ICE/FORTH Greece.

- Development of the Steam Sampler – WSOC
- Theoretical analysis of the off-line WSOC measurement.
- Finokalia Aerosol Measurement Experiment (FAME – 2008) field campaign, Finokalia, Greece. Field measurements using the Steam Sampler-WSOC.
- MEGAPOLI 2009 - Summer field campaign, Paris, France. Field measurements using a TSI Scanning Mobility Particle Sizer (SMPS) and a CCN counter.
- MEGAPOLI 2010 - Winter field campaign, Paris, France. Field measurements using a TSI Scanning Mobility Particle Sizer (SMPS) and a thermodenuder.
- Finokalia Aerosol Measurement Experiment (FAME – 2011) field campaign, Finokalia, Greece. Field measurements using the Steam Sampler-WSOC.
- Pan-European Gas-Aerosols Climate Interaction Study (PEGASOS) 2012 -Summer field campaign, Patras, Greece. Field measurements using a TSI Scanning Mobility Particle Sizer (SMPS), 2 CCN counters and a Steam Sampler-WSOC.
- THALIS 2013 - Winter campaign in Athens, Greece during biomass burning events. Field measurements using a TSI Scanning Mobility Particle Sizer (SMPS) and a CCN counter.
- Smog chamber study: Production and photochemical aging of α-pinene SOA. Simultaneous measurements with AMS, PTR-MS, CCNc, SMPS.

Publications

- **Psichoudaki M.,** S. Bezantakos, A. Nenes, G. Biskos, S.N. Pandis (2014). *Hygroscopic properties of biomass burning emissions in Athens during winter*. In preparation.
- Wang, N. E. Kostenidou, A. Tasoglou, A., **M. Psichoudaki**, E. Louvaris, S.N. Pandis (2014). *SOA yield, CCN and volatility properties from a-pinene aging*. In preparation.
- Kaltsonoudis, C., E. Kostenidou, K. Florou, **M. Psichoudaki,** S.N. Pandis (2014). *Temporal variability of VOCs in the Eastern Mediterranean*. In preparation.
- Pikridas M., E. Kostenidou, **M. Psichoudaki**, L. Hildebrandt, G. Engelheart, J. Sciare, A. Schwarzenboeck, S. Crumeyrolle, U. Baltensperger, A. Wiedensohler, M. Kulmala, and S. N. Pandis (2014) *Ultrafine particle sources and in-situ formation in a European Megacity*, Atmos. Chem. Phys., submitted for publication.
- Paciga A., E. Kostenidou, L. Hildebrandt, **M. Psichoudaki**, G. Engelheart, B. H. Lee, M. Crippa, U. Baltensperger, and S. N. Pandis (2014). *Volatitility of atmospheric organic aerosol components*, Atmos. Chem. Phys., submitted for publication.
- **Psichoudaki, M.**, S.N. Pandis (2013). *Atmospheric aerosol*

water soluble organic carbon measurement: A theoretical analysis. Environ. Sci. Technol. 47, 9791-9798.

- Pikridas, M., A. Bougiatioti, L. Hildebrandt, G. J. Engelhart, E. Kostenidou, C. Mohr, A. S. H. Prevot, G. Kouvarakis, P. Zarmpas, J. F. Burkhart, B.-H. Lee, **M. Psichoudaki**, N. Mihalopoulos, C. Pilinis, A. Stohl, U. Baltensperger, M. Kulmala, and S. N. Pandis (2010) "*The Finokalia Aerosol Measurement Experiment – 2008 (FAME-08): an overview*" Atmos. Chem. Phys., 10, 6793-6806.
- **Psichoudaki, M.**, H. Papaeythymiou (2008). "*Natural radioactivity measurements in the city of Ptolemais (Northern Greece)*" Journal of Environ. Radioact. 99, 1011-1017.

Visiting Researcher	2013	Georgia Institute of Technology, School of Earth and Atmospheric Sciences, Atlanta, GA. Training on CCN data analysis with Prof. A. Nenes.
Computer Skills		Windows, Microsoft Office, Igor, Matlab, SPSS, Linux.
Instrumentation Skills		AMS, PTR-MS, SMPS, CCNC, TOC, Ion Chromatography, GC-MS, gas monitors, nephelometers, air samplers
Languages		Greek (native speaker) English (fluent, teaching license) Spanish (poor)
Conference presentations	22/9/2014-26/9/2014	E. Kostenidou, N. Wang, **M. Psichoudaki**, E. Louvaris, C. Kaltsonoudis, S.N. Pandis. "Photochemical aging of α-pinene ozonolysis SOA". 13th IGAC Science Conference on Atmospheric Chemistry, Natal, Brazil.
	28/8/2014-2/9/2014	E. Kostenidou, K. Florou, C. Kaltsonoudis, M. Tsiflikiotou, **M. Psichoudaki**, E. Louvaris, D.K. Papanastasiou, G.I. Gkatzelis, A. Bougiatioti, S. Bezantakos, N. Mihalopoulos, A. Nenes, G. Biskos, C. Pilinis, K. Eleftheriadis, S.N. Pandis. "Temporal and spatial variability of fine PM in the Eastern Mediterranean". International Aerosol Conference, Busan, Korea.
	28/5/2014-31/5/2014	E. Kostenidou, K. Florou, C. Kaltsonoudis, M. Tsiflikiotou, **M. Psichoudaki**, E. Louvaris, S.N. Pandis. "Chemical characterization and sources of ambient aerosol and gas pollutants during summer 2012 in two urban background locations in the Eastern Mediterranean". *12th International Conference on Meteorology, Climatology and Atmospheric Physics*. Heraklion, Greece. (presentation)

27/4/2014-2/5/2014	D.K Papanastasiou, E. Kostenidou, G.I. Gkatzelis, **M. Psichoudaki**, E. Louvaris, S.N. Pandis. "*Photochemical aging of oranic aerosols: A laboratory study*". European Geosciences Union General Assembly 2014, Vienna, Austria. (poster)
30/9/2013-4/10/2013	E. Kostenidou, K. Florou, C. Kaltsonoudis, M. Tsiflikiotou, **M. Psichoudaki**, S.N. Pandis. "Sources and chemical processing of organic aerosol during the summer in the Eastern Mediterranean". *AAAR 32nd International Conference*, Oregon, USA. (Platform presentation)
1-6/9/2013	**M. Psichoudaki**, E. Kostenidou, E. Bougiatioti, S. Bezantakos, G. Biskos, A. Nenes, S.N. Pandis. "Summer and wintertime aerosol levels at an urban Mediterranean environment: Impacts of biomass burning". *European Aerosol Conference*, EAC, Prague, Czech Republic. (poster)
2-7/9/2012	**M. Psichoudaki**, S.N. Pandis. "Water soluble organic carbon (WSOC) measurement: A theoretical analysis". European Aerosol Conference, EAC, Granada, Spain. (poster)
3-5/9/2009	N. Dima, **M. Psichoudaki**, H. Papaeythymiou. "Temporal variation in mass concentration of $PM_{2.5}$ in Patras, Greece". 11th International Conference on Environmental Science and Technology, Chania, Crete, Greece. (poster)
30/9/2007-4/10/2007	**M. Psichoudaki**, K. Eleftheriadis, M. Soupioni, H. Papaefthymiou. "Mass and chemical characterization of $PM_{2.5}$ in ambient air of Patras, Greece". *5th International Conference on Instrumental Methods of Analysis: Modern Trends and Applications*, Patras, Greece. (poster)

Honors & Awards	2007	Award of Excellence in the MS of Environmental Analysis, Department of Chemistry
Professional Affiliations		Hellenic Association for Aerosol Research (HAAR) Hellenic Association of Chemistry